2014

FINITE ELEMENT MODELING AND FABRICATION OF AN SMA-SMP SHAPE MEMORY COMPOSITE ACTUATOR

Mohammad Souri
University of Kentucky, m.souri@elmusa.com

STUDENT AGREEMENT:

I represent that my thesis or dissertation and abstract are my original work. Proper attribution has been given to all outside sources. I understand that I am solely responsible for obtaining any needed copyright permissions. I have obtained needed written permission statement(s) from the owner(s) of each third-party copyrighted matter to be included in my work, allowing electronic distribution (if such use is not permitted by the fair use doctrine) which will be submitted to UKnowledge as Additional File.

I hereby grant to The University of Kentucky and its agents the irrevocable, non-exclusive, and royalty-free license to archive and make accessible my work in whole or in part in all forms of media, now or hereafter known. I agree that the document mentioned above may be made available immediately for worldwide access unless an embargo applies.

I retain all other ownership rights to the copyright of my work. I also retain the right to use in future works (such as articles or books) all or part of my work. I understand that I am free to register the copyright to my work.

REVIEW, APPROVAL AND ACCEPTANCE

The document mentioned above has been reviewed and accepted by the student's advisor, on behalf of the advisory committee, and by the Director of Graduate Studies (DGS), on behalf of the program; we verify that this is the final, approved version of the student's thesis including all changes required by the advisory committee. The undersigned agree to abide by the statements above.

Mohammad Souri, Student

Dr. Haluk Karaca, Major Professor

Dr. James McDonough, Director of Graduate Studies

FINITE ELEMENT MODELING AND FABRICATION OF AN SMA-SMP SHAPE MEMORY COMPOSITE ACTUATOR

DISSERTATION

A dissertation submitted in partial fulfillment of the
requirements for the degree of Doctor of Philosophy in the
College of Engineering
at the University of Kentucky

By
MOHAMMAD SOURI
Lexington, Kentucky

Director: Dr. Haluk E. Karaca, Professor of Mechanical Engineering
Lexington, Kentucky

2014

ABSTRACT OF DISSERTATION

Finite Element Modeling and Fabrication of an SMA-SMP Shape Memory Composite Actuator

Shape memory alloys and polymers have been extensively researched recently because of their unique ability to recover large deformations. Shape memory polymers (SMPs) are able to recover large deformations compared to shape memory alloys (SMAs), although SMAs have higher strength and are able to generate more stress during recovery.

This project focuses on procedure for fabrication and Finite Element Modeling (FEM) of a shape memory composite actuator. First, SMP was characterized to reveal its mechanical properties. Specifically, glass transition temperature, the effects of temperature and strain rate on compressive response and recovery properties of shape memory polymer were studied. Then, shape memory properties of a NiTi wire, including transformation temperatures and stress generation, were investigated. SMC actuator was fabricated by using epoxy based SMP and NiTi SMA wire. Experimental tests confirmed the reversible behavior of fabricated shape memory composites.

The Finite Element Method was used to model the shape memory composite by using a pre-written subroutine for SMA and defining the linear elastic and plastic properties of SMP. ABQUS software was used to simulate shape

memory behavior. Beside the animated model in ABAQUS, constitutive models for SMA and SMP were also developed in MATLAB® by using the material properties obtained from experiments. The results of FEM simulation of SMC were found to be in good agreement with experimental results.

KEYWORDS: Shape Memory Polymer, Shape Memory Alloy, Shape Memory Composite, Finite Element Modeling, Actuators

Mohammad Souri

_____

Student's Signature

_____

Date

Finite Element Modeling and Fabrication of an SMA-SMP Shape Memory Composite Actuator

By

Mohammad Souri

Dr. Haluk Karaca
_____
Director of Dissertation

Dr. James McDonough
_____
Director of Graduate Studies

_____

Finite Element Modeling and Fabrication of an SMA-SMP Shape Memory Composite Actuator

By

Mohammad Souri

Dr. Haluk Karaca
_____
Director of Dissertation

Dr. Charles Lu
_____
Co-Director of Dissertation

Dr. James McDonough
_____
Director of Graduate Studies

_____

To Marjan - my wife, my love, and my best friend, who has supported me unconditionally

ACKNOWLEDGEMENTS

I would like to thank my advisor, Dr. Haluk E. Karaca, who helped me to develop the basic principles of this study. This work could not be accomplished without his persistent guidance and motivation. I greatly appreciate his unconditional and continuous support.

I am really grateful for having Dr. Y. Charles Lu as my co-advisor who helped me a lot during the project. I would like to thank Dr. Rouch, Dr. Cheng, and Dr. Bazrgari for serving as committee members and for their time.

I would also like to thank my parents to whom I am indebted for their unconditional support despite being far away from me.

I am very lucky to have developed such great friendships during the course of my studies. I would like to express my deepest gratuities to Gurdish Singh Ded, Sayed Mohammad Saghaian, Dr. Burak Basaran, Dr. Hirobumi Tobe, Ali Sadi Turabi, Irfan Kaya, Peizhen Li, Dr. Adnan Kaya, Emre Acar, Anil Erol, Rayan Schulte, Kevin Wieman, Spandana Pulla, Vitali, Masoud Jabbari, and Amirhossein Ghasemi.

And lastly, without help of my dear friends, Sonia Erfani, and Katherine George, my work would not expressed as good.

TABLE OF CONTENTS

TABLE OF CONTENTS iv
LIST OF TABLES vi
LIST OF FIGURES vii
1 INTRODUCTION 1
1.1 PRELIMINARY INTRODUCTION 1
1.2 MOTIVATION 2
1.3 LITERATURE REVIEW 3
1.4 RESEARCH OBJECTIVES 6
2 SHAPE MEMORY POLYMER, CHARACTERIZATION AND MODELING 8
2.1 INTRODUCTION 8
2.2 HISTORY OF SMP CHARACTERIZATION 8
2.3 SAMPLE PREPARATION 10
2.3.1 EXPERIMENTAL SETUP 11
2.4 EXPERIMENTAL RESULTS 15
2.4.1 GLASS TRANSITION TEMPERATURE 15
2.4.2 SHAPE MEMORY EFFECT 17
2.4.3 DEFORMATION LIMIT ON NGDE3 SMP 19
2.4.4 COMPRESSION RESPONSES AND RECOVERY 20
2.4.5 EFFECTS OF TEMPERATURE ON DEFORMATION BEHAVIOR 22
2.4.6 CONSTRAINT SHAPE RECOVERIES 24
2.4.7 EFFECTS OF THERMO-MECHANICAL HISTORY 27
2.5 SMP MODELLING 30
2.5.1 LITERATURE REVIEW 30
2.5.2 SMP CONSTITUTIVE MODEL FOR SMALL DEFORMATIONS 31
2.5.3 FINITE ELEMENT MODELLING OF SMP IN ABAQUS® 35
3 NiTi WIRE CHARACTERIZATION AND MODELLING 40
3.1 EXPERIMENTAL CHARACTERIZATION OF NiTi WIRE 40
3.1.1 DSC RESULTS ON NiTi WIRE 40

3.1.2 STRESS INCREASE OF CONSTRAINED NiTi WIRES WITH TEMPERATURE SCAN 41
3.2 SMA MODELLING 42
3.2.1 LITERATURE REVIEW 43
3.2.2 LAGOUDAS APPROACH FOR SMA CONSTITUTIVE MODEL 45
3.2.3 ANSYS MODEL OF A DOG-BONE TENSILE SMA SAMPLE 49
3.2.4 SMA MODEL IN ABAQUS 54
4 SHAPE MEMORY COMPOSITE ACTUATOR: FABRICATION AND FINITE ELEMENT MODELING 59
4.1 BACKGROUND 59
4.2 SMA-SMP COMPOSITES 61
4.2.1 RULE OF MIXTURE 66
4.2.2 EXPERIMENTAL RESULTS AND DISCUSSION 68
4.3 SMC MODEL IN ABAQUS 71
4.3.1 Wire SMC FEM 71
4.3.2 Spring-SMC FEM 75
4.3.3 SMC with SMA-SMP bending plates 77
5. CONCLUSIONS 79
REFERENCES 80
VITA 84

LIST OF TABLES

Table 2-1: Chemical formulations of the NGDE3 SMP 10
Table 2-2: Calibrated functions for strain calculation 33
Table 2-3: Material specification of SMP in different temperatures..... 36
Table 2-4: Plastic definition for SMP at room temperature for 50% compression according to ABAQUS requirements 36
Table 3-1: ANSYS SMA material constant definitions 50
Table 3-2: Comparison of the results for the maximum von-misses stress in different temperatures 53
Table 3-3: SMA material parameter's values..... 56
Table 4-1: Main material properties of NiTi SMAs and SMPs [17]..... 62
Table 4-2: Calculated the number of needed wires for SMC according to rule of mixture..... 67

LIST OF FIGURES

Figure 2-1: Lindberg/BlueM box furnace (BF514841) 11
Figure 2-2: Illustration of MTS and its components 12
Figure 2-3: Servo-Hydraulic Mechanical Tester (MTS) setup schematic 12
Figure 2-4: Perkin Elmer Pyris DMA 7E 13
Figure 2-5: Pyris1 DSC used for finding the glass transition temperature of SMP and transition temperature of SMA wire 15
Figure 2-6: Results of DSC for NGDE3 SMP 16
Figure 2-7: Schematic of the three-point bending test [41] 16
Figure 2-8: Results of the three-point bending test for the NGDE3 epoxy-based SMP 17
Figure 2-9: Shape memory effect of SMP with illustrated schematics 19
Figure 2-10: Failure test result of NGDE3 SMP 20
Figure 2-11: Compression test results for SMP at room temperature 21
Figure 2-12: Recovery of compressed SMP samples by increasing the temperature 22
Figure 2-13: SMP compression test in different temperatures 23
Figure 2-14: Recovery tests on compressed specimens at different temperature 23
Figure 2-15: Strain-temperature profiles of constraint shape recoveries of the SMP 24
Figure 2-16: Stress-temperature profiles of constraint shape recoveries of the SMP 26
Figure 2-17: The maximum stress generated during constraint shape recovery as a function of fixing strain 27
Figure 2-18: (a) Schematic of the mechanical behavior of the SMP at $T<T_g$, (b) Schematic of the mechanical behavior of the SMP at $T>T_g$, and (c) Combined view of (a) and (b) 28
Figure 2-19: 3D stress-strain-temperature profile showing the shape recoveries of the SMP under complex thermo-mechanical cycles 29
Figure 2-20: SMP composed of active and frozen phases in the model proposed by Lagoudas et al. [53] 31
Figure 2-21: a) Strain-temperature and b) Calibrated frozen volume fraction-temperature graphs of SMP 34
Figure 2-22: Comparison between the experimental shape memory effect (colored) and the theoretical results (black) 35
Figure 2-23: (a) Applying constraint on the bottom end of the SMP, (b) Applying load on the top end of SMP 37

Figure 2-24: Illustration of shape memory effect on SMP FE model. a) Loading, b) Cooling, c) Unloading, d) Heating 38
Figure 2-25: Comparison between experimental SME and ABAQUS results 39
Figure 3-1: DSC result of NiTi wire 41
Figure 3-2: Stress generation test for a SMA wire 42
Figure 3-3: Super-elastic behavior of SMA with definitions of the important variables (from ANSYS online help and [1]) 50
Figure 3-4: Transformation stress versus temperature curves for SMA material 51
Figure 3-5: Superelastic responses at selected temperatures 51
Figure 3-6: Dog-bone tensile specimen dimensions 52
Figure 3-7: Load and boundary condition that applied to the dog-bone tensile specimen 53
Figure 3-8: The contour plot of generated stress at 70 °c 54
Figure 3-9: Pseudo-elastic behavior of SMA with definition of SMA parameters [30] 55
Figure 3-10: Contour plot of SMA bar under load 57
Figure 3-11: Superelasticity results of a SMA that was defined in ABAQUS at selected temperatures 57
Figure 3-12: ABAQUS results: shape memory effect of a SMA wire a) in 2D and b) in3D 58
Figure 4-1: Change of a) elastic modulus and b) yield stress with temperature of SMA, SMP and steel [104] 63
Figure 4-2: SMC actuation illustration 64
Figure 4-3: Stress-strain graph for NiTi wire 67
Figure 4-4: SMC sample made with NGDE3 SMP matrix and Flexinol NiTi wires 68
Figure 4-5: SMC actuation results with 1 °C/min 69
Figure 4-6: Alternative SMC cycle done by adjusting the thermal cycling range with a rate of 5 °c/min 70
Figure 4-7: SMC model in ABAQUS 72
Figure 4-8: SMC FEM in action, a) cooled down b) heated up 73
Figure 4-9: Comparison between finite element model results and experimental results of SMC 74
Figure 4-10: SMC results with SMP plastic behavior 75
Figure 4-11: Contour plots of spring SMC 76
Figure 4-12: Displacement versus temperature graph for spring-SMC actuation 76

Figure 4-13: Contour plots of SMC bending plates 77
Figure 4-14: Angle versus temperature graph for bending plates SMC 78

1 CHAPTER I: INTRODUCTION

1.1 PRELIMINARY INTRODUCTION

As a new "smart" material, shape memory polymers (SMPs) are one of the most interesting subjects research groups have studied in recent years. Many applications are being explored because of their rare benefits, such as large recoverable deformation, easier pretreatment procedure, low fabrication cost and adjustable recovery temperatures. As soon as the shape-memory effects in shape memory polymers were found out, a lot of applications have been introduced. Heat shrinkable tapes and tubes made with radiation-cross-linked polyethylene, information storage that can allow thermally reversible recording [1-3], temperature sensors and actuators are some of the examples of their applications [1]. However, novel applications are mostly focused on medical devices, such as biodegradable sutures [4, 5], actuators [6], catheters, and stents [1, 7].

The other novel shape memory materials are shape memory alloys (SMAs). SMAs can produce very high recoverable shape changes (~4-8%) as a result of reversible martensitic phase transformations that can be triggered by changes in temperature, stress state or magnetic field. Their remarkable mechanical property features, such as high recovery force to weight ratio and large recoverable deformation have enabled them to be utilized for actuators and sensors in a diversity of fields. SMAs have higher energy density than pneumatic actuators, D.C motors or other active materials and are equivalent in performance to hydraulic actuators while being compact, robust, lightweight, frictionless, quiet, easier and less costly to be inspected and maintained [8]. Due to these unique properties, industries such as aerospace, automotive, oil and gas and many others have become increasingly interested in SMAs [8-10].

A composite is a hybrid of two or more constituent materials with significantly different physical or chemical properties that remain discrete on a macroscopic level within the finished structure. A composite is designed to display a

combination of the best characteristics of each of the constituent materials. Consequently, a composite's performance is superior to those of its constituents acting independently [11]. SMAs have high strength, good thermal conductivity, and ability to generate high forces, but are more expensive, denser and show lower recovery strain in comparison to SMPs [12]. On the other hand, SMPs are lightweight, inexpensive, have good formability and provide high recovery strain; however, they lack strength, have low modulus at high temperatures and do not have the ability to perform reversible actuation [11, 12]. A SMC can be created by embedding SMA components (e.g. in wire or powder forms) in a SMP polymer matrix resulting in a low density composite with increased strength and modulus. Also, the addition of SMA wires, through electrical resistance, can supply heat energy to the overall polymer matrix to trigger the actuation motion. The size, distribution, and volume fraction of wires can be adjusted to control the SMC properties in accordance with the application requirements. The temperature range at which the SMC will function is one of the design variables that should be engineered and designed according to SMA and SMP transition temperatures.

This project focuses on a novel shape memory composite actuator that is designed with a shape memory polymer cylinder specimen and a NiTi shape memory alloy wire. The actuator is triggered by temperature and combines the shape memory effect of both SMP and SMA. The actuator shows reversible shape change with temperature.

1.2 MOTIVATION

Smart materials are engineering materials that have inherent sensing, actuating, and controlling or information processing capabilities in their microstructures. They have the ability to respond to changes in temperature, electric field, or magnetic field owing to their intrinsic intelligence. Shape memory materials, piezoelectric materials, fiberoptics, magneto-(electro-)strictive materials, magneto-(electro-)rheological fluids and some functional polymers are some examples of smart materials [13, 14]. They all have great potential in a variety of applications; however, shape memory materials (SMAs and SMPs) are the major elements of

smart composites because of their unusual properties of shape memory effect, pseudoelasticity, damping capacity, and adaptive properties.

In SMPs, the modulus changes significantly at the glass transition temperature (Tg), decreasing as the polymer is heated above the transition temperature [15, 16]. As a result, strain can be introduced into the polymer with relative ease at temperatures above the transition temperature. If the strain is maintained and the temperature of the material is decreased below the transition temperature, the strain is 'frozen in'.

This strain is recovered when the polymer is heated above the transition temperature again [17, 18]. SMPs have found use in structural applications in which epoxy-based materials are often used owing to their intrinsically high mechanical properties, chemical resistance, thermal stability, and tunable transition temperatures. SMPs can be employed in open cellular (foam) form as low mass, low volume, and low-cost self-deployable structures for space and commercial applications [19]. Their advantages include low mass, low storage volume, high reliability (no deployment mechanisms are required), high dynamic damping, ease of fabrication, impact and radiation resistance, and thermal and electrical insulation and low cost [20]. Because SMPs exhibit physical properties similar to those of human tissues, they are thought of as ideal candidates for many medical applications.

1.3 LITERATURE REVIEW

Shape memory composite, as described above, is a state-of-the-art actuator for which few groups have studied.

Tobushi *et al*. made a bending actuator using SMA and SMP properties in 2009. By putting a super-elastic kind SMA tape and a shape memory effect type SMA tape inside of a SMP tape. The two different kinds of SMAs have memory by heat-treatment in different directions. When SMC heated the recovery force increases and the SMC changes the shape and when cooled the recovery force is decreases and it will get back to the original shape [21].

Tobushi *et al*. fabricated the SMC belt, composed of SMA tapes and a SMP in which they showed that a small rotary actuator can be developed using the torsion properties of SMA-tape. They have fabricated the SMC belt with the SMA tapes covered by SMP tape. By using the characterizations of SMA and SMP, a three-way bending movement of the SMC belt during heating and cooling was observed [22].

In another effort, Tobushi *et al*. made a composite belt with a SMA wire and SMP sheet and the thermomechanical properties of the SMC matrix has been investigated [23].

Dapino and Noeth have tried to fabricate a shape memory composite by inserting pre-deformed shape memory alloy texture in shape memory polymer plate to achieve a fully reversible actuator. They have explained the techniques that they have used to embed the wire into the polymer by creating surface modifications using shape memory wires and modifying polymer using vacuum actuation [24].

Bollas *et al*. have investigated the stress generated in a shape memory wire embedded in fibrous polymer. The stress fields measured have confirmed that SMA wires can serve as effective stress-actuators. The wire composition and level of pre-strain turned out to be very important factors on efficiency of stress generation. The maximum value of stress recorded in the fibers at a distance of almost one wire radius was 227 MPa [25].

Turner has showed the results from experimental validation of a recently developed model for predicting the thermo-mechanical behavior of shape memory alloy hybrid composite (SMAHC) structures, composite structures with an embedded SMA constituent. The model captures the material nonlinearity of the material system with temperature and is capable of modeling constrained, restrained, or free recovery behavior from experimental measurements of fundamental engineering properties. A brief description of the model and analysis procedures is given, followed by an overview of a parallel effort to fabricate and characterize the material system of SMAHC specimens. Static and dynamic experimental configurations for the SMAHC specimens are described and experimental results for thermal post-buckling and random response are

presented. Excellent agreement is achieved between the measured and predicted results, fully validating the theoretical model for constrained recovery behavior of SMAHC structures [14].

Initial experimental efforts by Tobushi *et al*. provided data from small deformation experiments with applied extensions of 2%, 4%, and 10% [21]. The tests investigated the stress-strain relationship of thin polyurethane SMPs. The results obtained during this experimental investigation represent one of the first attempts to capture the entire shape memory effect of SMPs. In particular, the stress due to constrained cooling and the shape recovery upon subsequent heating was noted. Additional efforts by Tobushi *et al*. involved deforming the thin films to extensions of 20% and 100% [26]. The thermo-mechanical response of specimens loaded at different temperatures were captured. In addition, the stress-strain relationship upon loading was observed to be nonlinear for extensions greater than approximately 20%.

The preliminary cyclic effects on the shape recovery were investigated, and a shift in the stress-strain-temperature results was noted for subsequent thermo-mechanical cycles [26]. In particular, the accumulated amount of irrecoverable deformation continued to increase for each of the ten thermo-mechanical cycles, and Tobushi noted that the SMPs recovered approximately 98% of the applied deformation during each thermo- mechanical cycle.

Extensive efforts on the thermo-mechanical behavior of SMPs for small deformations were also conducted by Liu *et al.* [27]. These experiments characterized dog-bone shaped specimens, and the data was subsequently used to calibrate and validate the proposed constitutive model. The experiments performed by Liu not only aimed to obtain the material properties above and below the glass transition temperature, but also characterize the thermo-mechanical response when deformed to a range of values, up to 9% in magnitude, of applied tensile and compressive strains. In these experiments, both the stress increase due to constrained cooling and the nonlinear strain-temperature relationship during zero load recovery were captured and observed to occur in a smooth, nonlinear manner.

Recent experimental efforts have shifted from the characterization of the response due to small deformations to the large deformation response of SMPs processed in a dog-bone shape. For instance, Baer *et al*. [28] tested polyurethane SMP specimens to tensile extensions of 20% and 100% for use in medical applications. In these experiments, the SMP recovered approximately 90% of the applied deformation, and the effects of cyclic deformation at a range of temperatures were investigated. The results from the cyclic deformation study indicated the greatest shift in material response from the first cycle to the second cycle with an apparent training, or stabilization in material response, occurred from the second to fifth cycles.

Additionally, Atli *et al*. thermo-mechanically characterized SMPs for applied tensile strains up to 75% for dog-bone specimens [29]. The experiments performed by Atli are similar in principle to those presented in this work such that the same Veriflex*TM* shape memory polymer is used and subjected to a similar thermo-mechanical load path. Due to experimental apparatus limitations, however, the complete shape recovery profile during heating was not captured by Atli.

1.4 RESEARCH OBJECTIVES

Review of available literature on SMCs reveals that only limited work has been done on them. In order to be able to fabricate SMCs, there are critical steps to undertake. First, properties of SMPs must be characterized thoroughly to determine their glass transition temperature, fracture stress level, effects of temperature, and the amount of stress that can be generated.

The SMC was made with epoxy-based SMP cylinder and NiTi SMA wire. Thus, shape memory properties of NiTi wire should be characterized as well. For SMA wire, the transition temperature and the amount of stress that the SMA wire can generate were characterized.

For modeling, both SMA and SMP models were used. For SMA model, a subroutine that has developed by Lagoudas *et al*. (based on Tanaka, Boyd and Lagoudas, and Liand and Rogers constitutive models) was used [30]. This subroutine implements the SMA behavior in ABAQUS. In this study, this subroutine

was used for finite element modeling of the SMC. The required geometry was created and meshed with appropriate hexagonal elements and the material properties were assigned by the subroutine. For SMP, it is important to know its shape memory behavior and material properties very well. For SMC, SMP can be modeled as a linear-elastic material with plastic definition. SMP behavior is highly temperature dependent and it has to be considered in the material definition. A constitutive model for SMP that has proposed by Volk and Lagoudas [31] also was coded in MATLAB®.

In conclusion, the objectives of this study are:

- Thermo-mechanical characterization of the SMP that includes:
    - Fabrication of epoxy-based SMPs
    - Determining the glass transition temperature
    - Determining the critical stress for failure
    - Revealing shape memory effect
    - Investigating stress-strain tests as a function of temperature
    - Revealing stress generation as a function of strain
    - Studying the effects of loading history on SMP behavior
    - Modelling the SMP behavior
- Thermo-mechanical characterization of SMA wire that includes:
    - Determining the transition temperature
    - Revealing the critical stress for failure
    - Determining the elastic modulus
- Fabricating the SMC
- Determining the thermo-mechanical behavior of SMC
- Modelling of the SMC by using a commercial FEM software

2 CHAPTER II: SHAPE MEMORY POLYMER, CHARACTERIZATION AND MODELING

2.1 INTRODUCTION

The main focus of this chapter is the characterization of shape memory polymers and modeling its behavior by using a constitutive model from Volk and Lagoudas and a hyper-elastic model in ABAQUS. SMP characterization including the fabrication process to tailor the glass transition temperature, introduction of the experimental setup to perform the needed experiments, and detailed discussion of the characterization processes including the glass transition temperature, failure test, and shape memory effect, effects of temperature, recovery tests, stress generation tests, and effects of loading history, were investigated.

2.2 HISTORY OF SMP CHARACTERIZATION

The origin of SMPs can be traced back to the French company CdF-Chimie in 1984, and in less than a year, SMPs gained attention by Nippon Zeon Company in Japan because of their processability. Over the two decades, there have been great improvements to the understanding and applications of SMPs, but recently it gained greater interest [32].

SMPs function in two phases, separated by its glass transition temperature (Tg). The first state, below Tg, is a solid, fixed state, often times referred to as the glass state. When the SMP's temperature is increased above its Tg, the material transitions into a softer, rubber-like phase. During this state, the material is thermally reversible; the SMP will recover most, if not all, of its initial shape. It should be noted that the Tg can be adjusted by the composition of SMP and can be increased to 100 °C or more.

The mechanical properties of shape memory polymers were first characterized in 1992 by Tobushi *et al*. [33]. This first study tested the resistance to deformation of polyurethane above Tg by running tensile cycles with a strain level of 50%. The results showed that resistance to deformation increased with the number of cycles [33]. In four years, the research group of Tobushi published another paper that reported several results from different experiments on polyurethane, including

isothermal stress-strain responses in tension at constant strain rate, creep tests, and relaxation tests at different temperatures [34].

The shape fixity and recovery were examined in tension for polyurethane thin films at different temperatures by Tobushi *et al.* [35]. In 2003, Abrahamson *et al.* conducted isothermal tensile tests with constant strain rate experimentally [36]. In 2004, Liu and Gall *et al*. have done uniaxial compression and tension on shape memory polymer [37]. In 2009, Atli *et al.* characterized SMPs in a dog-bone shape for values of extensions up to 75% [29]. In 2011, Lagoudas *et al*. also have done a complete thermo-mechanical characterization of SMP in tension [31]. A few researchers have studied the effect of polymer structure on recovery properties at moderate strains. Baer *et al.* examined the thermo-mechanics and shape-memory behavior for thermoset polyurethanes intended for medical applications as a function of curing temperature, *Tr,* and deformation strain [28, 38].

Although, a great increase in the understanding of the constitutive response of SMPs was evident, there has been little effort to connect the effects of SMP structure, temperature, and strain limits to one another. Due to this deficiency of knowledge, it is difficult to optimize the strain recovery of an SMP by altering its structure and/or deformation temperature.

Currently, research is being focused on the characterization of thermo-mechanical properties of epoxy-based SMPs. Several approaches are being investigated to help our understanding of these properties, such as compression and recovery tests, failure tests, effect of temperature, etc. The epoxy-based SMPs were fabricated based on an approach introduced in the study by Xie *et al*. [39]. A series of epoxy-based SMPs was introduced in the aforementioned work with various glass transition temperatures. They have named NGDE1 to NGDE4 based on their glass transition temperature. In this project, one epoxy-based shape memory polymer that will be specifically focused on is the NGDE3 (part of the NGDE series). NGDE3 has been selected because of the appropriate range of glass transition that it has and needed to fabricate SMC.

2.3 SAMPLE PREPARATION

The SMP used for our experiments is epoxy-based and composed of an epoxy monomer (EPON 826), Jaffamine D230 (curing agent) and NGDE (neopentyl glycol diglycidyl ether). The detailed formulations of the epoxy SMP are summarized in Table 2-1. EPON 826 was weighed in a glass bottle and melted at 70 °C. After melting EPON 826, weighed Jeffamine D230, and NGDE (or decylamine) were introduced into the bottle, which was then shaken vigorously by hand for about 10 seconds to mix the components. Next, the mixture was poured into a Teflon container to get a cylindrical shape for compression tests. The epoxy samples were thermally cured at 100 °C for 1.5 hours and post-cured at 130 °C for 1 hour.

Upon the completion of the cure, the epoxy cylindrical samples could be cut into appropriate lengths for compression and recovery tests and the thin plates into rectangular shapes with needed dimensions for DMA three-point bending tests [39].

Table 2-1: Chemical formulations of the NGDE3 SMP

Samples	EPON826 (mol)	D230 (mol)	NGDE (mol)
NGDE3	0.005	0.01	0.015

A Lindberg/BlueM BF514841 Box furnace (Figure 2-1) was used for curing the polymer. Equipped with a UT150 controller, the furnace could be programmed to a single set-point while using a desired ramp rate. The furnace was set to the desired temperature and allowed to reach the set temperature before the sample was place in the furnace. After putting the liquid polymer or a sample in the furnace, the time was noted once the temperature reached the set temperature again [40].

Figure 2-1: Lindberg/BlueM box furnace (BF514841)

2.3.1 EXPERIMENTAL SETUP

All experiments for this project were performed at the Smart Material's Laboratory at the Mechanical Engineering Department of University of Kentucky. The compression tests are performed by a Landmark 370.10 MTS (Servo-hydraulic Mechanical Tester) with 100kN capacity. As shown in Figure 2-2, MTS has a temperature controller. The specimen was heated in a furnace and cooled via convection using liquid nitrogen introduced near the bottom of the furnace at a rate of 10 °C/min. An Omega CN8200 series temperature controller ensured stable heating-cooling rates with K-type thermocouples attached to both the specimen and grips. A cryogenic grade, on/off solenoid valve commanded by the temperature controller was used to control the flow of liquid nitrogen [40].

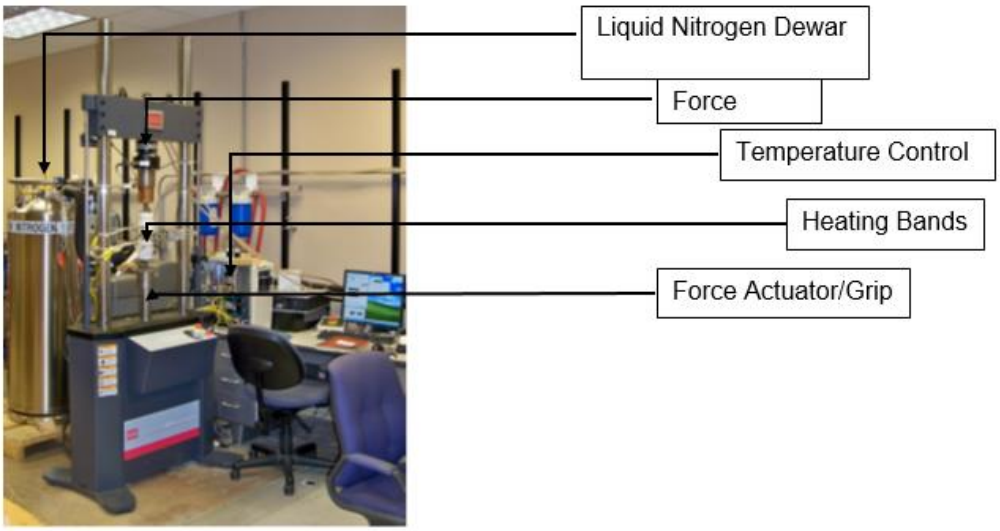

Figure 2-2: Illustration of MTS and its components

Figure 2-3 shows a schematic of MTS and its main parts.

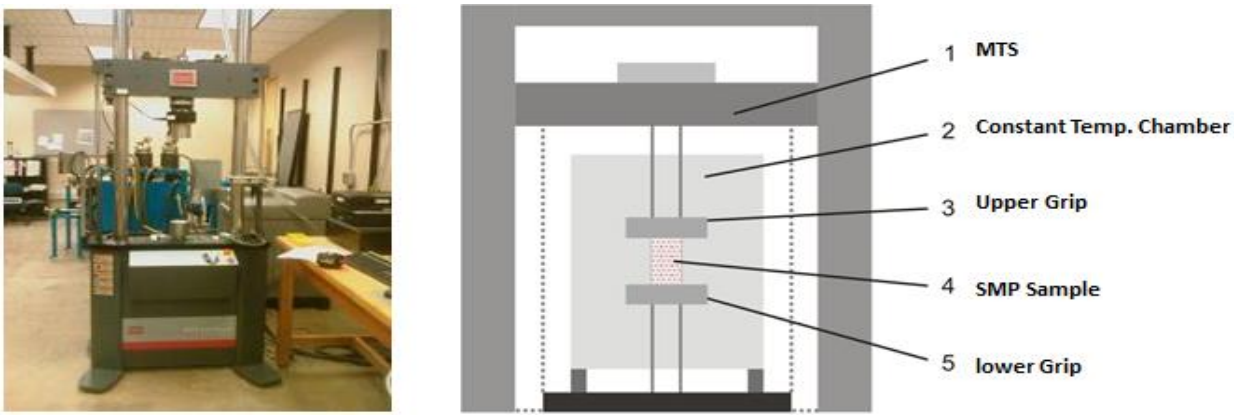

Figure 2-3: Servo-Hydraulic Mechanical Tester (MTS) setup schematic

The compression sample was polished mechanically with 600-grit paper to remove any residue after being removed of its Teflon container Teflon container. Once the sample was ready, a K-type thermocouple was attached to the sample by fastening it with fine gauge copper wire, followed by placing the sample between the test setup in proper position. Typical strain rate used for isothermal cycling was ($2*10^{-4}$) mm/sec for loading. The sample was unloaded with 100 N/sec.

For recovery tests, a DMA (Dynamic Mechanical Analyzer) was used (Figure 2-4). The Perkin Elmer DMA 7e provides the performance and flexibility necessary for

the characterization of a broad range of materials from soft samples, such as elastomers, thin films and single filament fibers, to hard samples, like composites, ceramics and metals. The DMA 7e's multiple measuring systems accommodate most sample types, and its multiple operating modes, including temperature, time, frequency scan, stress scan, creep-recovery, and constant force (TMA), further enhance flexibility and accurate material characterization. The temperature range for Perkin Elmer Pyris DMA 7e is from -170 ˚C to 500 ˚C [40].

For the SMP recovery test, the sample was placed inside the chamber of DMA underneath of the probe after which the temperature was increased from 20 °C to 80 °C. By recording the change in the length of the sample, strain could be calculated.

The three-point bending test is another important test that can be performed on a SMP thin plate by the DMA. This test has mainly performed to confirm the glass transition temperature of SMP.

Figure 2-4: Perkin Elmer Pyris DMA 7E

The Perking Elmer Differential Scanning Calorimeter (Pyris 1) has been used to determine the glass transition temperature of SMP and also the transition temperature of SMA wire (Figure 2-5). Differential scanning calorimetry (DSC) is a thermo-analytical technique in which the difference in the amount of heat required

to increase the temperature of a sample and reference are measured as a function of temperature. Both the sample and reference are maintained at nearly the same temperature throughout the experiment. The heating and cooling rate used to run the experiments was fixed at 5°C/minute. The temperature scale was calibrated using the furnace calibration feature in Pyris software. The minimum and maximum set-point is entered in the sub menu for furnace calibration and the software calculates seven other points between the desired ranges, as specified by the user. The thermocouple temperature is matched to the programmed furnace temperature when this calibration is complete. The enthalpy scale was calibrated using the observed delta-H from an accurately known amount of indium.

Samples were encapsulated in disposable aluminum pans, typically using 20 to 40 milligrams of sample. There are two styles of pans available, one used for solids, and a hermetically sealed version for liquids. Aluminum pans (Perkin Elmer part number 0219-0041) with a temperature range of -170°C to 600°C and volume capacity of 40 µL were used. The sample pans ensured safety against material that can leak out into the DSC can contaminate and cause permanent damage to the DSC's furnace, particularly if there are metals present in the sample that could make an alloy with the platinum furnace holders.

There is a sample side and a reference side in the furnace. A blank pan was inserted into the reference side. For all samples, it was noted that the sample maintained good contact with the bottom of the pan, thus ensuring good contact with the sensor, especially when using large samples since the thermal gradient effects can increase. Large samples produce larger transition, hence are preferred for study even the small changes, but thermal gradient should be taken into account while using them [40].

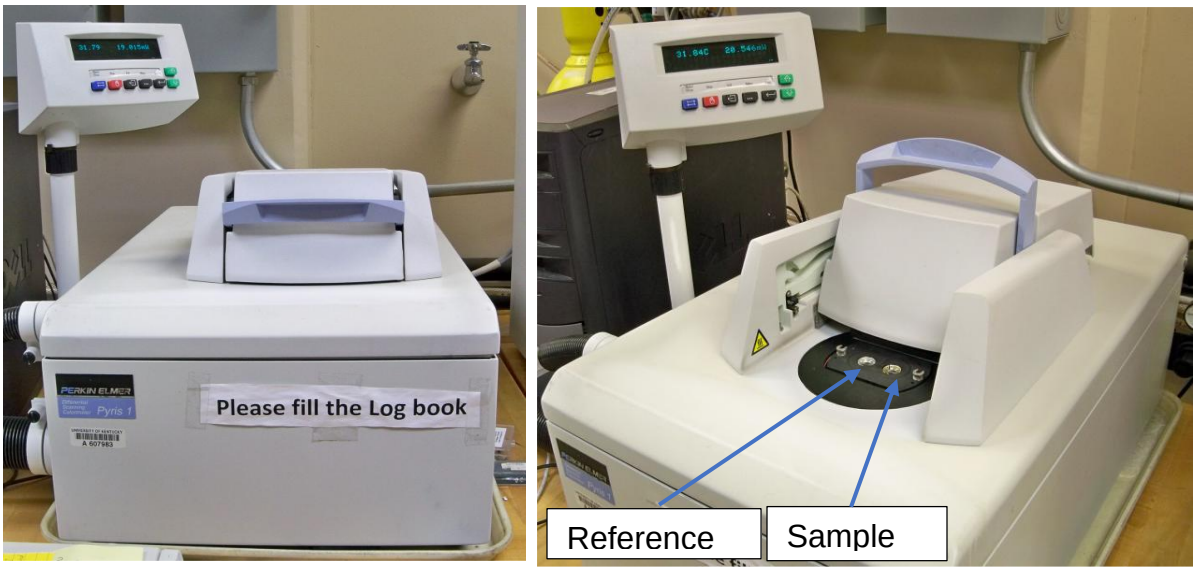

Figure 2-5: Pyris1 DSC used for finding the glass transition temperature of SMP and transition temperature of SMA wire

2.4 EXPERIMENTAL RESULTS

In this section, all experiments necessary for characterizing SMP behavior will be discussed. The detailed information about the devices and performing the experiments are presented and the results were inputted for subsequent modeling.

2.4.1 GLASS TRANSITION TEMPERATURE

Glass transition temperature (T_g) of an SMP is the temperature at which a substance transitions from a fixed phase to a rubber phase. The T_g can vary among the different types of SMPs and can be manipulated by altering the chemical composition of the SMP. Determining this glass transition temperature is a crucial step prior to the thermo-mechanical testing of an SMP.

In order to find the T_g of an SMP, a technique called Differential Scanning Calirometry (DSC), as described in the previous part, is used. For SMPs, as temperature increases, the internal energy steadily changes, and the T_g is marked by a fluctuation of the internal energy. As illustrated in the graph of Figure 2-6, the glass transition temperature of NGDE3 SMP is around 43 °C.

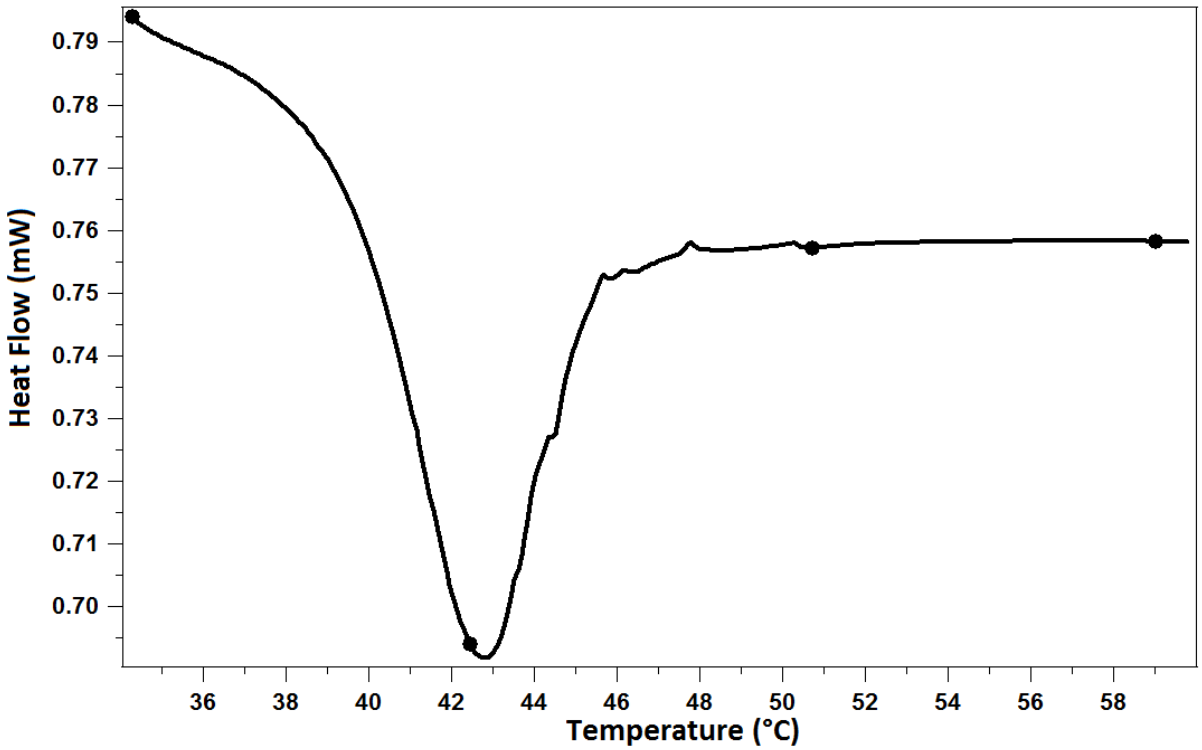

Figure 2-6: Results of DSC for NGDE3 SMP

Another common test that is performed on materials to characterize the transition temperature is three-point-bending test. This test was performed by DMA device. Figure 2-7 shows a schematic of the three-point-bending test clamp.

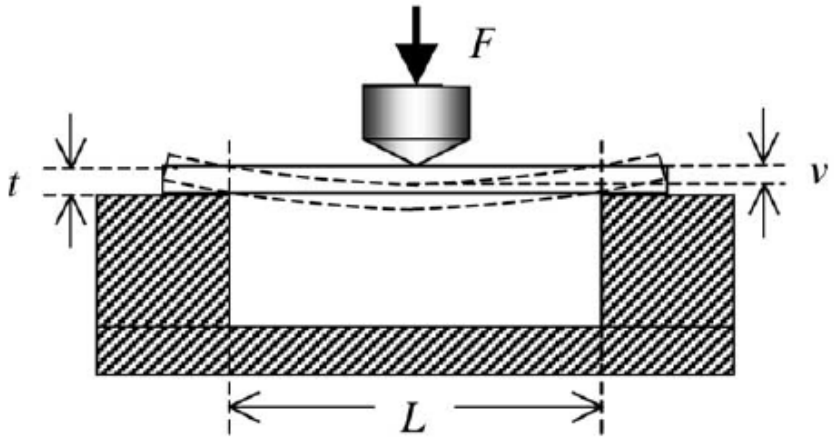

Figure 2-7: Schematic of the three-point bending test [41]

A rectangular 1 mm thick (t) SMP specimen was cut to 5 mm in width and 15 mm in length and put in the furnace of DMA while clamped on a special grip. The

distance between the 2 sides of the grip is 12 mm (L). Once the probe touches the middle of the sample and with amplitude of 20 mN for dynamic force and static force of 100 mN, the test begins. The temperature range is from 15 °C to 75 °C. The peak for heat flow will show the transition temperature. Figure 2-8 shows the results for the NGDE3 specimen. The glass transition temperature obtained from this test is consistent with the results from DSC (~43 °C).

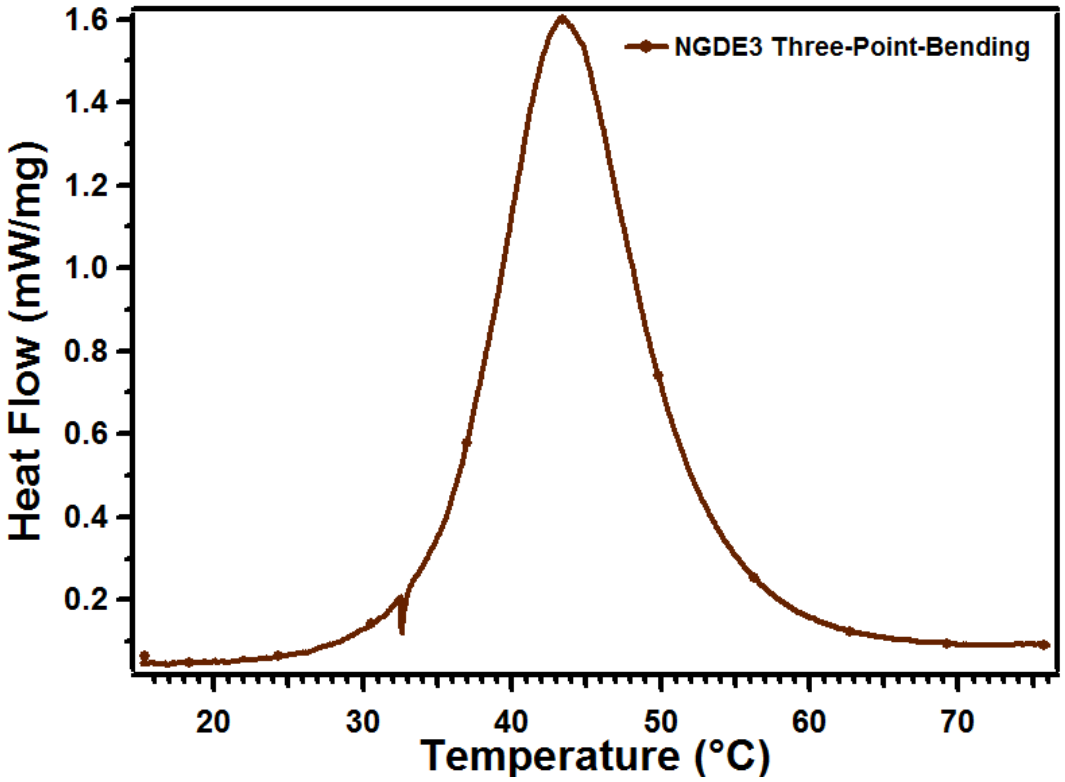

Figure 2-8: Results of the three-point bending test for the NGDE3 epoxy-based SMP

2.4.2 SHAPE MEMORY EFFECT

The driving force for shape recovery in a polymer is the elastic strain generated during the deformation. Deformation at high temperature is much easier due to the lower rubbery modulus of the polymer that makes the orientation of polymer more feasible. However, the orientation will be partly relaxed before the structure is frozen in during the subsequent cooling cycle. On the other hand, deformation at low temperature is more difficult due to the higher glassy state modulus of the polymer but chain orientation will remain at a higher degree as the relaxation

process is slowed down. A high glassy state modulus (E_g) will provide the material with high shape fixity during simultaneous cooling and unloading, whereas a high rubbery modulus (E_r) will provide high elastic recovery at high temperature [13].

Shape recovery is important to SMPs because it is the material's ability to completely return to its original shape after stretching. Shape recovery is most often studied by loading and unloading an SMP at various temperatures, then heating it up to above the glass transition temperature.

Figure 2-9 shows the complete cycle of the shape memory effect of an SMP.

The thermo-mechanical cycle in which SMP is recovered can be summarized as follows:

1. While kept at a zero stress, heat the material above its glass transition temperature (Point 1).
2. At high temperature, compress the SMP to the desired strain level (Point 2).
3. Cool the material down to a temperature below its glass transition temperature while keeping the strain constant (Point 3).
4. Unload the stress from the specimen (Point 4).
5. To recover the original shape, heat the material above its T_g (Point 1).

The SMP's recovery characteristics are best illustrated by producing a shape-memory plot of strain vs. temperature. This plot also shows the material's shape fixity or its ability to hold a shape after it has been deformed. Figure 2-9 gives a breakdown of the shape-memory plot and what each section represents. The material is first loaded to 2.75 MPa at a constant temperature above T_g which is 60 °C (process 1: Heating). The loading is then held constant for one minute to determine if there is any creep present (process 2: Loading). Then, the material is cooled down to 12 °C (below T_g) under the constant stress of 2.75 MPa (process 3: Cooling). After cooling, the load is released (process 4: Unloading). Finally, the material is reheated to the original temperature above T_g (which was 60 °C) and recovery profile is seen in the final section of the graph (process 5: Heating)

During the shape memory effect, 19% strain was recovered, and recovery process shows a glass transition temperature of 43 °C which is consistent with DSC results described in the previous section.

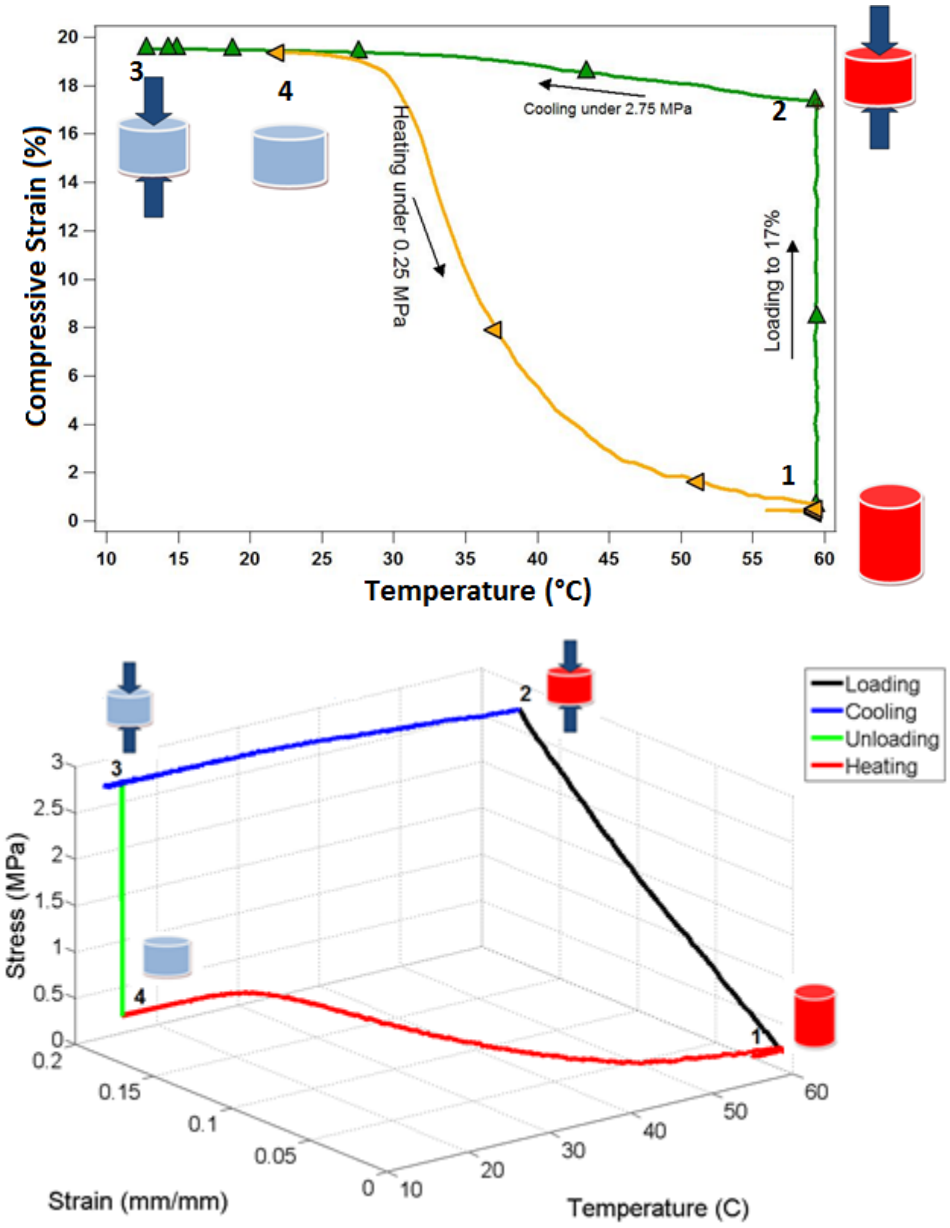

Figure 2-9: Shape memory effect of SMP with illustrated schematics

2.4.3 DEFORMATION LIMIT ON NGDE3 SMP

Figure 2-10 shows the stress versus strain graph for an NGDE3 SMP sample in compression at room temperature. It indicates that 65% strain compression is needed for an SMP sample to fail which is relatively high for rubbery materials. The graph shows that the stress level does not exceed 30 MPa until the material is roughly compressed to about 55%. Even though the area of the sample is increased, after this point the stress level is increasing at a much higher rate

suggesting that the material is going to fail. At a strain of 65%, the SMP fails at a compressive stress of 75 MPa. It has been reported that some SMPs could be stretched up to 800% in tension [1], but tensile test study was not performed in the current project. The modulus of elasticity calculated from the compressive stress-strain curve and is found to be 1.3 GPa and the yield strength (the maximum stress in stress-strain curve) is determined to be 22 MPa. Strain rate is very important in determining these factors.

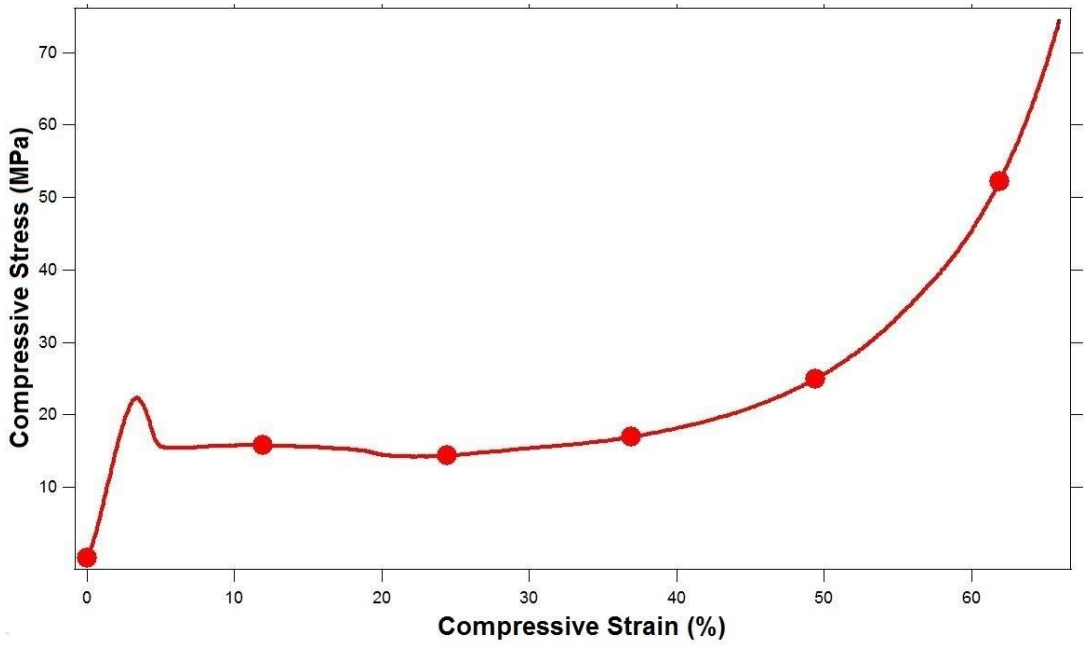

Figure 2-10: Failure test result of NGDE3 SMP

2.4.4 COMPRESSION RESPONSES AND RECOVERY

Epoxy-based SMP has a unique behavior on compression. It behaves like an elastic material up to some extent of deformation after which the stress level decreases and plastic deformation occurs. A compression test for NGDE3 SMP sample was performed with MTS at room temperature. It is important to note that the strain rate significantly affects the stress level that is obtained in this test. Compression tests have been done up to 40% of the original length at room temperature. After loading to the pre-determined strain levels of 10%, 20%, 30%, and 40% in compression (Figure 2-11), the sample was unloaded. Upon unloading the material has unrecovered strain at room temperature,

After loading and unloading at room temperature, the sample was heated in DMA, where the probe was touching the sample in stress control. By tracking the position of the probe, recovery graphs can be created. Figure 2-12 shows recovery tests that were done with DMA from room temperature to 80 ^{0}C with a heating rate of 5 ^{0}C/min. The other important information from the recovery tests is the observing glass temperature for NGDE3 as 43 ^{0}C which is in good agreement with DSC results. The recovery of the SMP is 100% after the temperature is reached above its glass transition temperature.

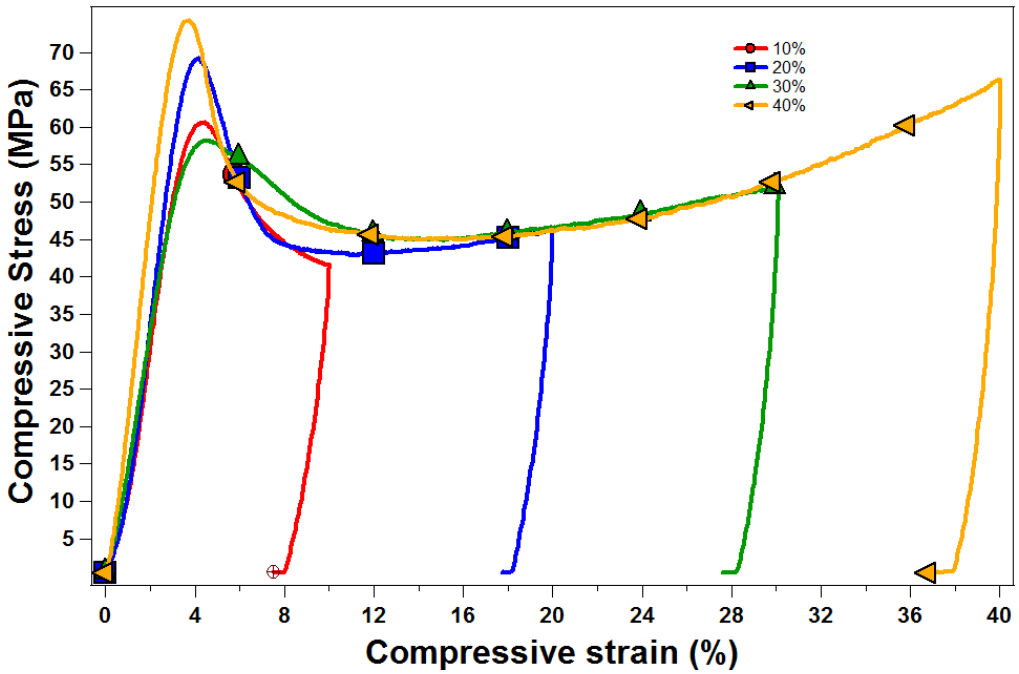

Figure 2-11: Compression test results for SMP at room temperature

The recovery characteristics of the SMP can be illustrated by producing a shape-memory plot of strain vs. temperature. From this plot, the linear shape recovery ratio, R, can be estimated

$$R = (1 - \frac{h_f}{h_i}) \cdot 100$$

Where h_i and h_f are the initial and final heights of the cylindrical specimens. After the final step, the SMP has returned completely to its original position. The linear

shape recovery ratio was calculated as ~100%, indicating that the SMP exhibits perfect shape recovery.

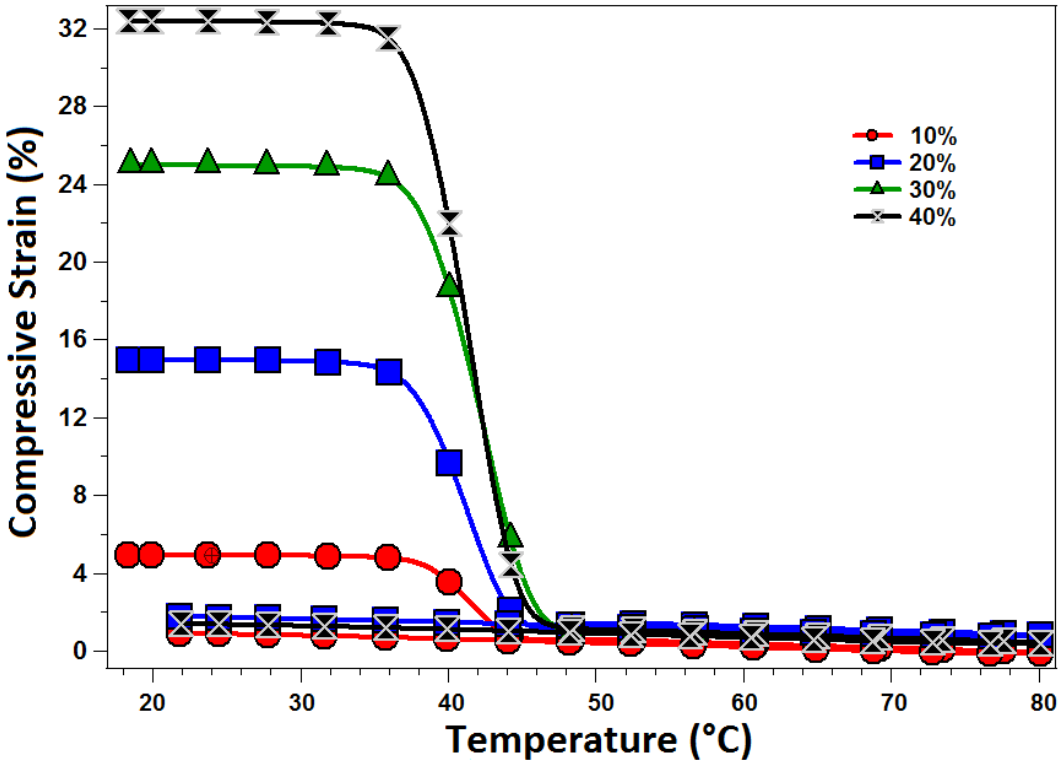

Figure 2-12: Recovery of compressed SMP samples by increasing the temperature

2.4.5 EFFECTS OF TEMPERATURE ON DEFORMATION BEHAVIOR

In this section the effects of temperature on SMP recovery and produced stress are discussed. As temperature increases, the material softens and requires less stress for the same amount of deformation inflicted. Basically, the SMP behaves like rubbery material at temperatures higher than the glass transition temperature and no plastic deformation is observed.

The compression/recovery tests are done at five selected temperatures from 15°C to 55 °C (Figure 2-13). The amount of compressive strain was fixed to 10%. It is clear that as the temperature increases, the mechanical behavior of SMP more closely resembles pure elastic material. Its behavior is completely linear at 55°C, above the glass transition temperature. The required applied stress for 10% deformation was decreased considerably as SMP softened.

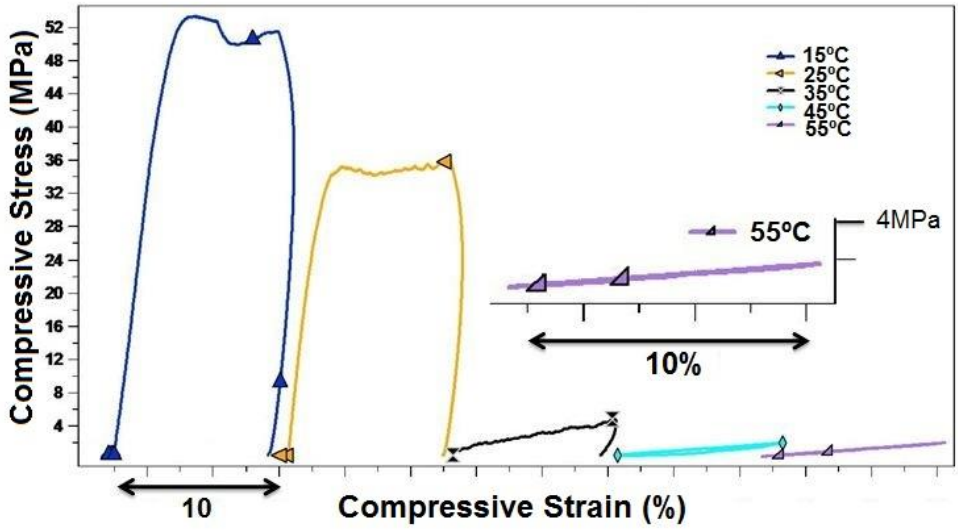

Figure 2-13: SMP compression test in different temperatures

Figure 2-14 shows the recovery tests of the same sample that is compressed at selected temperatures (see figure 2-13). Upon heating, complete recovery was observed for the deformed specimens. SMPs compressed above the transition temperature exhibited elastic behavior

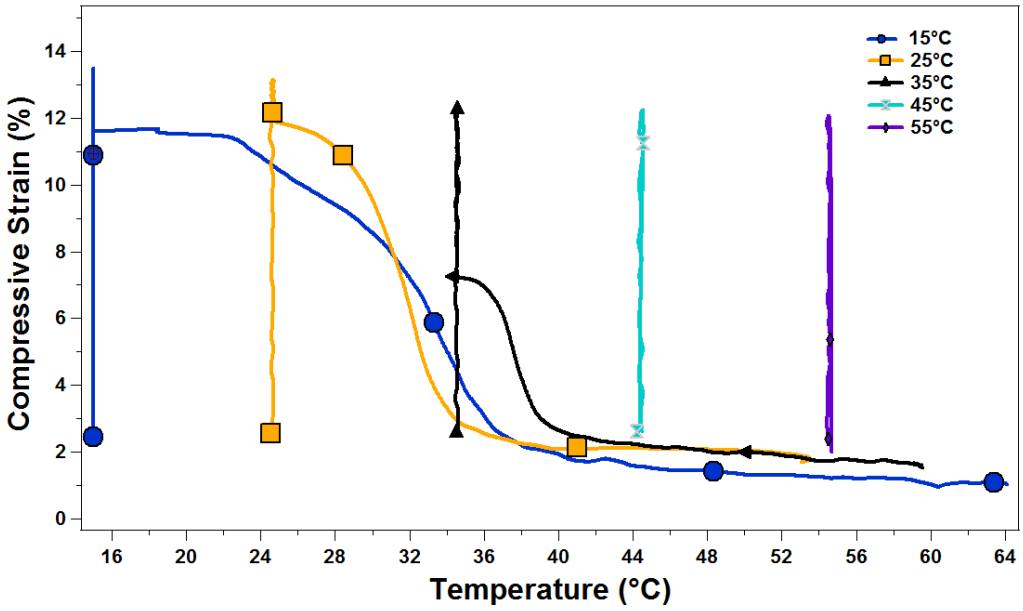

Figure 2-14: Recovery tests on compressed specimens at different temperature

2.4.6 CONSTRAINT SHAPE RECOVERIES

From the practical application point of view, the ability for a programmed SMP to recover its original shape under loads is critical. The process of heating a deformed SMP under constant stress is called the constraint shape recovery. In this study, the constraint shape recovery tests began by deforming the cylindrical SMP specimens in the glassy phase to a compressive strain of 10%. Then, the samples are unloaded to the loads of 2 MPa and 3 MPa and the loads are kept constant. The specimens were heated to 70°C at a rate of 5°C/min. The stress was held constant to allow the shape change. Finally, the materials were cooled down to the glassy phase under the same constant loads. Figure 2-14 shows the thermal cycling under constant stress results. Upon heating after deformation the material is trying to recover (in tensile direction) the pre-deformation amount of 10%. However, since load is applied and the elastic modulus of SMP decreases dramatically above Tg, The recovery stops and the sample is deformed in compression. Thus, during heating the pre-deformed sample initially elongated but then shortens under constant stress. It should be noted that there is an optimum stress level for fully reversible behavior. In this study it is founf to be 2 MPa. If lower stress of 1 MPa is applied, the recovery is more pronounced than the compression due to modulus change and vice versa if 3 MPa is applied.

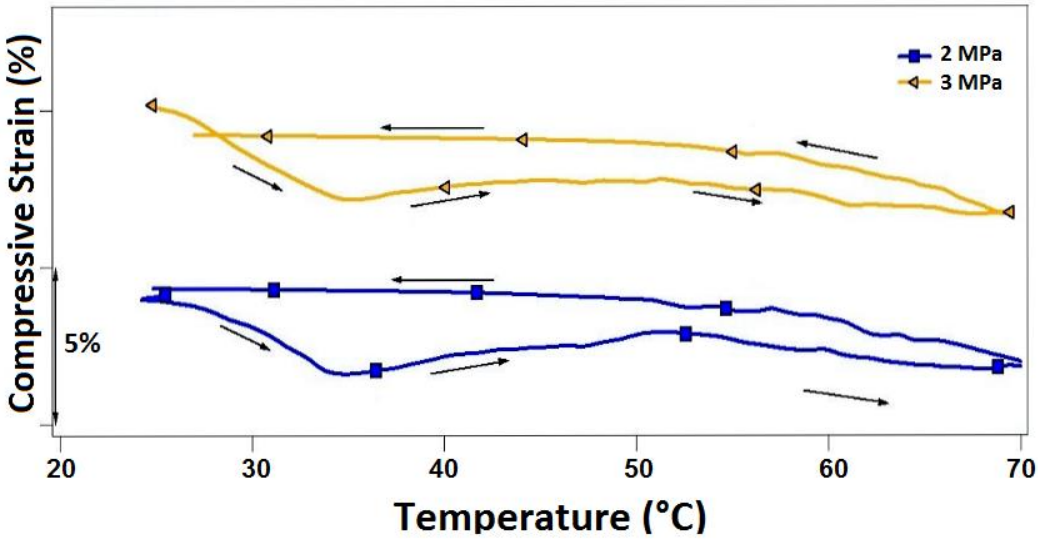

Figure 2-15: Strain-temperature profiles of constraint shape recoveries of the SMP

Figure 2-15 is indicating an important achievement in SMPs since normally, they do not show reversible shape memory behavior during thermal cycling. By applying the optimized stress two-way-shape-memory-effect (TWSME) can be observed in SMPs. In other words, SMPs could be used as an temperature activated actuator that is acting reversibly by temperature cycling.

Another version of the constraint shape recovery test is to hold the SMP at a constant strain during the heating which would allow measuring the stress generation of SMPs. The amount of stress generated during the recovery process is a very useful actuator property of the SMPfor designs. In this test, cylindrical SMP specimens were deformed to selected compressive strains ranging from 10% to ~50%. Then the samples were unloaded to 0.5 MPa and the ends of the SMP are fixed by displacement control. Specimens were then heated to elevated temperatures while maintaining the strain constant. As the temperature increased, the material tried to recover to initial length by expansion, however since the ends of the SMP are fixed, it exerted reaction loads. As expected, such loads reached to the maximum level around the glass transition temperature and then decreased as temperatures continued to increase (Fig. 2-16). The load decreased after the glass transition temperature due to low elastic modulus and elastic behavior of the SMP at higher temperatures.

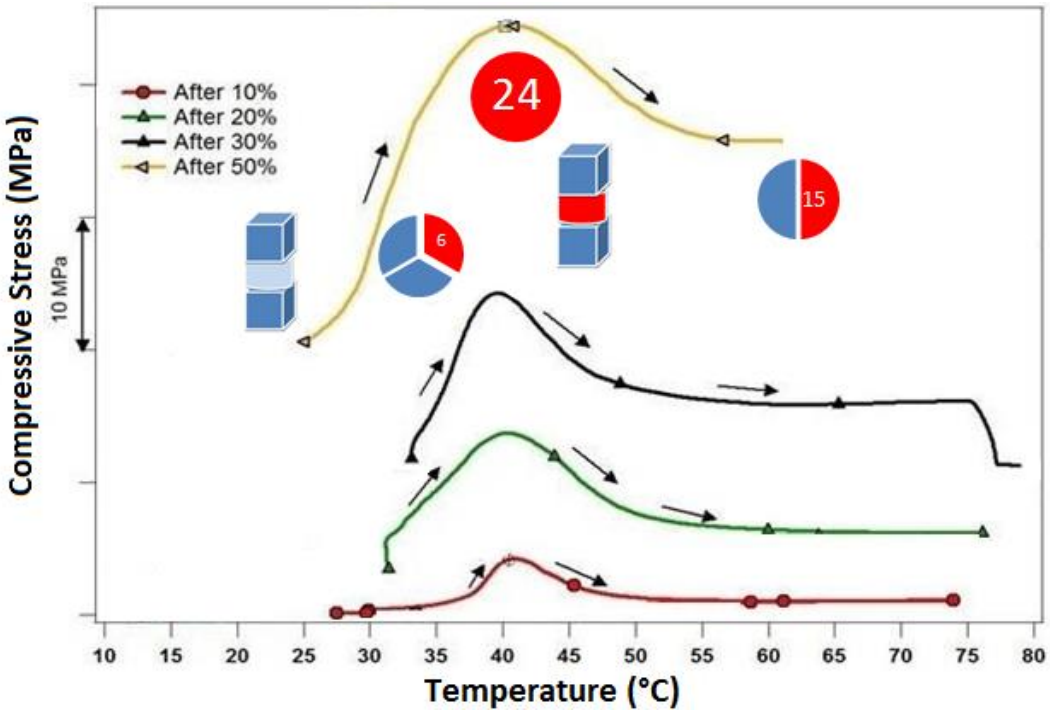

Figure 2-16: Stress-temperature profiles of constraint shape recoveries of the SMP

The amount of stress generated is almost linearly dependent upon the amount of compressive strain applied to the SMP prior to the test (Fig. 2-17). It is seen that the present SMPs can generate a maximum stress of 24 MPa after pre-strain of 50%. Such high magnitude of stress generation from an SMP is promising and even comparable to that generated from shape memory alloys [16, 25].

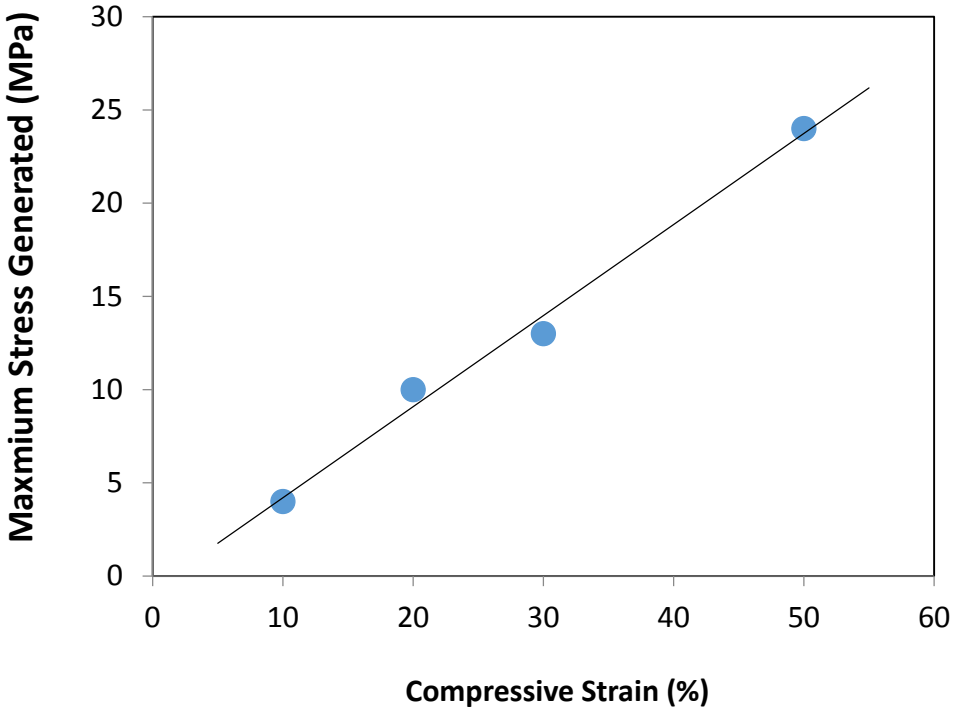

Figure 2-17: The maximum stress generated during constraint shape recovery as a function of fixing strain

2.4.7 EFFECTS OF THERMO-MECHANICAL HISTORY

Earlier mechanical tests have shown that the present SMP has very distinct behaviors at glassy and rubbery states. These temperature-dependent mechanical behaviors can be sketched as shown in Fig.15. In the glassy state ($T<T_g$), the material exhibits elastic and perfect plastic deformation (Fig. 2-18 (a)). While in the rubbery state ($T>T_g$) the material exhibits revisable hyper-elastic deformation (Fig. 2-18 (b)). So, for any applied stress at low temperature there exist two different strains (points 1 and 3 in Fig. 2-18 (c)). For any applied stress at elevated temperatures, there exists only one strain (point 2 in Fig. 2-18 (c)).

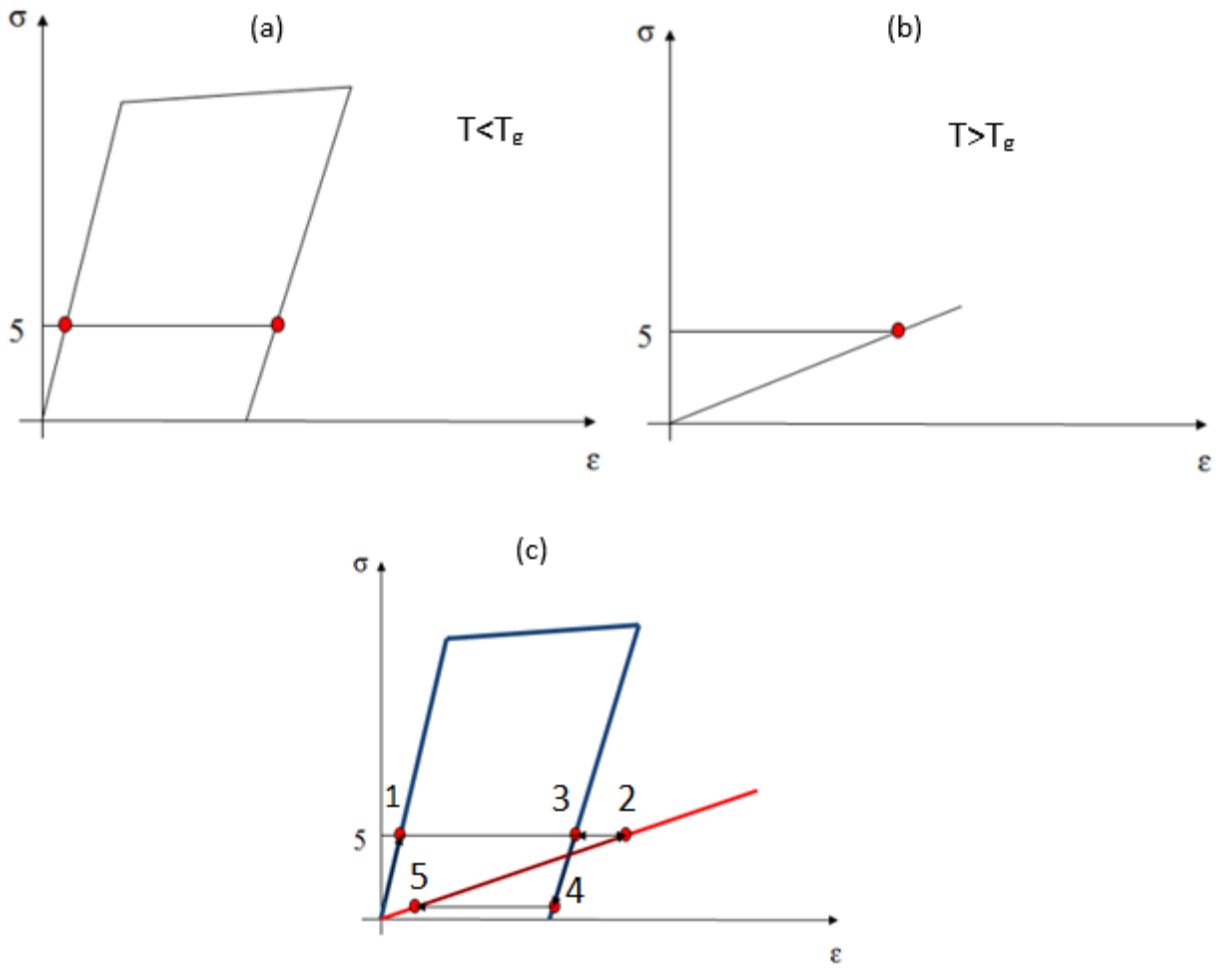

Figure 2-18: (a) Schematic of the mechanical behavior of the SMP at $T<T_g$, (b) Schematic of the mechanical behavior of the SMP at $T>T_g$, and (c) Combined view of (a) and (b)

According to this unique material behavior, different loading histories might be used to reach the same stress-strain condition for the same material. Fig. 2-19 depicts a three-dimensional stress-strain-temperature plot showing the shape recoveries of the present SMP under two selected thermo-mechanical cycles. The first cycle started from point 0, in which the SMP was at room temperature under zero load/displacement. The specimen was then loaded to 5 MPa at the same temperature (point 1). The material was heated to an elevated temperature (60°C) under the applied load, which resulted in a large strain (point 2). The constraint material was subsequently cooled down to room temperature (point 3). The second

cycle started from point 3, where the SMP was at room temperature under constrained load. To begin the cycle, the material was unloaded at low temperature and the strain was stored (point 4). Next, the material was heated to a rubbery state (60°C), after which the material recovered to its original shape (point 5). The material was loaded again to reach point 2 and cooled down again to reach point 3. The entire thermo-mechanical process involved two distinct cycles: 0123 – the constraint recovery and 34523 – the free recovery. The SMP is seen to have fully recovered its shape (from point 1 to point 5) in this very complex thermo-mechanical cycle.

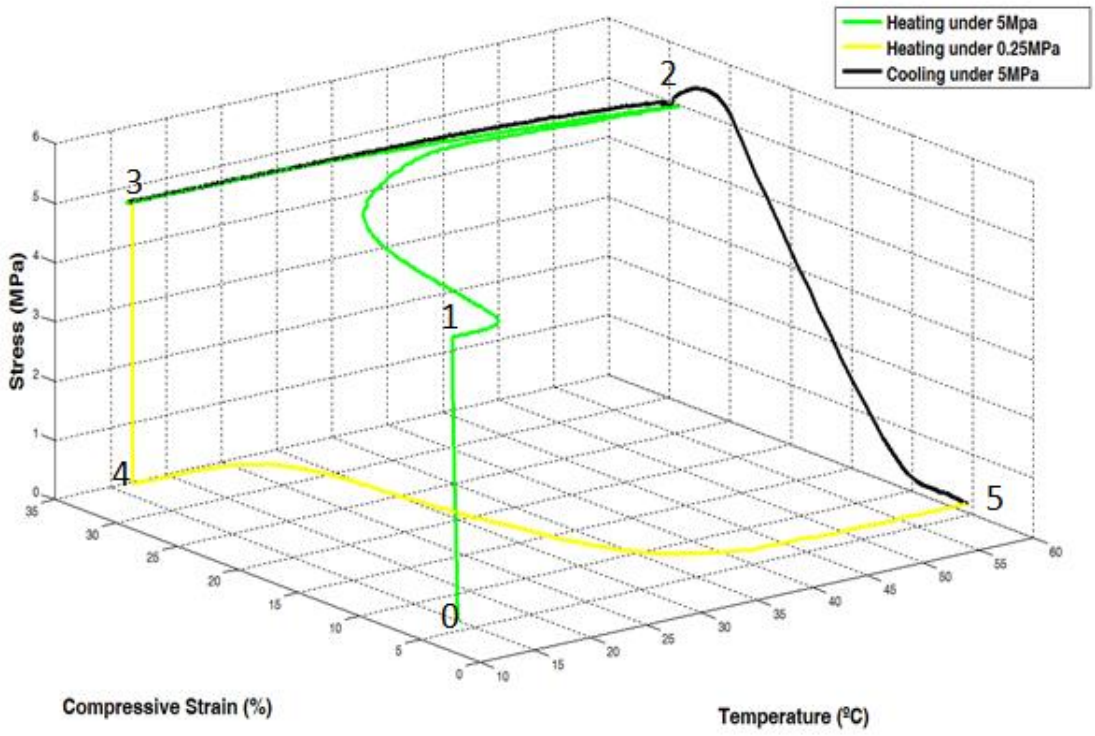

Figure 2-19: 3D stress-strain-temperature profile showing the shape recoveries of the SMP under complex thermo-mechanical cycles

2.5 SMP MODELLING

2.5.1 LITERATURE REVIEW

There have been various efforts to develop constitutive modeling for SMPs, but most efforts concentrate on small deformations, namely 10% nominal strain for compression or tension.

Tobushi had developed a spring-dashpot system to model the behavior of SMP for small deformations [42, 43]. In 2000, Tobushi and Bhattacharyya developed the model further [44] and in 2001, Tobushi *et al*. added more details on constitutive modeling. They incorporated nonlinear elastic terms, thermal expansion and viscosity in the model after which the viscoelasticity of SMP for small deformations was studied [45]. In 2007, Hong encountered the relaxation modulus in different temperatures for model input [46]. Srinivasa and Gosh developed a rheological model and used a spring-dashpot system and based on Gibbs potential approach, solved the state of the material with the result of differential equations [47]. The shape memory behavior and the process that SMP encountering during the shape memory effect, including the formation of different phases has been developed by Rao [48]. The model by Rao stated that the crystalline phase stores the deformation and the melting of the crystalline returns the material to its original shape. Liu *et al*. also proposed a model that predicted the small deformation [27, 49]. Liu's model proposed the frozen volume fraction and stored strain as two state variables and defines the strain as fractions of elastic, thermal and stored components. Then, the model describes the deformation in the frozen phase contributes to the stored strain. By heating up the stored deformation returns to its permanent shape. In 2008, Chen and Lagoudas proposed a model that can support three-dimensional SMP constitutive model for large deformations [50, 51]. This model continues the framework of Liu et al. [49] and uses the same concepts such as the stored strain and frozen volume fraction.

2.5.2 SMP CONSTITUTIVE MODEL FOR SMALL DEFORMATIONS

Lagoudas' model is on the basis of nonlinear thermo-elasticity and formulated according to Gibbs free energy [31, 52-54]. It is assumed that individual material particles transform from the frozen (glass) phase to the active (rubber) phase, and vice versa, until the entire material has transformed into a single phase. Based on this theory, SMP is assumed to be a mixture of these particles. Initially, the equations for a single phase are proposed. The model is formulated in terms of a general deformation gradient. SMP is composed of individual particles, as can be seen in Figure 2-20, that may be transformed to another phase at different temperatures. Deformation is continuous during the transformations and an integral technique is used over the entire volume to determine the average deformation gradient.

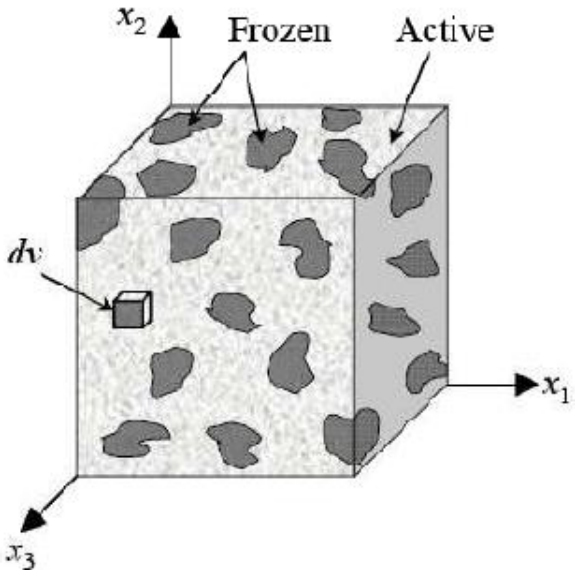

Figure 2-20: SMP composed of active and frozen phases in the model proposed by Lagoudas et al. [53]

The average deformation gradient for the entire SMP undergoing homogenous deformation was calculated via the volume integral of individual material particles in each phase (introducing frozen volume fraction and net cooling history). In general, the deformation gradient is defined by the following equation:

$$\overline{\mathbf{F}}(t) = \left[1 - \phi\left(\theta(t)\right)\right]\hat{\mathbf{F}}_a\left(S(t), \theta(t)\right) + \int_0^t \hat{\mathbf{F}}_f\left(S(t), \theta(t)\right)\hat{\mathbf{F}}_f^{-1}\left(S(\tau), \theta(\tau)\right)\hat{\mathbf{F}}_a\left(S(\tau), \theta(\tau)\right)\phi'\left(\theta(\tau)\right)\tilde{\theta}'(\tau)d\tau$$

where $\overline{\mathbf{F}}(t), \hat{\mathbf{F}}_a, \hat{\mathbf{F}}_f$ are the deformations from active to frozen, from active reference to deformed active and from frozen reference to frozen deformed, respectively. S(X,t) and θ(X,t) represent the two state variables of Piola-Kirchhoff stress and ϕ is the frozen volume fraction. The term, τ, represents the last time at which the material point **X** was frozen. The term $\tilde{\theta}'(\tau)$ represents the net cooling history. The second term in the equation above calculates the shape recovery of the material during heating dictated by change in volume fraction.

In the case of one-dimensional deformation, the assumptions that have been made are as follows:

- SMP is isotropic-linear elastic: $E = E^t(\theta) + M(\theta) : \sigma$
- The cross-sectional area changes negligibly as result of loading, so Piola-Kirchhoff stress will be equal to Cauchy stress: $S \approx \sigma$
- Infinitesimal strain tensor: $E \approx \frac{1}{2}(F + F^T) - I$
- Isotropic material behavior: $E^t(\theta) = \varepsilon^t I = \alpha \Delta\theta I$
- Uni-axial tension: $\sigma_{11} = \sigma(t)$
- Compliance tensor, assuming linear elastic behavior, independent of temperature: $M_{11}(\theta) = \frac{1}{E}$

For calibrating the linearized model, the following equation is used for calculating the axial strain:

$$\bar{\varepsilon}(\theta) = \left[1 - \phi\left(\theta(t)\right)\right]\left\{\alpha_a \Delta\theta(t) + \frac{\sigma(t)}{E_a}\right\} + \phi\left(\theta(t)\right)\left\{\alpha_f \Delta\theta(t) + \frac{\sigma(t)}{E_f}\right\} + \int_0^t \left\{\alpha_a \Delta\theta(\tau) - \alpha_f \Delta\theta(\tau) + \frac{\sigma(\tau)}{E_a} - \frac{\sigma(\tau)}{E_f}\right\}\phi'\left(\theta(\tau)\right)\tilde{\theta}'(\tau)d\tau$$

Calibration is necessary for the five functions that are listed below:

- Elastic modulus for active and frozen phases: E_a, E_f
- Thermal expansion coefficients for the active and frozen phases: α_a, α_f

- Frozen volume fraction: $\phi(t)$

The above functions will be calibrated by using the experimental data. The elastic modulus for the current epoxy-based SMP used for characterizing the active and frozen phases and also the thermal expansion coefficient are listed in Table 2-2.

Table 2-2: Calibrated functions for strain calculation

	Active Phase	**Frozen Phase**
Elastic Moduli	1.3 GPa	0.2 GPa
Thermal Expansion Coefficient	1.17e-5 K^{-1}	2.3e-6 K^{-1}
Frozen Volume Fraction	$\phi(\theta(t))$	$\phi(\theta(t))$

The frozen volume fraction should be normalized according to the strain-temperature graph of the SMP. Figure 2-21a shows the strain-temperature behavior of the SMP. By normalizing the graph to the range of 0 to 1, the frozen volume fraction function will be generated as shown in Figure 2-21b. At temperatures below the glass transition temperature, the function has the value of 1 for frozen volume fraction, indicating that the material is fully in the frozen phase. By increasing the temperature to above the glass transition temperature, the frozen volume fraction has the value of almost zero, consistent with the material being in the active phase. During the transition, the function returns a value between 0 and 1 depending on the temperature.

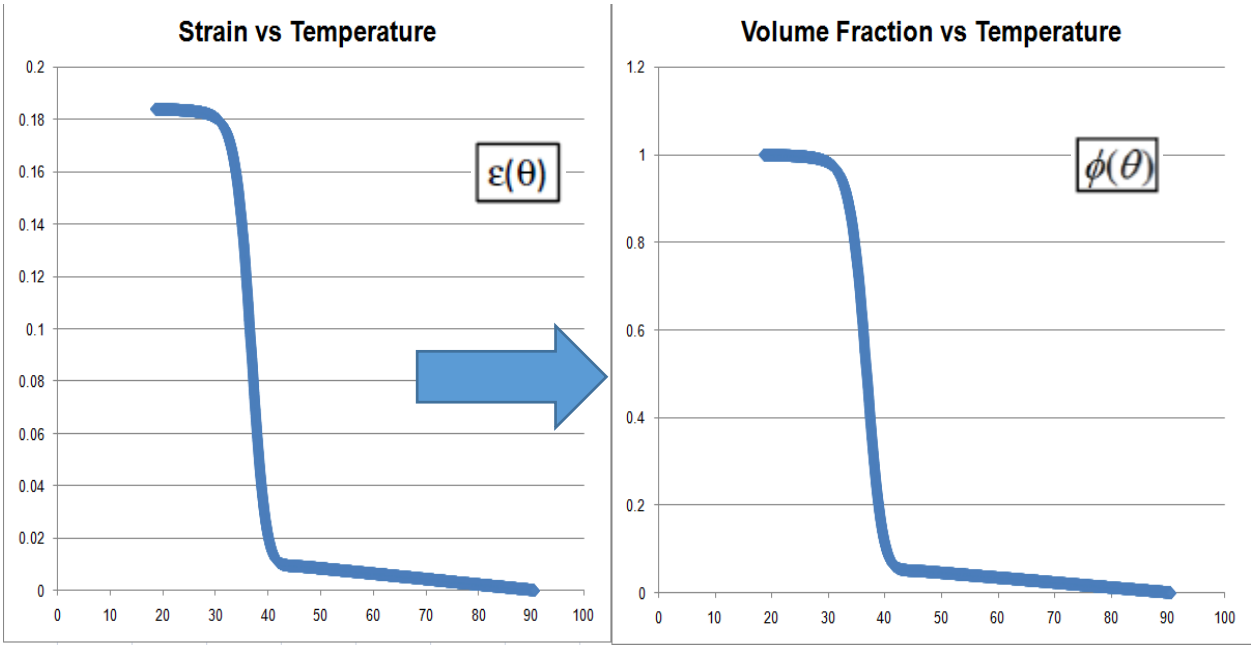

Figure 2-21: a) Strain-temperature and b) Calibrated frozen volume fraction-temperature graphs of SMP

After determining the calibrated volume fraction function, the shape memory effect modeling requires four steps, as described in the experimental results section. Each step has to be identified correctly and then implemented in MATLAB® program with ode45 function. The governing equation for each step is as follows:

- At a temperature greater than glass transition temperature, the sample will be loaded:

$$\varepsilon(t) = \left[1 - \phi\big(\theta(t)\big)\right]\frac{\sigma(t)}{E_a} + \phi(\theta(t))\frac{\sigma(t)}{E_f}$$

- While the load is held constant, the temperature decreases to below the glass transition temperature:

$$\frac{d\sigma'(\theta)}{d\theta} = -\frac{[1-\phi(\theta)]\alpha_a + \phi(\theta)\alpha_f}{[\frac{1-\phi(\theta)}{E_a} + \frac{\phi(\theta)}{E_f}]}$$

- In the third step, the material will be unloaded at the temperature below the glass transition temperature:

$$\varepsilon(t) = \varepsilon_{pre} + \left[\frac{1-\phi(\theta_2)}{E_a} + \frac{\phi(\theta_2)}{E_f}\right][\sigma(t) - \sigma(\theta_2)]$$

- In the last step, recovery occurs while the temperature increases to above the transition temperature and load remains zero:

$$\frac{d\varepsilon'(\theta)}{d\theta} = [1-\phi(\theta)]\alpha_a + \phi(\theta)\alpha_f + [\frac{1}{E_a} - \frac{1}{E_f}]\phi'(\theta)\sigma'(\theta)$$

The above equations were implemented in MATLAB® with appropriate material specifications determined from the experimental characterization results shown before (see Table 2-2). The predicted results are matching very well with experimental results as shown in Figure 2-22. It should be noted that In this graph, the cooling was done on strain control, while stress control was used by Volk *et al*. [53].

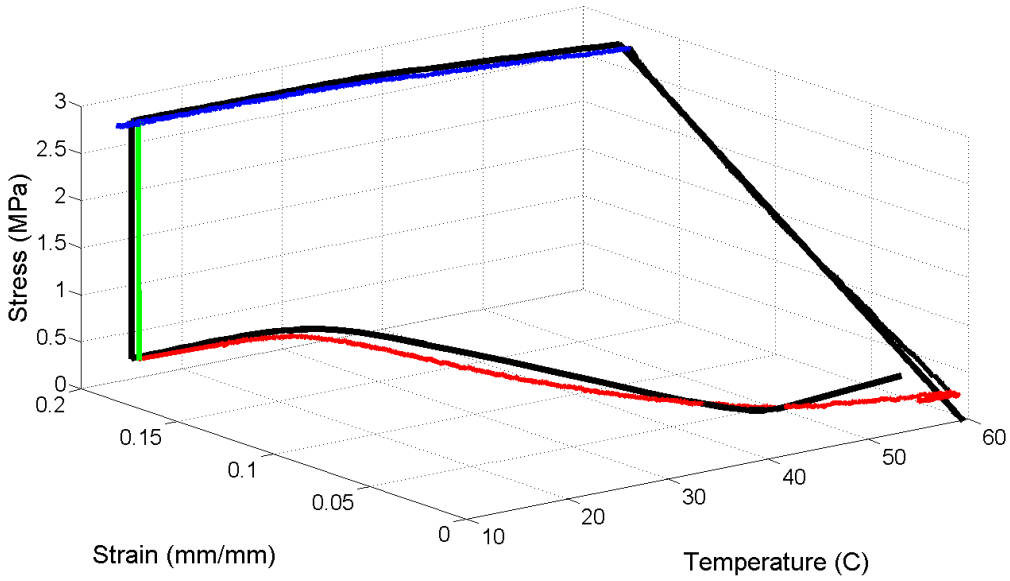

Figure 2-22: Comparison between the experimental shape memory effect (colored) and the theoretical results (black)

2.5.3 FINITE ELEMENT MODELLING OF SMP IN ABAQUS®

There have been several studies of finite element modeling of SMP in which commercial software was used. For example, Khanokar *et al*.[55] reported a subroutine for glassy shape memory polymers based on the constitutive model developed by Rao *et al*. [48]. However, a simpler model is used in this study since SMP is deformed only in compression and temperature-dependent elastic

modulus and the plastic behavior is known. Thus, it could be modeled in ABAQUS as an elastic material with plastic definitions. The material specifications at different temperatures, according to experimental results, are indicated in Table 2-3.

Table 2-3: Material specification of SMP in different temperatures

TEMPERATURE (K)	**ELASTIC MODULI (GPA)**	**POISON'S RATIO**	**THERMAL EXPANSION COEF.**
288	1.3	0.3	2.3e-6
298	0.9	0.3	2.3e-6
308	0.4	0.4	2.3e-6
318	0.3	0.4	1.17e-5
328	0.2	0.45	1.17e-5
373	0.1	0.45	1.17e-5

The plastic behavior of the material was defined according to the experimental results for 50% compression at room temperature with regards to ABAQUS requirements as shown in Table 2-4.

Table 2-4: Plastic definition for SMP at room temperature for 50% compression according to ABAQUS requirements

STRESS (MPA)	**STRAIN (%)**
70	0
45	5
50	18
70	50

The model that was created in ABAQUS is a cylindrical specimen with the diameter of ¼" and length of 3". The geometry created in ABAQUS matches with the sample dimensions and was meshed with average size hexagonal elements. In order to prevent the rigid body motion in FEM simulation, the bottom end of the cylindrical

sample has to be constrained for all degrees of freedom. In order to do so, a reference point was defined and the kinematic motion of the reference point was coupled with the bottom surface. With applying constraint on the reference point, the whole surface will be constrained as shown in Figure 2-23a. On the top end, another reference point was defined that was coupled for kinematic motions with the top surface. The load was applied to the top reference point as pictured in the Figure2-23b.

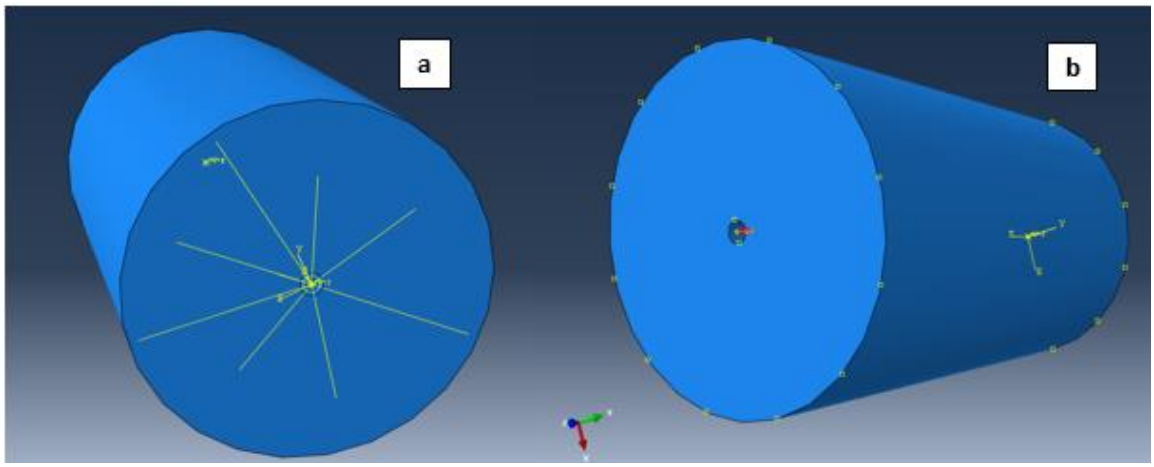

Figure 2-23: (a) Applying constraint on the bottom end of the SMP, (b) Applying load on the top end of SMP

For shape memory effect modeling in ABAQUS, material properties given in Tables 3 and 4 were used, along with the following steps:

Initial step: In this step, all the initial conditions were set. The temperature was set to 363 K, which is above the glass transition temperature, and load at zero. The boundary conditions were defined in this step.

Step 1: In this step, the temperature was kept at 363 K and a compressive load of 1500 N (approximately 75 MPa) was applied to the top surface. The applied load resulted in the deformation amount of around 20% (Figure 2-24a).

Step 2: While the load was kept constant, the temperature decreased with a constant rate to 263 °K, which is lower than the glass transition temperature. (Figure 2-24b).

Step 3: The load was removed and the temperature was kept constant. Thus, the elastic deformation was released and the sample remained deformed (Figure 2-24c).

Step 4: The temperature was increased with a constant rate up to 363 K, which is above the glass transition temperature at which the sample will recover back to its original shape (Figure 2-24d).

A summary of the shape memory effect that was done in ABAQUS on the created SMP sample is illustrated in Figure 2-24.

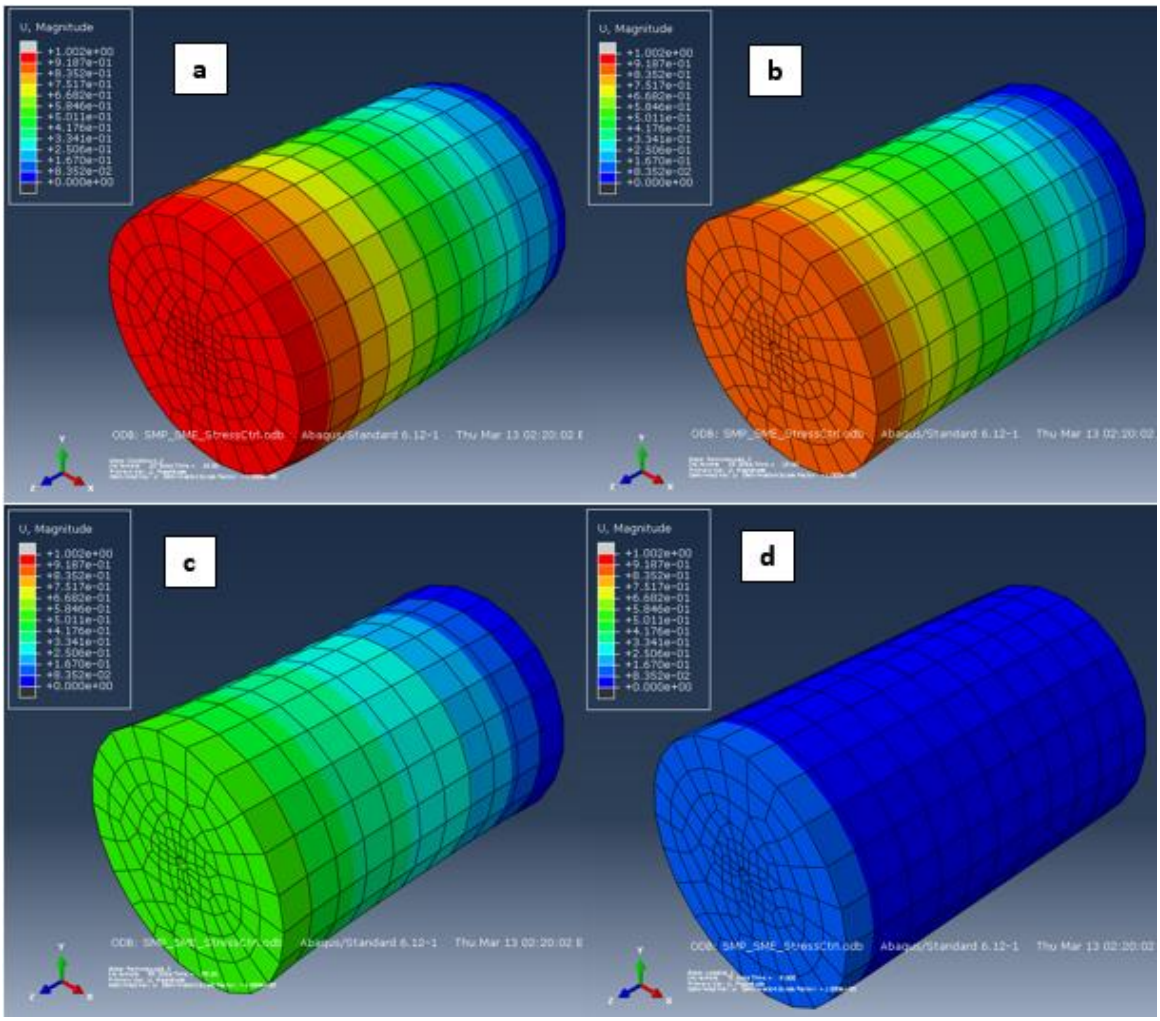

Figure 2-24: Illustration of shape memory effect on SMP FE model. a) Loading, b) Cooling, c) Unloading, d) Heating

The graph on Figure 2-25 shows the shape memory effect in a 3D plot for temperature-strain-stress variations that compares the FEM results with

experimental results. The SME graph from ABAQUS shows a difference in experimental SME. Although both cooled by the same method, ABAQUS shows a strain release. The reason is because a constant force was applied to the SMP for loading that was maintained during cooling as well. The elastic modulus is increasing in different temperatures and the reaction force from SMP is also increasing because of that. The increased reaction force causes the strain release. In the current model there is no control over this behavior.

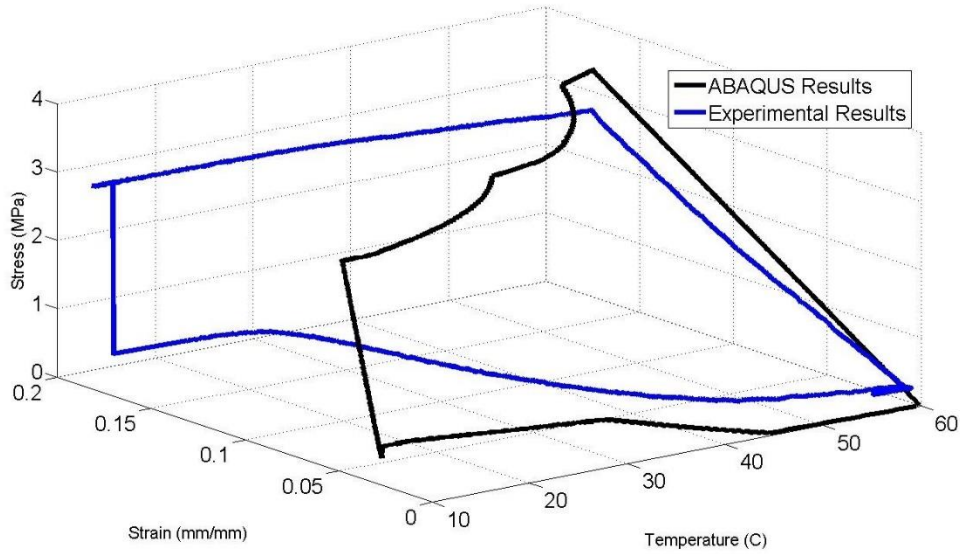

Figure 2-25: Comparison between experimental SME and ABAQUS results

CHAPTER III: NiTi WIRE CHARACTERIZATION AND MODELLING

3.1 EXPERIMENTAL CHARACTERIZATION OF NiTi WIRE

For the SMC fabrication, the shape memory properties of NiTi should be characterized. Flexinol NiTi wires were ordered from DYNALLOY© and used in as-received form. Flexinol wires were heat treated by the factory to show shape memory behavior. To determine the transition temperature, DSC testing was performed on the NiTi wires. Also, stress-strain and recovery tests were conducted on the wires to determine the elastic modulus and plastic strain. Moreover, the fracture stress of the wire was also determined. The stress generation tests were conducted by loading the wire at room temperature and heating it up above the transition temperature while keeping the strain constant.

3.1.1 DSC RESULTS ON NiTi WIRE

Figure 3-1 shows the results of DSC response of the NiTi wire that was used to fabricate the SMC actuator. The results show the martensite to austenite transformation of the wire. The peak observed at DSC during heating corresponds to martensite to austenite transformation. This transition does not happen suddenly. Martensite to austenite transformation starts at 68 °C and finishes at 78 °C. Thus, austenite start temperature is 68 °C and austenite finish temperature is 78 °C. For the cooling part, the peak shows austenite to martensite transformation. Martensite start temperature is 50 °C and martensite finish temperature is 40 °C.

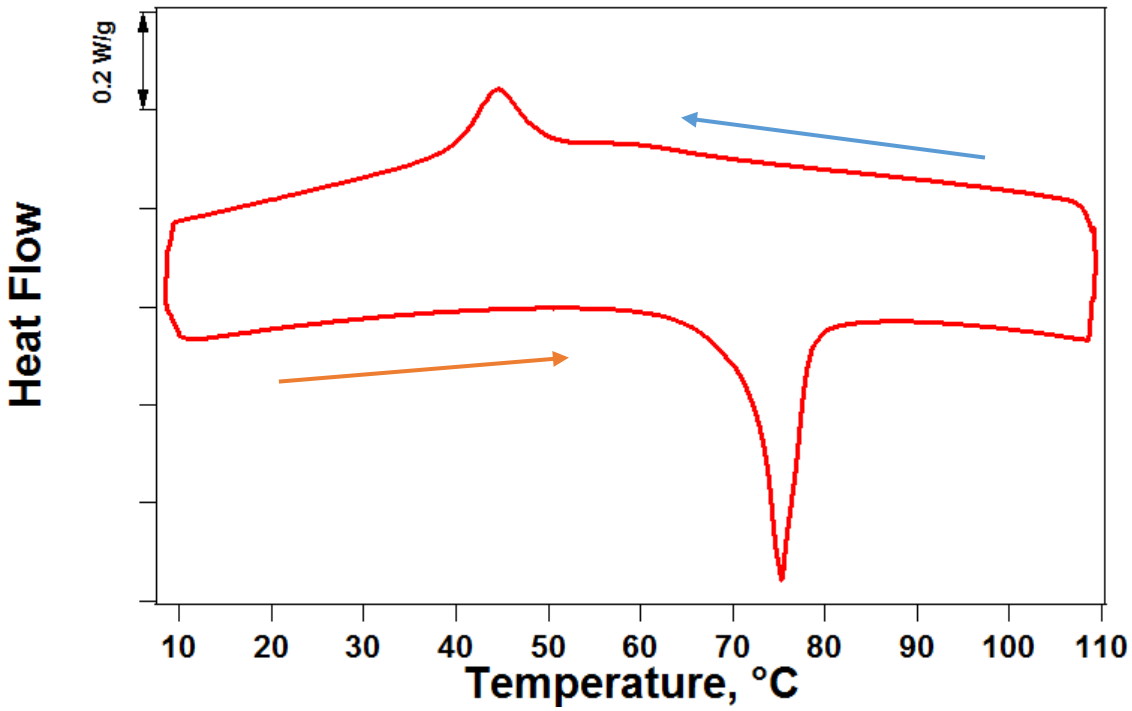

Figure 3-1: DSC result of NiTi wire

3.1.2 STRESS INCREASE OF CONSTRAINED NiTi WIRES WITH TEMPERATURE SCAN

To determine the stress generation of NiTi wires, MTS Landmark test setup with custom heating system was used. The wire was clamped to both grips and then loaded to tensile stress of 10 MPa at room temperature when it is martensite. Then, the wire was heated up to 200°C in displacement control mode which means that the distance between the end points of the wire kept were kept constant during the temperature scan. As the temperature increases, the NiTi wire has a tendency to transform to austenite. Since NiTi wire wants to contract as it transforms to austenite, additional stress was applied to keep the length of the wire constant. At the end, the wire generated a stress level up to 800 MPa, as shown in Figure 3-2. The graph is not smooth since the servo-hydraulic MTS controller has to constantly adjust the applied force to a thin wire to keep the length of the wire constant as temperature increases. The initial increase of the force up to 120 °C is related to the change of the elastic modulus and strength of martensite. At temperatures

above 120 °C, the force is applied to prevent the martensite to austenite transformation, resulting in a steeper slope. At temperatures above 180 °C, the stress generation becomes saturated due to plastic deformation or completion of martensite to austenite transformation.

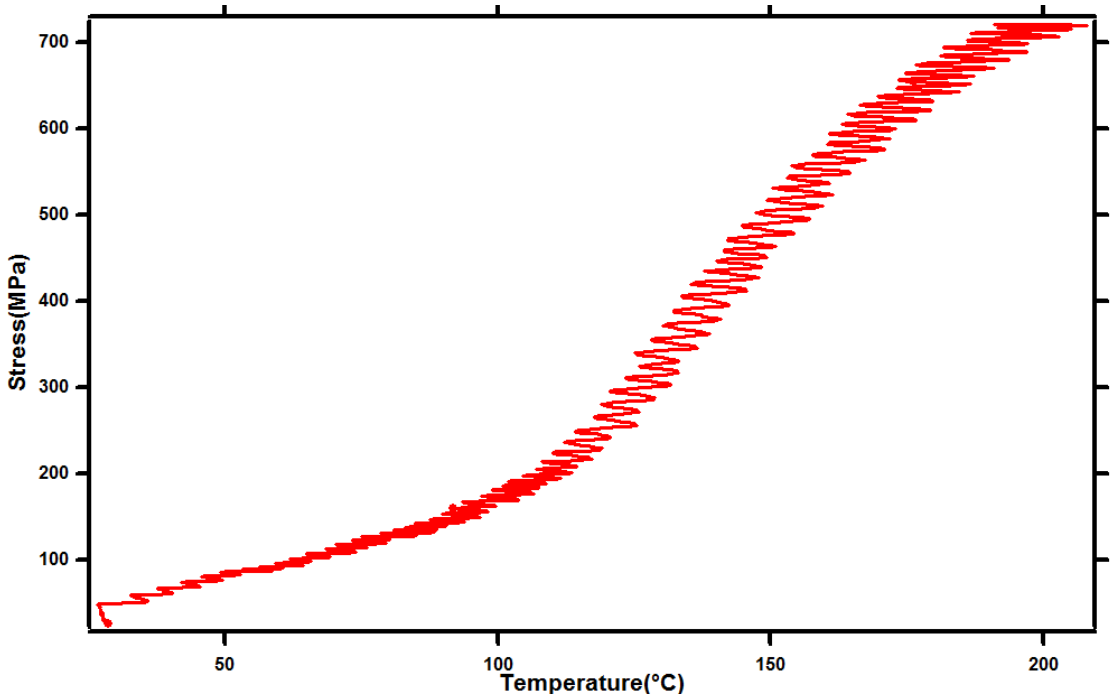

Figure 3-2: Stress generation test for a SMA wire

3.2 SMA MODELLING

In this part, the constitutive SMA model, developed by Lagoudas *et al*., [50, 51] will be reviewed. The subroutine is based on this constitutive model. In another effort, a dog-bone shape tensile sample was created in ANSYS with the built-in SMA predefined material in its library. The built-in SMA material in ANSYS was developed according to constitutive model that has provided by Auricchio *et al*. [56], for isothermal analysis Finally, the modeling of the SMA wire by ABAQUS will be described. Shape memory effect has been demonstrated by implementing a subroutine USERMAT that was developed by Lagoudas *et al*. [30]. The modeled NiTi wire was later used to simulate the behavior of shape memory composite in ABAQUS.

3.2.1 LITERATURE REVIEW

One-dimensional SMA modeling was first reported in 1986 [57]. Tanaka proposed to use an exponential hardening function for the phase transformation. However, the model was very simple in which the material properties remained constant during the transformation [57]. Achenbach proposed a model with two different phases including austenite, martensite in tension and compression by utilizing potential energy wells [58]. Later, Seelecke and Muller expanded the work by Achenbach [59]. Helmholtz free energy has been used in Liang and Rogers model [60] in which, similar to Tanaka's model, the material properties were kept constant, but cosine hardening function was used instead of exponential hardening function [60]. Brinson and Abeyaratne used Helmholtz free energy in their works as well. Brinson uses a cosine hardening function and the model allows twinned martensite [61]. Abeyaratne did not use martensitic volume fraction, instead strain was presented in each phase [62]. Govindjee and Kasper used a phase diagram based model in which not only martensitic phase in compression and tension were considered, but the coefficient of thermal expansion and the plasticity as well [63]. Auricchio and Sacco also developed a phase diagram based model for isothermal super-elasticity. A linear hardening function with critical temperatures input has been used for model development [64]. Bekker and Brinson also used a phase diagram based model with cosine hardening function [65]. Ivshin and Pence have used hyperbolic function to model the transformation hysteresis. The model considered both hysteretic and non-hysteretic conditions [66]. Rajagopal and Srinivasa, as well as Savi and Paiva, have used Helmholtz free energy to construct models as reported in two different works. In Savi and Paiva's work, two-way shape memory effects and internal sub-loops in tension and compression were also considered [67, 68].

Three-dimensional SMA models have been developed by several groups. In 1987, Patoor *et al*. used Gibbs free energy formulation to simulate transformation of a single crystalline SMA. The model was then extended to predict the polycrystalline behavior as well [69]. Liang and Rogers developed their one-dimensional model based on transformation surfaces and Helmholtz free energy [70]. Sun and Hwang

used Gibbs free energy to formulate a model in macro-scale by using the microstructure variables martensitic volume fraction and re-oriented martensitic volume fraction [71]. Boyd and Lagoudas used Gibbs free energy and a polynomial hardening function to model the phase transformation. Martensitic volume fraction was used as an internal variable [72]. Auricchio *et al*. extended the work previously done by Auricchio and Sacco [64] for a three-dimensional case. An exponential hardening function was used and FEM implementation of the model has been described [73]. Lagoudas *et al*. generated a unified framework from the works of Tanaka [74], Liang [70] and Boyd [72] by Gibbs free energy formulation [75]. Leclercq and Lexcellent also used Helmholtz free energy and exponential hardening function in their model. Two internal variables were used to allow both twinned and detwinned martensitic transformation [76]. Raniecki and Lexcellent have used Gibbs free energy and exponential hardening function to model tension and compression asymmetry [77]. Bo and Lagoudas have extend their work to include transformation induced plasticity as well [78]. Qidwai and Lagoudas have also used Gibbs free energy to extend the work of Boyd and Lagoudas [72] by adding several different transformation surfaces [79]. Govindjee *et al*. extended their phenomenological model by allowing arbitrary numbers of martensitic variants. They have also focused on the numerical implementation of their model [80]. Brocca, Brinson and Bazant have developed a microplane-based model that allows for nonproportional loading paths [81]. Juhasz *et al*. considered the effects of reorientation by taking the whole transformation strain as an internal variable instead of just the detwined martensite volume fraction [82]. Lagoudas and Entchev have extended upon the work of Bo and Lagoudas that was reported in 2003 [30]. Helm and Haupt used Helmholtz free energy and considered both temperature and stress induced cases. They used kinematic hardening for both the forward and reverse cases [83]. Anand and Gurtin have also developed a model based on Helmhotz free energy and derived a finite deformation framework. Tension and compression in single crystal has been considered [84]. Popov and Lagoudas considered three different phases of twinned and detwinned martensite and austenite and developed a three-dimensional implementation based on Gibbs

free energy [85]. Reese and Christ [86] used Helmholtz free energy to focus on large deformation of SMAs. Only isothermal pseudo-elasticity has been considered. They used kinematic hardening function based on Helm and Haupt model [83].

3.2.2 LAGOUDAS APPROACH FOR SMA CONSTITUTIVE MODEL

Qidwai and Lagoudas have developed constitutive models for shape memory and super-elastic materials based on the first principles of thermodynamics [79]. In their approach, the second law of thermodynamics is written in terms of the Gibbs free energy. Strain, temperature and martensitic volume fraction were state variables that must satisfy the second law of thermodynamics. An evolution equation for the martensitic volume fraction is derived from a dissipation potential and the effective transformation surfaces are evaluated as functions of the state variables. This approach also allows for temperature dependent elastic properties for austenite and martensite and accommodates both mechanical and thermal loading.

Modeling of the shape memory alloys using thermodynamic equations is important since this model can be used to predict the behavior of complex SMA parts in selected thermomechanical loading conditions.

The current work is based on Lagoudas' constitutive model since they have implemented their model in ABAQUS. The important equations of their constitutive model are discussed below.

The explicit form of the Gibbs free energy is given by [87]:

$$G(\sigma, T, \xi, \varepsilon^t) = -\frac{1}{2\rho}\sigma : S : \sigma - \frac{1}{\rho}\sigma : [\alpha(T - T_0) + \varepsilon^t] + c\left[(T - T_0) - Tln\left(\frac{T}{T_0}\right)\right] - s_0 T + u_0 + \frac{1}{\rho}f(\xi)$$

where G is the specific Gibbs free energy, σ represents Cauchy stress tensor, T is temperature tensor, ξ is martensitic volume fraction, ε^t is uniaxial transformation

strain, ρ represents mass density, α is thermal expansion coefficient, T_0 is reference temperature, c is specific heat capacity, s_0 and u_0 represent specific entropy and specific internal energy at reference point, respectively, and f is the hardening function.

After algebraic calculations and adding the explicit equations for stress and compliances, the following equation for thermodynamic force conjugated to ξ can be extracted:

$$\pi(\sigma, T, \xi) = \sigma : \Lambda + \frac{1}{2}\sigma : \Delta S : \sigma + \sigma : \Delta\alpha(T - T_0) - \rho\Delta c\left[(T - T_0) - Tln\left(\frac{T}{T_0}\right)\right] + \rho\Delta s_0 T - \rho\Delta u_0 - \frac{\partial f}{\partial \xi}$$

where π is thermodynamic force conjugated to ξ, Λ is transformation tensor, and S represents the compliance tensor.

By having the Clausius-Plank inequality as below:

$$\left(\sigma : \Lambda - \rho\frac{\partial G}{\partial \xi}\right)\dot{\xi} = \pi\dot{\xi} \geq 0$$

The conditions in which the forward and reverse martensitic phase transformations could happen can be defined.

• In forward martensitic transformation, $\dot{\xi}$ is positive because austenite is transforming to martensite. Now the Clausius-Planck inequality can only be satisfied if π is a positive value. For the forward martensitic transformation, $\dot{\xi} > 0$, the function π will take the condition of π = Y.

• In the reverse martensitic transformation, $\dot{\xi}$ will be negative because martensite is transforming back into austenite. Now the Clausius-Planck inequality can only be satisfied if π is a negative value. For the forward martensitic transformation, $\dot{\xi} < 0$, the function π will take the condition of π = -Y.

• While stress and temperature of the SMA is in the situation that there is no phase transformation occurring, the value of ξ remains constant and $\dot{\xi} = 0$.

Therefore, the Clausius-Planck inequality is always satisfied, regardless of the value of π, because $\pi\dot{\xi} = 0$.

The above constraints, called Kuhn-Tucker conditions, are presented below for both the forward and reverse phase transformations:

$$\dot{\xi} \geq 0; \quad \Phi(\sigma, T, \xi) = \dot{\pi} - Y \leq 0; \quad \Phi\dot{\xi} = 0;$$
$$\dot{\xi} \leq 0; \quad \Phi(\sigma, T, \xi) = -\pi - Y \leq 0; \quad \Phi\dot{\xi} = 0;$$

where Φ represents the transformation function and Y is the critical value for thermodynamic force to cause transformation.

The final step in the constitutive formulation is to define an appropriate hardening function, f (ξ). The hardening function defines the interactions between the austenitic and martensitic phases, and also among the martensitic variants themselves. Here, the hardening function that Lagoudas proposed is as follows:

$$f(\xi) = \begin{cases} \frac{1}{2}\rho b^M \xi^2 + (\mu_1 + \mu_2)\xi; & \dot{\xi} > 0 \\ \frac{1}{2}\rho b^A \xi^2 + (\mu_1 - \mu_2)\xi; & \dot{\xi} < 0 \end{cases}$$

where ρb^M, ρb^A, μ_1, and μ_2 are model parameters that could be determined from thermo-mechanical experiments and *M* and *A* represent the martensite phase and austenite phase, respectively.

Overall, after submitting the required criteria for the forward and reverse stages, five separate equations have to be considered as follows:

1. Beginning of forward phase transformation at zero stress:

$$\pi(\sigma, T, \xi) = Y \quad at \quad \sigma = 0, \qquad T = M_s, \qquad \xi = 0$$

2. Ending of forward phase transformation at zero stress:

$$\pi(\sigma, T, \xi) = Y \quad at \quad \sigma = 0, \qquad T = M_f, \qquad \xi = 1$$

3. Beginning of reverse phase transformation at zero stress:

$$\pi(\sigma, T, \xi) = -Y \quad at \quad \sigma = 0, \qquad T = A_s, \qquad \xi = 1$$

4. Ending of reverse phase transformation at zero stress:

$$\pi(\sigma, T, \xi) = -Y \quad at \quad \sigma = 0, \qquad T = A_f, \qquad \xi = 0$$

5. Continuity of Gibbs free energy:

$$f(\xi = 1)|_{\dot{\xi}>0} = f(\xi = 1)|_{\dot{\xi}<0}$$

Model parameters for the quadratic polynomial hardening function model are defined as below:

$$Y = \frac{1}{4}\rho\Delta s_0\left(M_s + M_f - A_f - A_s\right)$$

$$b^A = -\Delta s_0\left(A_f - A_s\right)$$

$$b^M = -\Delta s_0\left(M_s - M_f\right)$$

$$\mu_1 = \frac{1}{2}\rho\Delta s_0\left(M_s + A_f\right) - \rho\Delta u_0\right)$$

$$\mu_2 = \frac{1}{4}\rho\Delta s_0\left(A_s - A_f - M_f + M_s\right)$$

3.2.3 ANSYS MODEL OF A DOG-BONE TENSILE SMA SAMPLE

These are strong thermo-mechanically coupled problems due to the latent heat that is released and absorbed during austenite-martensite phase transformations. To facilitate the development of these new devices and obtain a better understanding of their working mechanism, an efficient computational tool such as finite element method (FEM) has to be used.

This work was performed to show the capabilities of the built-in SMA material in ANSYS. It is relatively easy to model the SMA behavior by ANSYS; however, the drawback of this software would be its limitation to isothermal condition. A dog-bone tensile sample was created to show the capability of the SMA material in ANSYS.

ANSYS is a general purpose finite element modeling package for numerically solving of a wide variety of mechanical problems and is used widely in industry to simulate the response of a physical system to structural loading, and thermal and CFD effects. ANSYS uses the finite-element method to solve the underlying governing equations and the associated problem-specific boundary conditions. In this report, ANSYS was used to analyze the nonlinear behavior of framed structures.

ANSYS 12.0 and later versions have SMA material in their built-in material library. This SMA material was developed by utilizing Auricchio's constitutive model [64] which is limited to isothermal loading. Thus, the tensile specimen was loaded at selected constant temperatures and the results were compared to each other.

The shape memory alloy material model implemented (accessed with TB, SMA which is the command for SMA material definition in ANSYS) is intended to model the super-elastic behavior of NiTi alloys in which the material undergoes large deformations without showing permanent deformation under isothermal conditions. Figure 3-3 shows the super-elastic behavior of SMA. The indicated points show the critical stress values for the start and finish of austenite to martensite and martensite to austenite transformation. The maximum residual strain is also indicated as $\bar{\varepsilon}_L$ in figure 3-3.

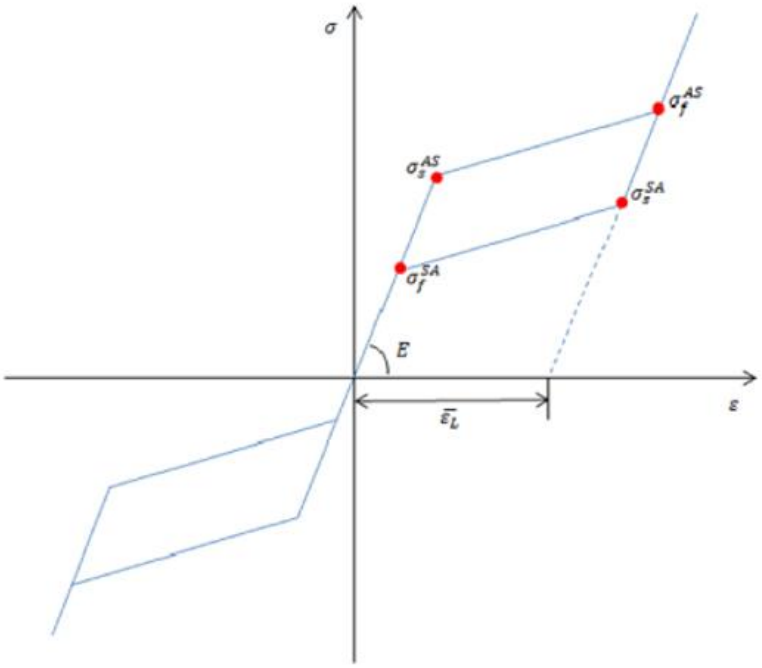

Figure 3-3: Super-elastic behavior of SMA with definitions of the important variables (from ANSYS online help and [1])

Table 3-1 shows the constants that have to be defined for SMA material in ANSYS.

Table 0-1: ANSYS SMA material constant definitions

Constant		Meaning
SIG-SAS (C1)		Starting stress value for the forward phase transformation
SIG-FAS (C2)		Final stress value for the forward phase transformation
SIG-SSA (C3)		Starting stress value for the reverse phase transformation
SIG-FSA (C4)		Final stress value for the reverse phase transformation
EPSILON (C5)		Maximum residual strain
ALPHA (C6)	α	Parameter measuring the difference between material responses in tension and compression

For the specimen, the material model was extracted from the following curves at selected temperatures as shown in Figure 3-4. Then, the specifications were defined in ANSYS according to the needed constants and are shown in Table 3-1.

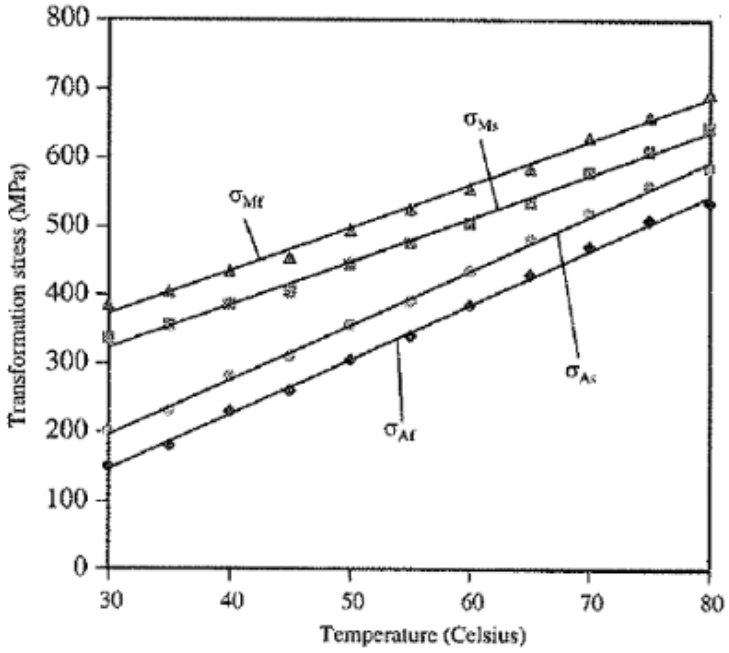

Figure 3-4: Transformation stress versus temperature curves for SMA material

The values for start and finish stresses for forward and backward transformations as a function of temperature can also be defined according to the results shown in Figure 3-5.

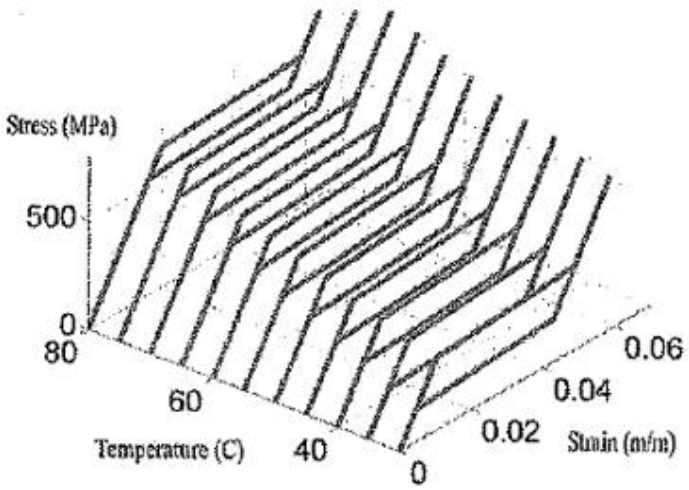

Figure 3-5: Superelastic responses at selected temperatures

The SMA specimen geometry was created in ANSYS with the following dimensions as showed in Figure 3-6. It was then meshed with a size of 4 in smart mesh.

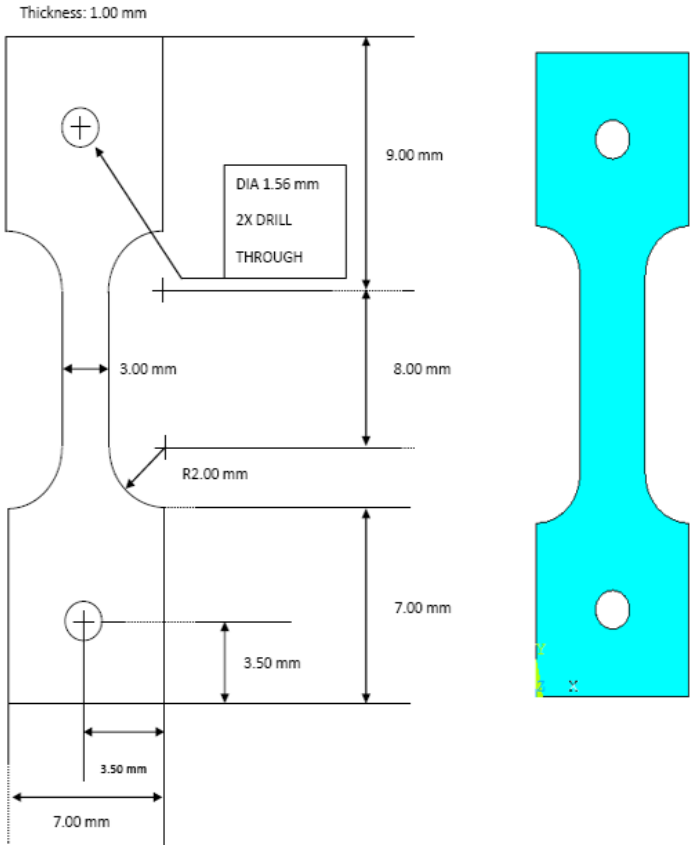

Figure 3-6: Dog-bone tensile specimen dimensions

Load and boundary conditions were applied to the specimen after being meshed. The load was applied on the top curve of the upper hole and the constraint was applied to the lower curve of the bottom hole. Figure 3-7 shows the pressure load on the upper curve of the upper hole and the constraint for all degrees of freedom was applied to the lower curve of the bottom hole.

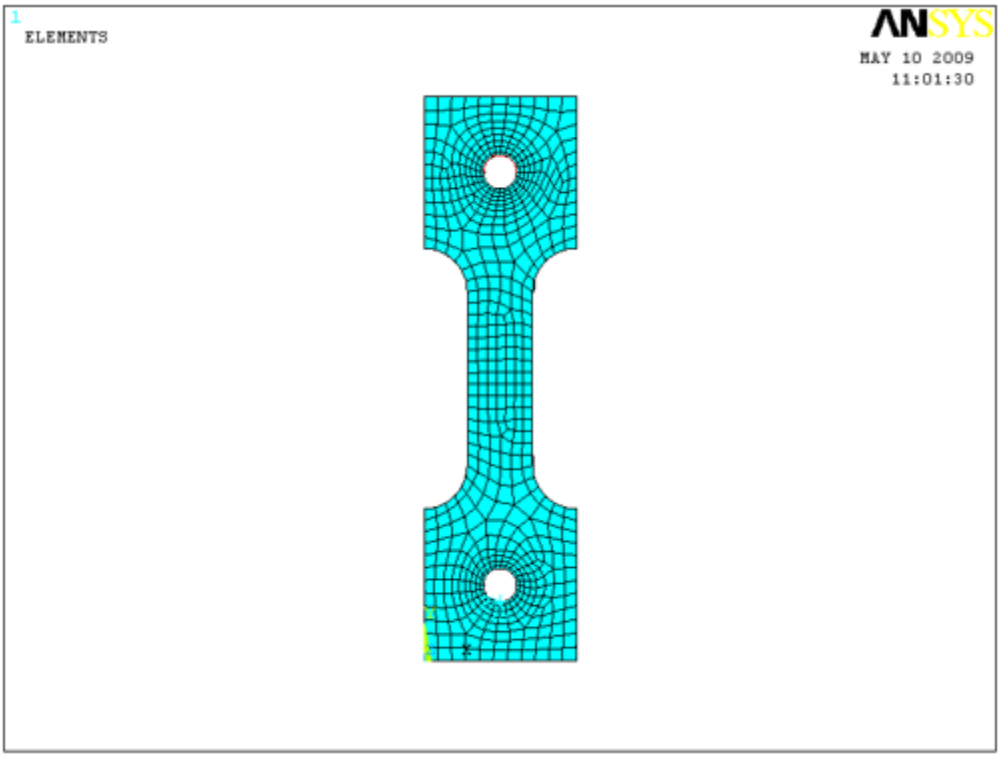

Figure 3-7: Load and boundary condition that applied to the dog-bone tensile specimen

Table 3-2 provides the maximum von-misses stresses that were generated because of the applied pressure at selected temperatures. It is clear that as temperature increases, the maximum stress increases.

Table 0-2: Comparison of the results for the maximum von-misses stress in different temperatures

Temperature (Celsius)	Von-Misses Stress (Pa)
30	396.05
40	486.65
50	573.98
60	675.80
70	723.11
80	780.37

Also, Figure 3-8 shows a contour plot of the SMA sample that was deformed at 70 °C. As expected, the maximum stress was generated by the holes where the load and constraint were applied.

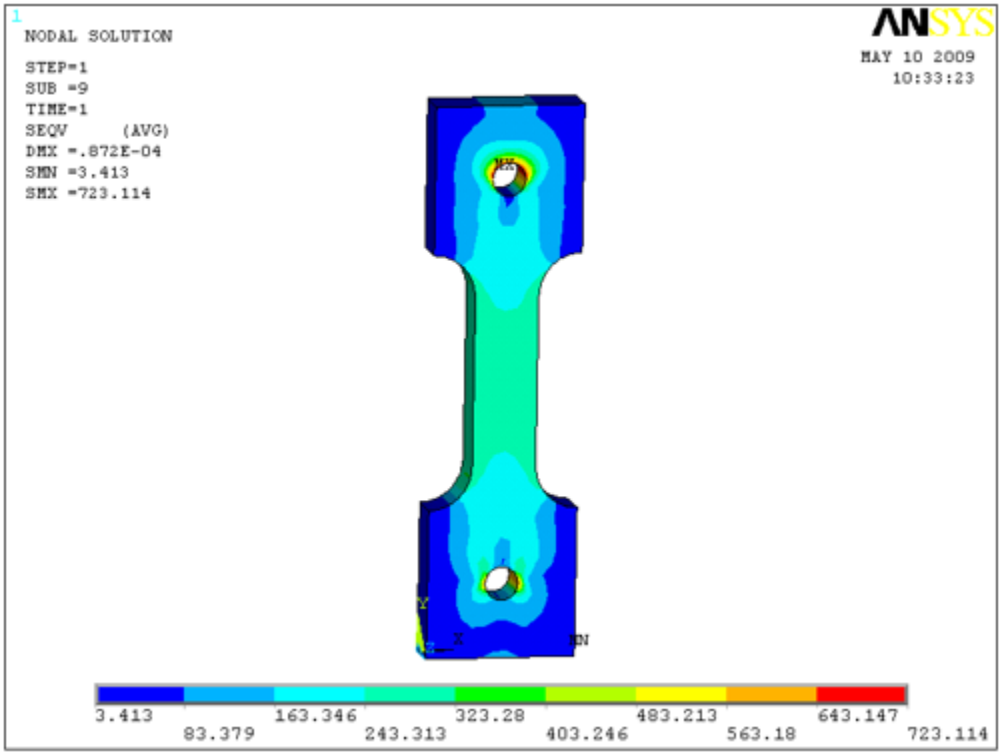

Figure 3-8: The contour plot of generated stress at 70 °c

3.2.4 SMA MODEL IN ABAQUS

As described in previous sections, the subroutine developed by Lagoudas' group for SMA modeling in ABAQUS was used [30]. The subroutine is a FORTRAN coded numerical implementation for SMA that is called SMA_UM (Shape Memory Alloy-Unified Model). The material has to be defined in a certain way and the required parameters have to be provided by the user.

The required material specifications are: the Young's modulus of both austenite and martensite phases (E^A and E^M), thermal expansion coefficients for both phases (α^A and α^M), martensite start and finish and austenite start and finish temperatures at zero stress (M^{0s}, M^{0f}, A^{0s} and A^{0f}), maximum transformation strain

(H), and austenite and martensite stress influence coefficients ($\rho\Delta s^A$ and $\rho\Delta s^M$). In addition, the subroutine is capable of using different hardening functions in which according to the selection, the hardening constants must also be defined [30]. Figure 3-9 shows the pseudoelasticity of SMA and the parameters that can be obtained.

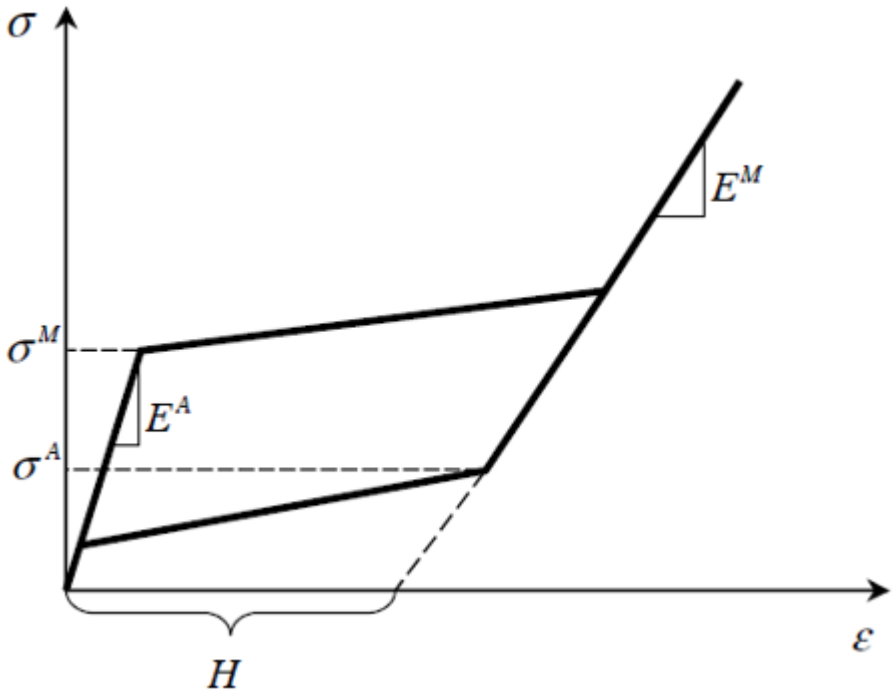

Figure 3-9: Pseudo-elastic behavior of SMA with definition of SMA parameters [30]

The stress influence coefficients for both phases could then be defined as:

$$\rho\Delta s^A = -\frac{\sigma^A}{T_{Test} - A^{0s}} H$$

$$\rho\Delta s^M = -\frac{\sigma^M}{T_{Test} - M^{0s}} H$$

The material parameters values that were used for the SMA wire are listed in Table 3-3:

Table 0-3: SMA material parameter's values

Material Parameter	Value
Austenite elastic modulus E^A	70 GPa
Martensite elastic modulus E^M	30 GPa
Poisson's ratio v	0.33
Austenite coefficient of thermal expansion α^A	22.0×10^{-6}/K
Martensite coefficient of thermal expansion α^M	22.0×10^{-6}/K
Martensite start temperature M^{0s}	291 K
Martensite finish temperature M^{0f}	271 K
Austenite start temperature A^{0s}	345 K
Austenite finish temperature A^{0f}	365 K
Maximum transformation strain H	0.08
Austenite stress influence coefficient $\rho\Delta s^A$	-0.35 MPa/K
Martensite stress influence coefficient $\rho\Delta s^M$	-0.35 MPa/K

For material verification, a simple model of a SMA bar was created in ABAQUS and loaded up to 5000 N (Approximately 1000 MPa) at selected temperatures. The bar was created with 2 cubic elements and the load was applied to the top surface. The bottom surface was constrained for all degrees of freedom. A contour graph of the model is shown in Figure 3-10.

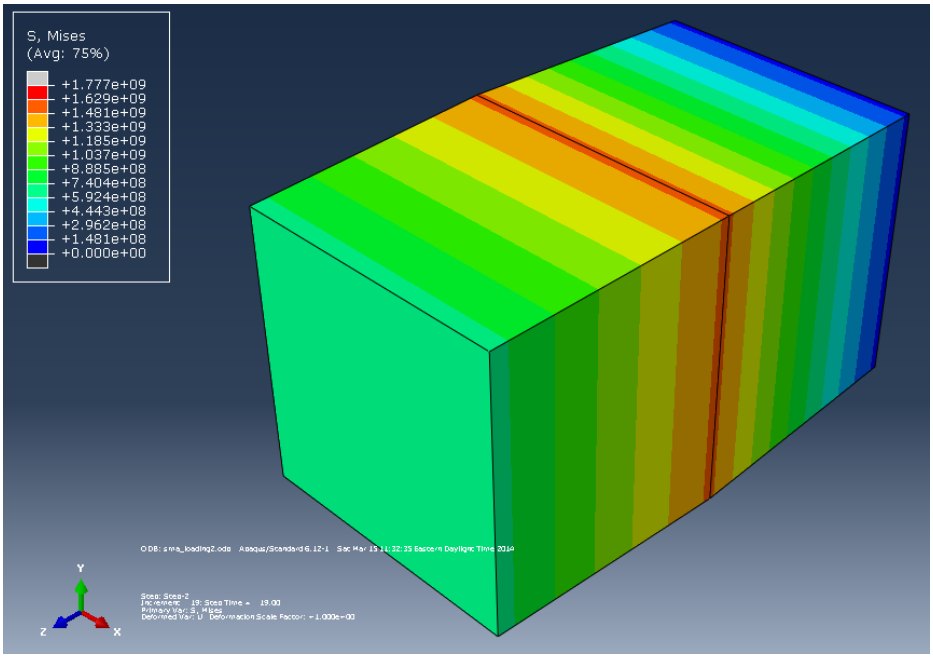

Figure 3-10: Contour plot of SMA bar under load

The simulated superelasticity results for SMA at selected temperatures are shown in Figure 3-11.

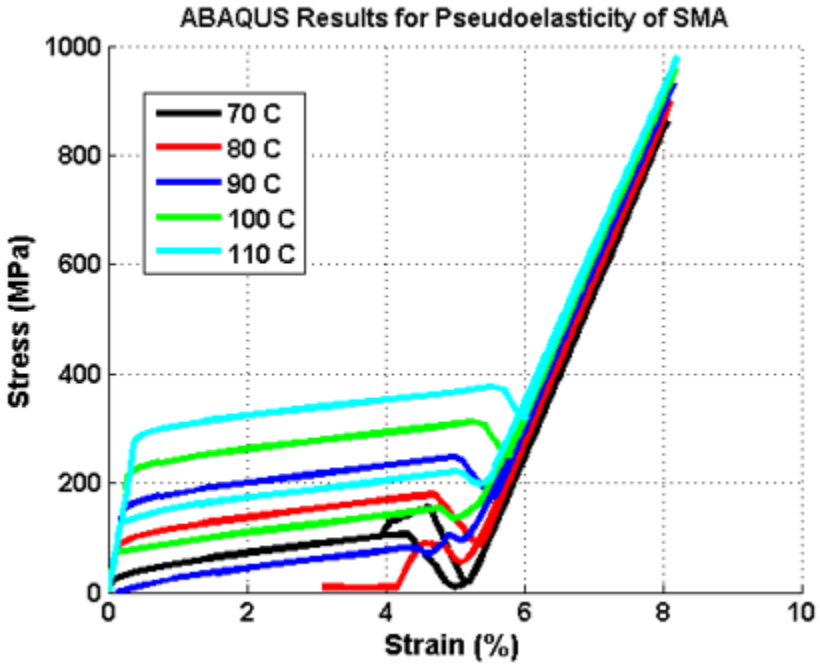

Figure 3-11: Superelasticity results of a SMA that was defined in ABAQUS at selected temperatures

In another effort, shape memory effect was examined on a SMA wire model. This model consisted of two beam elements. The bottom node was constrained for all degrees of freedom and the top node was loaded in tension while the temperature was kept above the austenite finish temperature right at 100 °C. Then, while the load was kept constant, temperature was lowered to below martensite finish temperature. The load was then removed and temperature was increased to 100 °C for recovery.

Figure 3-12a shows the simulated 2D results for strain versus temperature and Figure 3-12b shows the 3D results of the shape memory effect.

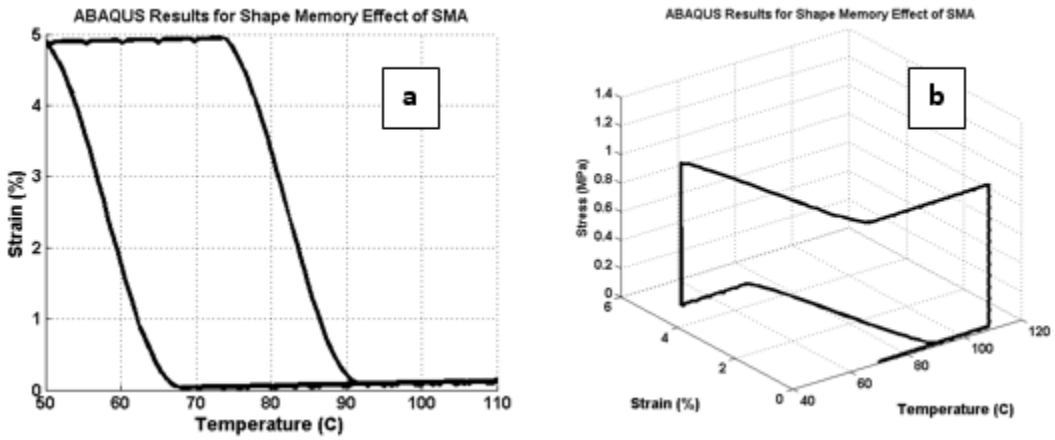

Figure 3-12: ABAQUS results: shape memory effect of a SMA wire a) in 2D and b) in3D

4 CHAPTER IV: SHAPE MEMORY COMPOSITE ACTUATOR: FABRICATION AND FINITE ELEMENT MODELING

4.1 BACKGROUND

Conventional SMAs are a unique class of shape memory materials with the ability to recover their shapes when temperature is increased. In addition, under specific conditions, SMAs can absorb and dissipate mechanical energy by undergoing a reversible hysteretic shape change when subjected to the applied mechanical cyclic loading. These unique characteristics of SMAs have made them popular for sensing and actuation, impact absorption, and vibration damping applications [88]. SMAs have two phases: a high temperature phase or *austenite,* and a low temperature phase or *martensite.* Martensite has a different crystal structure and therefore different properties than austenite. The transformation from one structure to the other does not occur by diffusion of atoms, but rather by shear lattice distortion which is known as martensitic transformation. Although the shape memory phenomenon has been observed in a variety of alloys, near equiatomic NiTi (49-51 at% Ni) has been the workhorse of research and applications due its excellent ductility and shape memory properties. In this proposal, unless it is stated otherwise, SMAs will refer to NiTi alloys.

SMAs have been utilized as smart composites in which SMA fibers (powders, wires) are used as reinforcements in the matrix. One example is to make composites by mixing NiTi SMA fibers or particles with other materials, such as metal powders and polymers, so that SMA fibers or particles are embedded in the matrix. In general, there are two main techniques by which to utilize SMAs embedded composite structures: active property tuning and active strain energy tuning [60]. Active property tuning refers to the increase of the Young's modulus, yield strength, and other properties of the SMA during the transformation of martensite phase to austenite phase. These changes in material properties, especially the Young's modulus, were used to modify the dynamic characteristics of the composite plate in which the SMA wires had been embedded. On the other hand, active strain energy tuning involves the embedment of the pre-strained SMA

wires in martensitic phase into a composite material. Upon the application of heat, the SMA wires are constrained from returning to their memorized length, thus creating the recovery force. This recovery force is used to increase the strain energy and the stiffness of the structure and thus improves structural problems (e.g., shifting natural frequency), suppresses vibration, increases critical and thermal buckling loads, controls post-buckling and thermal post-buckling deflections and prevents cracks and fatigues. When the composite is used in an application, the pre-existing internal compressive stress will compensate the tensile stress applied from the external load, thus improving the tensile and fatigue resistance of the composite [89]. Increase in tensile strength and decrease in crack propagation rate with temperature is observed in those composites indicating the strengthening mechanisms by SMAs [90]. It has also been observed that size and aspect ratio of fibers, pre-strain and thermo-mechanical history of SMAs, and the interface between the fibers and matrix affect the strength of composites [89, 91, 92].

In addition to strengthening, remarkable properties of SMAs have been utilized as a composite constitute to produce intelligent materials with improved and tunable stiffness, fracture toughness, damping properties. The resulting SMA-based composites exhibit unique properties or functions such as self-strengthening, active modal modification, high damping, damage resistance, and shape control that make them useful in many engineering applications [93].

SMAs are mostly added to polymer matrices, although they have also been used with metal matrices [89, 92]. It has been reported that SMA wire-reinforcement increases ductility and strength in fiberglass composites [94] and shifts the natural frequency of a structure away from its exciting frequency and as such controls the amplitude of the structure’s motion during vibration [95] and alters the stiffness properties when the SMAs are activated. The hybridized composites can also be utilized for shape control, as well as for various vibration controls, due to the excellent damping properties of the SMAs [96-98].

Due to their low thermal conductivity, lower mechanical properties, and reduction in shape memory performance over the first several thermo-mechanical cycles and

high-thermal-expansion coefficients, SMP composites are produced by adding inorganic particles or fibers (thermal conductivity) to improve their properties [16, 98]. The addition of inorganic particles increases thermal conductivity, but decreases shape recovery. Carbon nanotubes improve thermal conductivity slightly, but enhance the mechanical properties considerably. The addition of multi-walled carbon nanotubes increases shape recovery and recovery stresses, but decreases shape fixity [99]; while organically and carbon nano-fibers are found to be efficient in decreasing the coefficient of linear thermal expansion [100].

Electro-active shape-memory composites were synthesized using conducting polyurethane (PU) composites and multi-walled carbon nanotubes (MWNTs). Electro-active shape recovery was observed in the experiments for the surface-modified MWNT composites with an energy conversion efficiency of up to 10.4%, making these composites promising candidates for use as smart actuators [101]. In another study, a deployable shape memory polymer composite (SMPC) reinforced by carbon fiber fabrics was fabricated, followed by experiments to demonstrate the feasibility of using an SMPC hinge as a deployable structure with an aim of overcoming the relatively low modulus and low strength by fiber reinforced SMPC and utilizing the extremely high recovery strain, low density and low cost [102]. A shape recovery ratio of the SMPC upon bending above 90% was observed in the experiments conducted.

Additionally, fiber micro-buckling was found to be the primary mechanism for obtaining a large strain in the bending of the SMPC. As a result, an SMPC hinge was fabricated, and a prototype of a solar array actuated by the SMPC hinge was successfully deployed.

4.2 SMA-SMP COMPOSITES

The main properties of SMAs and SMPs are given in Table 4-1 [17]. It is clear that SMAs have one order of magnitude higher recovery stress, but also one magnitude of order lower recovery strain than SMPs. SMPs are softer at high temperature and have a lower density, easier formability and lower heat conductivity than SMAs. Moreover, the modulus decreases as the polymer is heated through the

glass transition temperature (T_g) or the crystalline melting temperature (T_m). The elastic modulus is normally observed to increase with heating for SMAs.

SMPs are lightweight and inexpensive and have good formability and provide high recovery strain. The main drawbacks of SMPs are their lack of strength, low modulus at high temperatures and an inability for reversible actuation [17, 103]. On the other hand, SMAs have high strength, good conductivity, and the ability to generate high forces, but are more expensive, dense and show lower recovery strain than SMPs [17]. A shape memory composite (SMC) can be created by embedding SMA components (e.g. wires) in SMP polymers that will result in low density composites with increased strength and modulus. Also, the addition of SMA wires can supply electrical resistive heat to the overall polymer matrix to trigger the actuation. The size, distribution, and volume fraction of wires can be adjusted to control the SMC properties.

Table 4-1: Main material properties of NiTi SMAs and SMPs [17]

	SMP	SMA
Density , kg/cm^3	0.9-1.1	6-8
Extent of Deformation (%)	Up to 500%	<8%
Young's Modulus, T< T_{trans}(GPa)	0.01-3	83
Young's Modulus, T> T_{trans}(GPa)	(0.1-10) * 10^{-3}	28-41
Stress Required for Deformation (MPa)	1-3 (Easy Shaping)	50-200 (Hard Shaping)
Stress Generated During Recovery (MPa)	1-3	150-300
Working Temperatures (°C)	-10-100	-10-100
Thermal Conductivity (W/mK)	0.15-0.3	18
Processing Condition	<200C, Low P	>1000C, High P
Cost	<$10/lb	~$250/lb

There have been only a few studies on SMA+SMP composites [21, 103, 104]. Tobushi and his team investigated two-way bending deformation and recovery force of shape memory composites [21]. Two kinds of SMA tapes showing SME

and the SE were heat-treated to memorize a round shape. Shape-memorized round tapes were arranged facing in opposite directions and were sandwiched by one SMP sheet in the middle part and by two SMP sheets from upper and lower sides. The fabricated SMC belt bends in the direction of the shape-memorized round shape of the SME-SMA tape during heating and bends in the direction of the shape-memorized round shape of the SE-SMA tape during cooling. The two-way bending deformation with an angle of 56 degrees was observed.

Figures 4-1a and 4-1b compare the elastic modulus and yield stress variations in different temperatures for SMA, SMP, and steel. This graph supports another reason for the use of SMA-SMP composites. By increasing the temperature, SMA's elastic modulus is increasing, while the elastic modulus of the SMP is decreasing and vice-versa. An SMA-SMP composite could have appropriate mechanical strength in all temperatures.

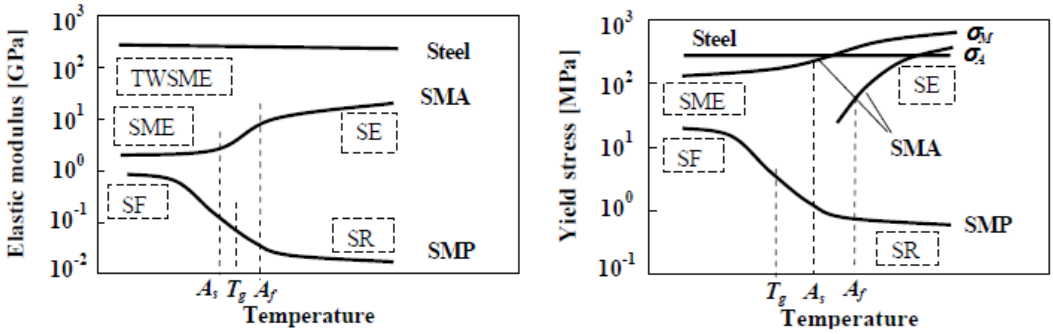

Figure 4-1: Change of a) elastic modulus and b) yield stress with temperature of SMA, SMP and steel [104]

In this project, shape memory composites will be studied in two novel research areas:

1) Novel functional composites: The material properties of both SMAs and SMPs are temperature dependent. SMA+SMP composites can be classified as a novel SMC with multifunctional material properties of which could be governed by temperature. Furthermore, the properties of SMA+SMP composites could be optimized for a specific application (by changing the chemical compositions of

SMP and SMA, applying heat treatments on SMA and altering the volume fraction of either constituent).

2) Reversible Actuation with SMA+SMP composites*:* There is a possibility of inducing reversible actuation in SMCs through a careful adjustment of the transformation temperatures of SMA and T_g of SMP. The proposed mechanism for a reversible SMC actuator and how to build this composite is explained as follows: In SMAs, the start and finish temperatures of the martensite to austenite transformation are given as A_s and A_f while start and finish temperatures of the austenite to martensite transformation are depicted as M_s and M_f, respectively. These temperatures are referred to as transformation temperatures (TTs) and are strongly composition and thermo-mechanical treatment dependent and can be adjusted. In order to achieve reversible actuation, we will use a SMP that has a T_g higher than M_s and lower than A_s. The original length of the SMA wires with self-accommodated (twinned) martensite structure is designated as "S" in Figure 4-2.

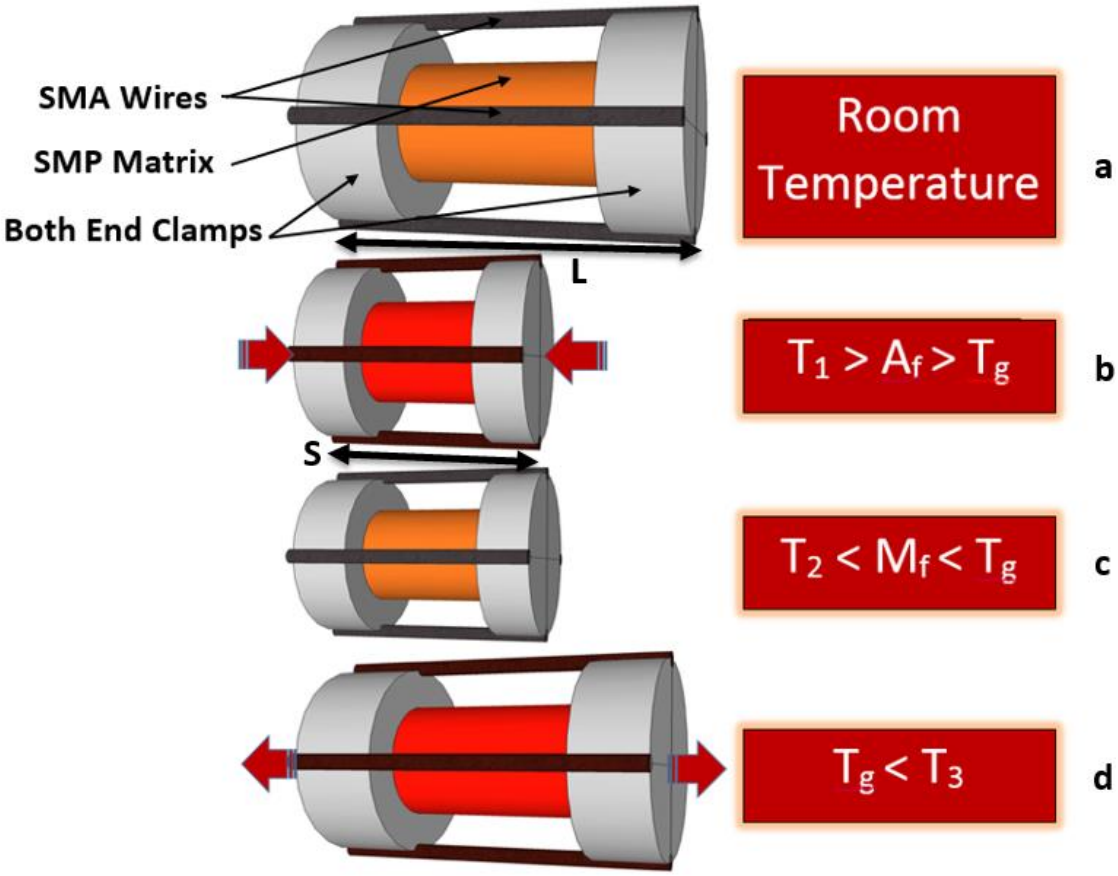

Figure 4-2: SMC actuation illustration

When stress is applied to the SMA wires in martensite phase, their length will increase from “S” to “L” due to detwinning of martensite and upon unloading it will not change but remain as “L”. The SMP cylinder, described previously, will be used as the matrix. After drilling a thorough hole at the center of SMP cylinder, the wire will go through that and from the sides. Both ends of the SMC will be rigid to ensure the compatibility and the transformation of the induced stress from one component to the other. Next, these steps should be realized in the given sequence for the SMC to successfully perform reversible actuation:

i) Heat the composite to T1>Af>Tg. Above Tg ,the SMP is soft and can be easily deformed, while the SMA will transform from detwinned martensite to austenite where the length of the SMA will shorten from initial length “L” to compressed length “S”. Since the ends of composite are rigid, SMA wires will apply force to the soft SMP, resulting in a decrease in the overall length of the composite as shown in Figure 4-2b.

ii) In the second step, the temperature will decrease down to T2 (Ms <T2< Tg). The SMP will harden in the compressed length “S”. Upon further cooling to T3<Mf, austenite will transform to twinned martensite and the length of the composite “S” will remain the same (Figure 4-2c).

iii) In the third step, the temperature will be increased to T4 (Tg <T4<As). In this case, the polymer will create a recovery force to change the length from its compressed length of “S” to initial length of “L”. Since the force required to transform twinned martensite to detwinned martensite is low in the SMA wire, the length of the composite will increase from “S” to “L” (Figure 4-2d).

iv) When the composite is cooled down to RT it will retain its length “L” and steps 1 to 3 can be repeated for reversible actuation (Figures 4-2c and 4-2d).

v) There is an alternative way to achieve reversible actuation: After step 2, the temperature can be increased to T4 first and then to T1 (T4< Af <T1) where the length of the composite will increase from “S” to “L” first and then decrease from “L” to “S”. Therefore, reversible actuation during heating can be observed.

Following the same cooling process as described in step 2, the shape of the SMC can be reset and the heating process can be repeated.

4.2.1 RULE OF MIXTURE

To be able to determine how many wires are needed for SMC that can show reversible actuation, the rule of mixture with exact dimensions and elastic modulus for both SMP and SMA wire is used. Importantly, the elastic modulus of SMP changes drastically with temperature, making the design a bit challenging. Rule of mixture has shown in the following equation [105]

$$0 = f^{\Omega}\bar{E}^{\Omega}(\varepsilon_P^{\Omega} - \gamma^{\Omega}) + f^{M}\bar{E}^{M}(\varepsilon_P^{M} - \gamma_t^{M})$$

where f, E, ε, and γ represent the volume fraction, elastic modulus, plastic strain and elastic strain, respectively, Ω and M represent SMA wire and SMP matrix, respectively. The first term is the total force that is generated by SMA wire and the second term is the total force that has been generated by SMP. The SMP cylinder "S" has the diameter of 0.25" and the wire has the diameter of 0.008". The elastic moduli of the SMP at selected temperatures are given in Figure 8. The elastic modulus of the wire was determined from the experiments to be around 30 GPa as shown in Figure 4-3.

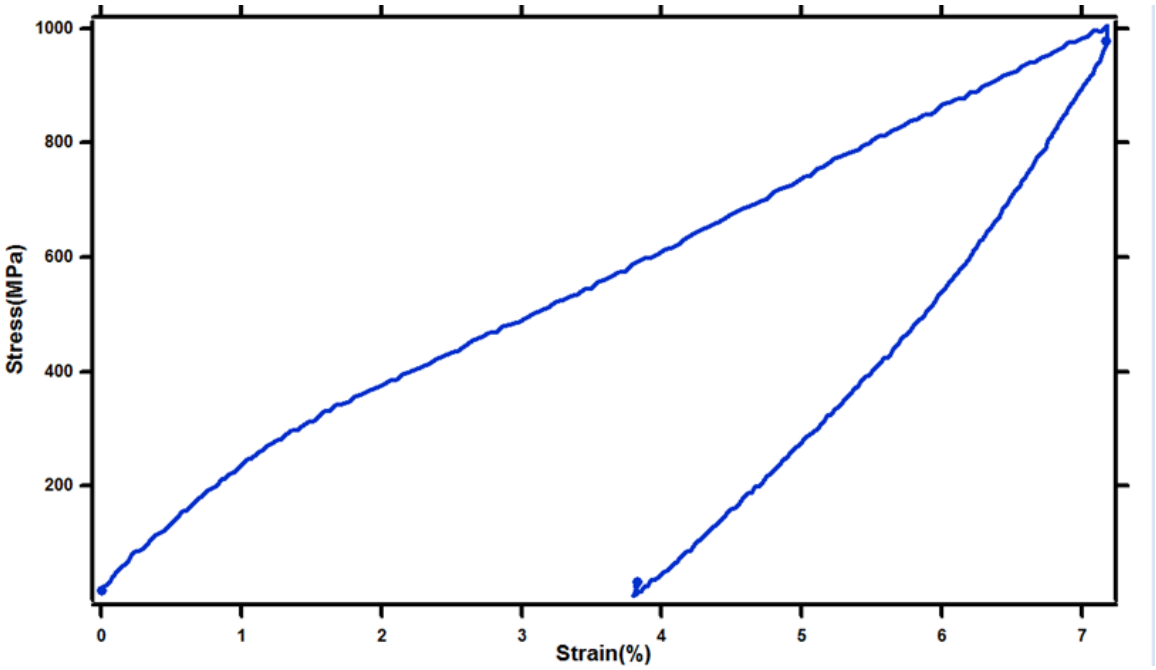

Figure 4-3: Stress-strain graph for NiTi wire

Table 4-2 shows the number of wires needed for equilibrium condition at selected temperatures.

Table 4-2: Calculated the number of needed wires for SMC according to rule of mixture

Temperature	15°C	25°C	35°C	45°C	55°C
SMP Matrix Elastic Modulus (GPa)	1.3	0.9	0.4	0.3	0.2
SMA Wire Elastic Modulus (GPa)	30	30	30	30	30
Wires Needed	43	29	13	9	6

As the temperature increases, the volume fraction of SMA should decrease to reach equilibrium. At low temperatures, there is no need for large number of wires since SMA will not contract. At higher temperatures, a few wires can do their job of deforming the SMP; however the force that SMA is producing should overcome the matrix's force. The most important stage is the time that SMP wants to recover. The SMP should be able to overcome the force that is created by wires. As indicated in Table 4-2, nine wires are needed for equilibrium at the glass transition temperature of SMP (43°C). If any fewer wires are installed, the SMP will be able to recover. Thus, eight wires were installed in SMC, with four at the center hole and four at the sides.

4.2.2 EXPERIMENTAL RESULTS AND DISCUSSION

The SMC was fabricated by using epoxy-based NGDE3 SMP and Flexinol NiTi wires from DYNALLOY©. The clamps were machined from stainless steel. Figure 4-4 shows the fabricated SMC used in experiments.

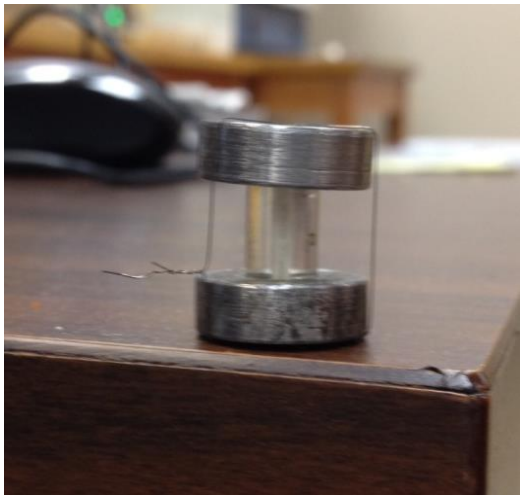

Figure 4-4: SMC sample made with NGDE3 SMP matrix and Flexinol NiTi wires

The SMC sample was tested in DMA. After placing the sample inside the chamber, the probe needs to touch the clamp. Thermal cycling was done between room temperature and 130 °C (above A_f) for complete recovery and maximum action. The temperature rate of 1 °C/min was used. The strain was calculated from the

displacement of probe. Strain versus temperature response of the SMC is shown in Figure 4-5.

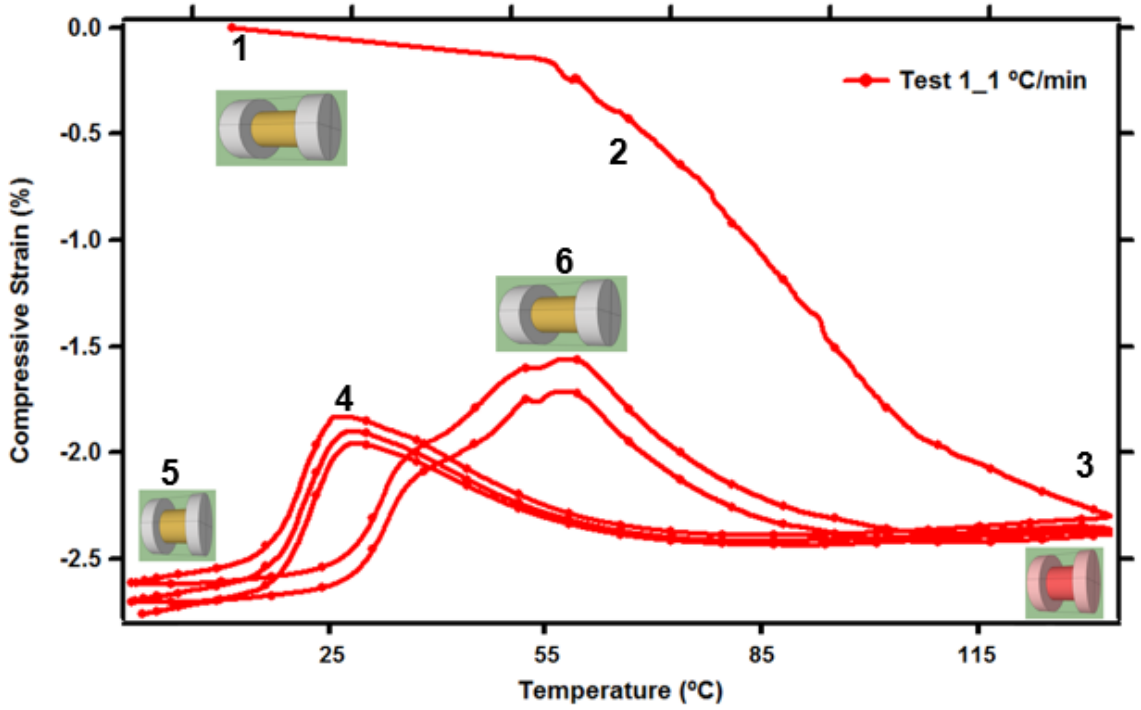

Figure 4-5: SMC actuation results with 1 °C/min

The SMC sample was been placed in DMA, reflected by point 1 on the graph. Point 2 shows the austenite start temperature where the wire is contracting and will deform the SMP matrix as well. At higher temperatures, the SMP has lower elastic modulus and is very elastic. NiTi wire can easily deform the SMP. At point 3, the wire contracts and transforms to austenite. When the sample is cooled down, the modulus of SMP increases, thus, SMP exerts additional force to NiTi wire which transforms to martensite, resulting in increased length of the composite. In order to understand why compressive strain increases when the sample is cooled further to point 5, figure 2-11 is needed to be reviewed. As the temperature is reduced, the elastic modulus of SMP was increased and SMP went from pure elastic behavior to elastoplastic type behavior. As the stress applied to SMP was increased, SMP was deformed plastically as shown in Figure 2-11. Therefore, the compressive strain of SMC was increased. At point 5, the sample is at its lowest

temperature in the cycle and as expected, the SMP matrix is in deformed condition. Upon heating, the SMC expands to recover and softens with temperature. Thus the wires are expanded due to variant reorientation. As temperature exceeds A_s, the wire transforms to austenite and contracts the SMC. The SMC was thermally cycled two more times to observe the reversible actuation behavior. It is clear that the response is fully reversible after the initial heating.

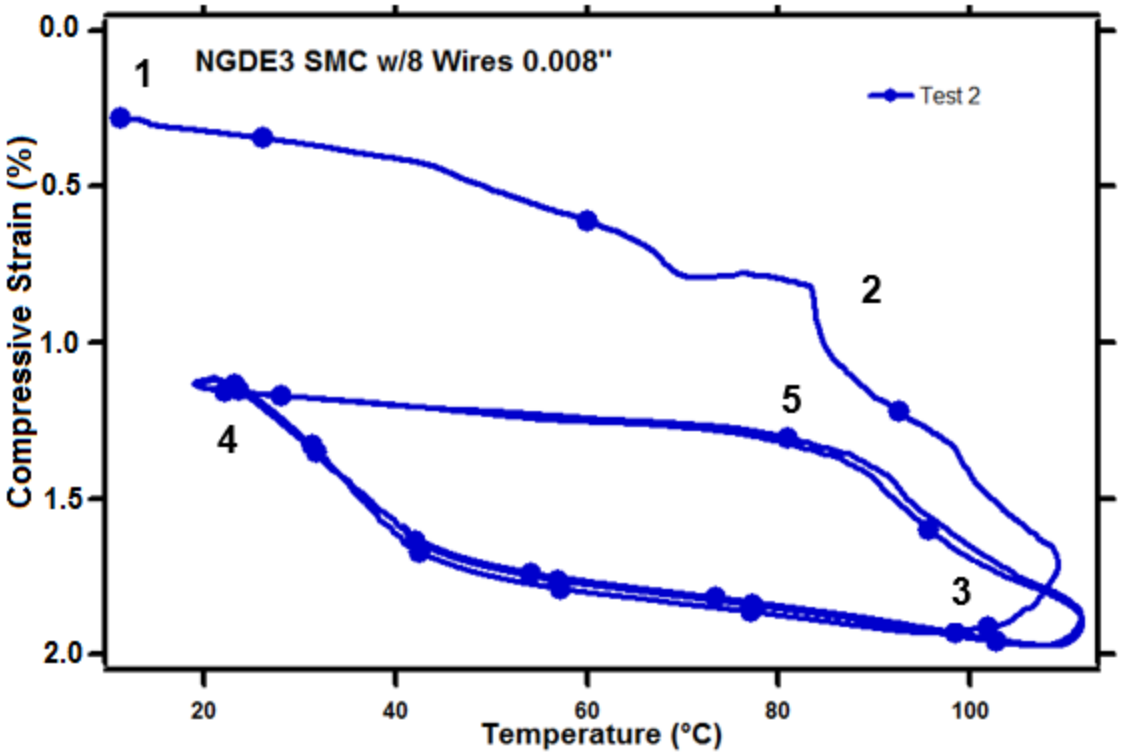

Figure 4-6: Alternative SMC cycle done by adjusting the thermal cycling range with a rate of 5 °c/min

The plastic behavior of SMP at temperatures below point 4, provides an alternative method to create reversible behavior. Instead of cooling the sample further from 4 to 5 shown in Figure 4-5, the temperature of the sample can be cycled between 3 and 4 shown in Figure 4-5. Figure 4-6 shows the alternative cycle that was done at the rate of 5°C/min. In this test, the sample was placed inside the furnace at point 1. After heating the sample up, the wires started to contract at point 2. At 110 °C, contraction was complete and the sample as it was transformed to austenite. Upon cooling, the SMA transforms to martensite where its modulus decreases

while SMP becomes harder with increased modulus, resulting in increased length of the SMC. Upon heating, martensite to austenite transformation results in contraction of the SMC. The alternative experiment was done for two additional cycles to check the repeatability.

4.3 SMC MODEL IN ABAQUS

Modeling of the behavior of SMC in ABAQUS will now be described. As described in the previous sections, SMP and SMAs models are individually created. For SMC modeling, not only are two types of materials needed, but the interactions between these materials play a very important role. In order to to model the SMC, either SMA has to be in tension before contraction or SMP needs to be in compression before they can be tied together.

4.3.1 Wire SMC FEM

ABAQUS has the capability to define a contraction between two separate parts. Also, it is possible to have a “model change” during the steps. This way contraction will not work for the steps that there is no need for that. This capability was used for the model. The only difference between the SMA model that was used for SMC and the one that was introduced in the previous section is that hexagonal elements were used as the element type instead of beams. The total area of the wires used in the experiments were superimposed and one bar with an area equal to the total area of the wires was created. The length of the SMA bar is considered a little shorter so it matches the length of SMP when in compression. Figure 4-7 shows the geometry of the SMC created in ABAQUS.

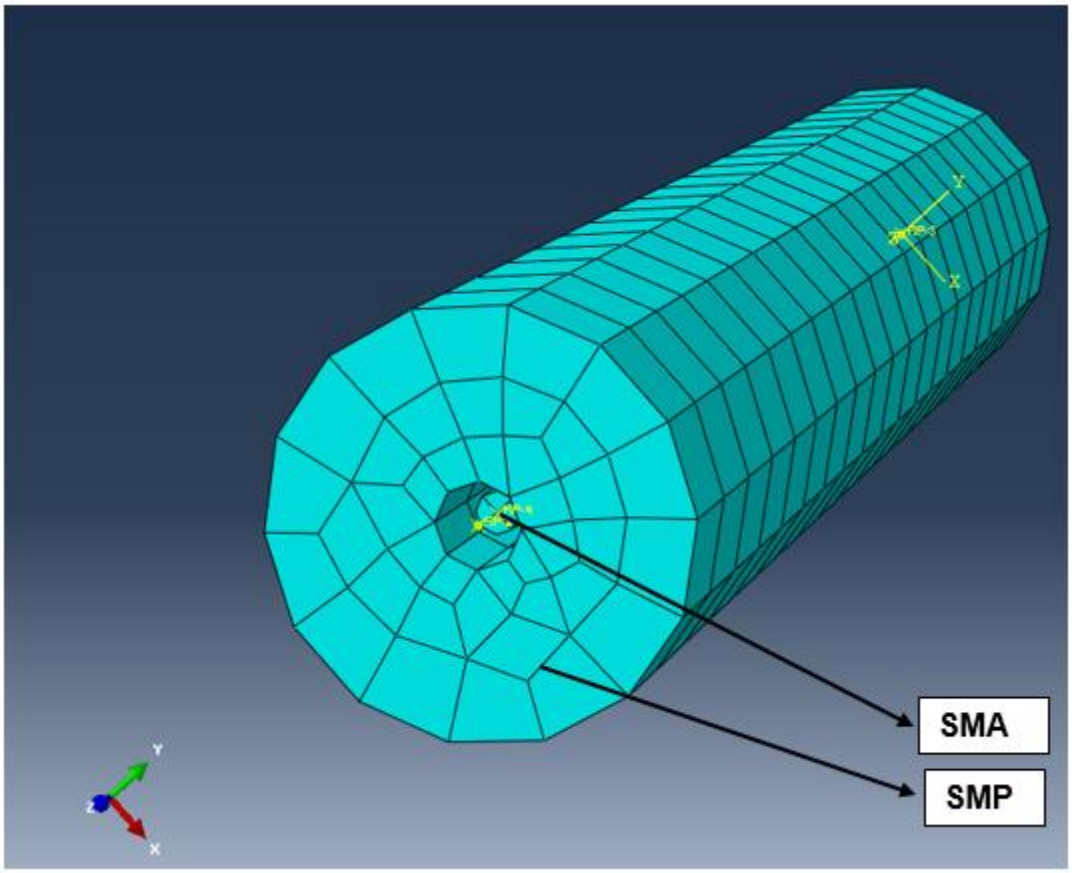

Figure 4-7: SMC model in ABAQUS

In this model, there are two reference points defined at the top and bottom of SMP. They are coupled with top and bottom surfaces of SMP cylinder, respectively. The bottom point was constrained for all degrees of freedom. SMC behavior was tested in ABAQUS through the following steps:

Step 1: SMP was compressed for 10% of its original length at 110 °C which is above its glass transition temperature.

Step 2: The temperature decreased to 20 °C which is below the glass transition temperature of SMP. The interaction between the two parts was also activated. The load was removed after cooling down from SMP in this step.

Step 3: The temperature was increased to 110 °C which is higher than the glass transition temperature of SMP.

Step 4: The deformed SMP tried to recover but it was tied to the SMA part. As a result, the SMA rod will be deformed in this step.

Step 5: The temperature increased to 110 °C which is more than the austenite finish temperature of SMA and activated the SMA to recover to its original shape. However, since SMA was tied to SMP, it also deformed the SMP.

The heating and cooling steps were added for two more cycles to ensure that the SMC actuator is moving back and forth only with altering the temperature.

Figure 4-8 shows the two slides of the SMC was after being cooled down and then heated up. The pictures show the same position for both SMA and SMP and also confirm that the movement is due only to changes in temperature, a main goal of this study.

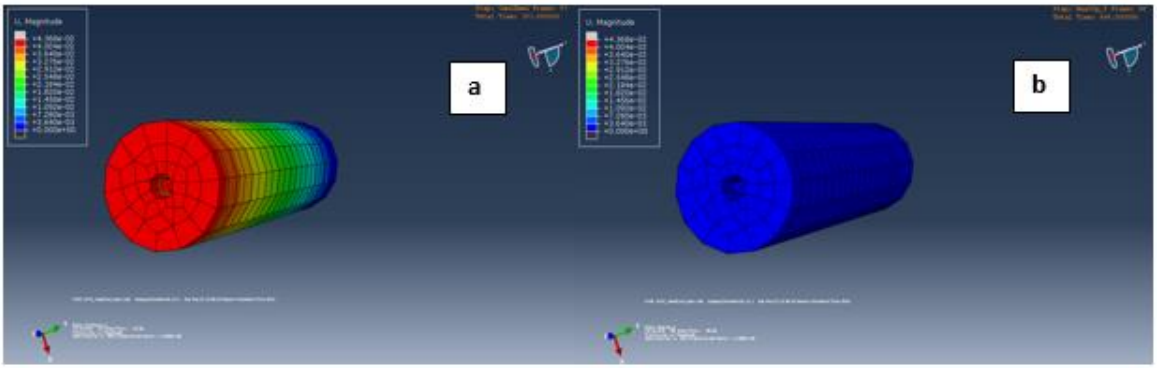

Figure 4-8: SMC FEM in action, a) cooled down b) heated up

Figure 4-9 shows both experimental and simulation results of SMC behavior with temperature.

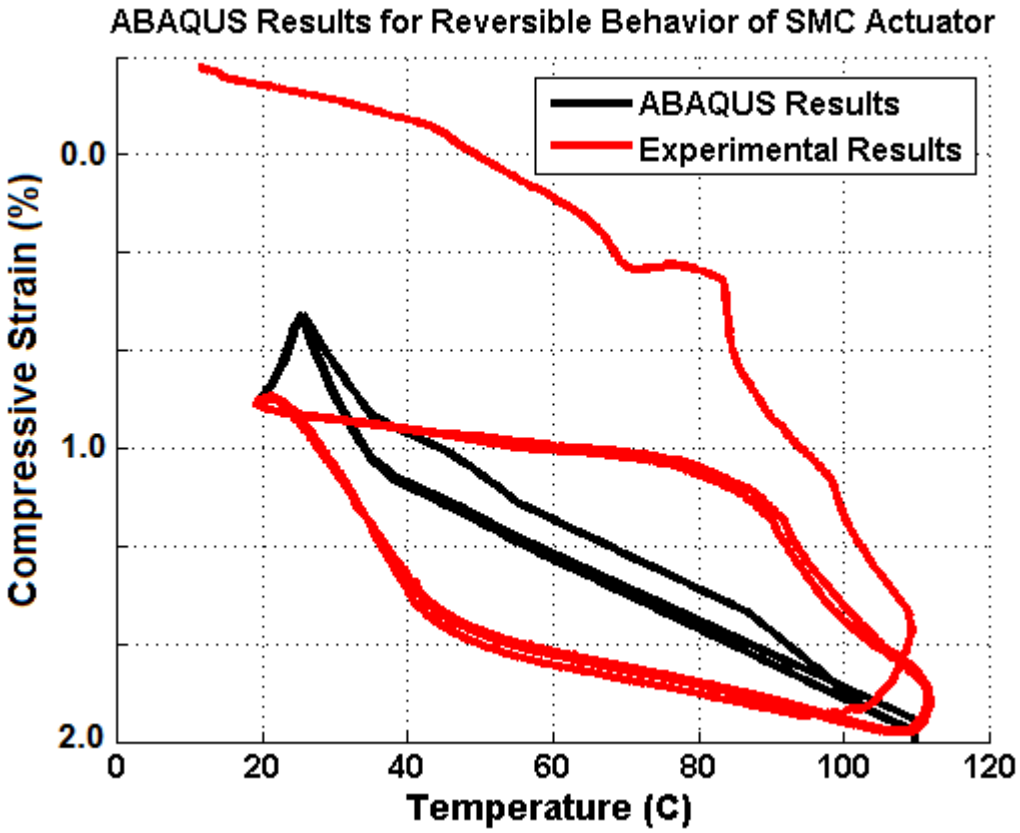

Figure 4-9: Comparison between finite element model results and experimental results of SMC

The FEM results match quite well with the experimental results with the exception that full recovery was achieved at each step and resulted in less hysteresis compared to the experimental results. This discrepancy is a result of how the SMP was defined in this project in experiments, the SMP properties change instantly with alterations in temperature, while in FEM, a gradual change in properties is noted with temperature, thus resulting in less hysteresis. The simulation results capture the general behavior of SMC actuation. However, because of the limitations of a simple SMP model, the simulation results do not exactly match with experimental results.

In order to confirm that the contraction with further cooling from point 4 to 5 in Figure 4-5 is due to plastic deformation of SMP, the temperature range was changed in ABAQUS model. Figure 4-10 shows the FEM results includes the plastic behavior of SMP. It shows the behavior that we observed in experiments.

However the hysteresis is lower in this case because after the heating the gained displacement is lower.

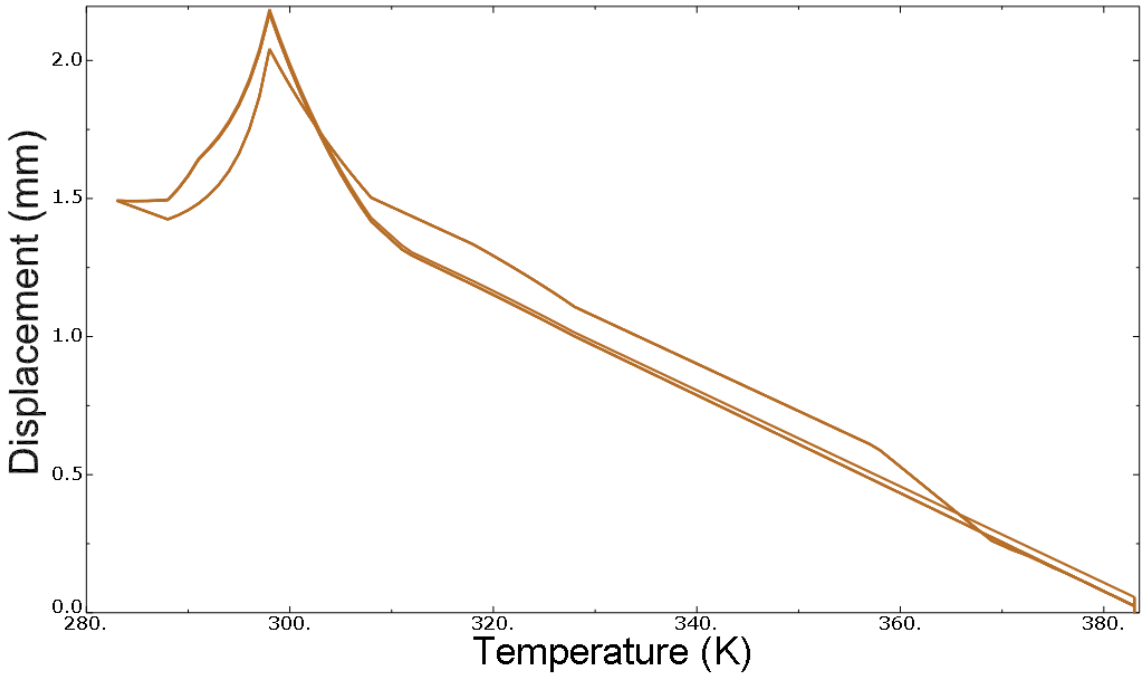

Figure 4-10: SMC results with SMP plastic behavior

4.3.2 Spring-SMC FEM

In another effort, a NiTi coil spring was used instead of NiTi wire to create a SMC by attaching it to a SMP cylinder. The concept is exactly the same beside the fact that we have to encounter the spring force according to Hooke's law in rule of mixture equation. As such, the equation becomes:

$$0 = f^{\Omega}\bar{E}^{\Omega}(\varepsilon_P^{\Omega} - \gamma^{\Omega}) + f^{M}\bar{E}^{M}(\varepsilon_P^{M} - \gamma_t^{M}) + K\Delta L$$

where K represents the spring stiffness and ΔL represents the SMC actuator stroke. Figure 4-11 shows contour plots of the SMC in two cases while it is in its upper and lower level of its stroke.

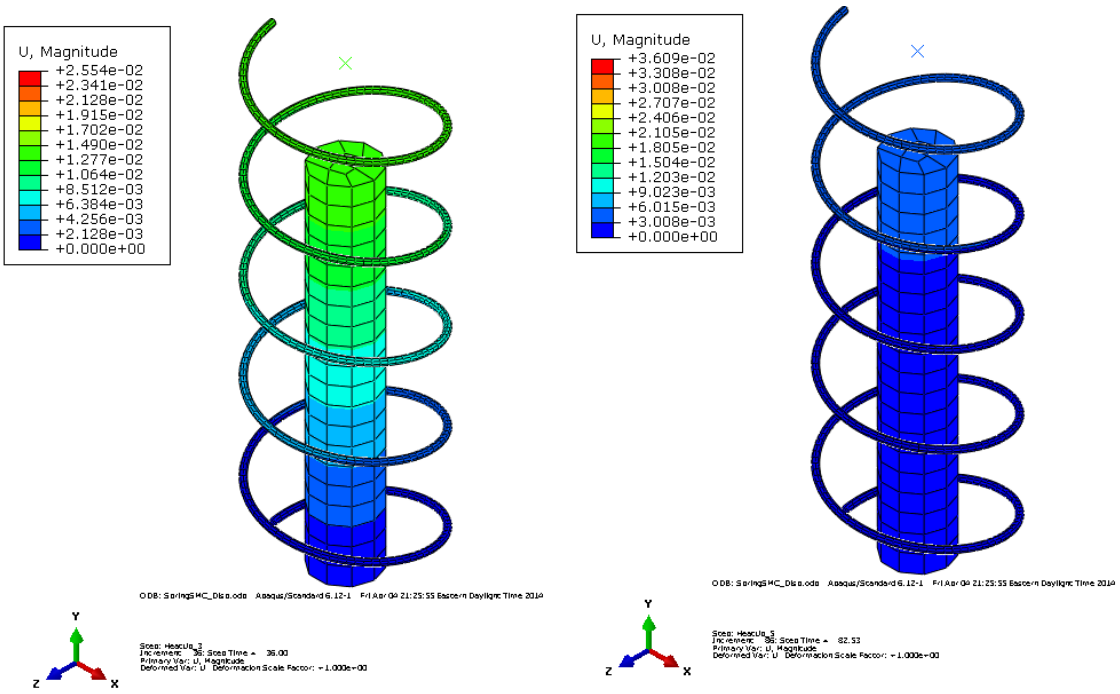

Figure 4-11: Contour plots of spring SMC

Figure 4-12 shows the spring SMC actuator behavior. It clearly shows a reversible motion with temperature cycling.

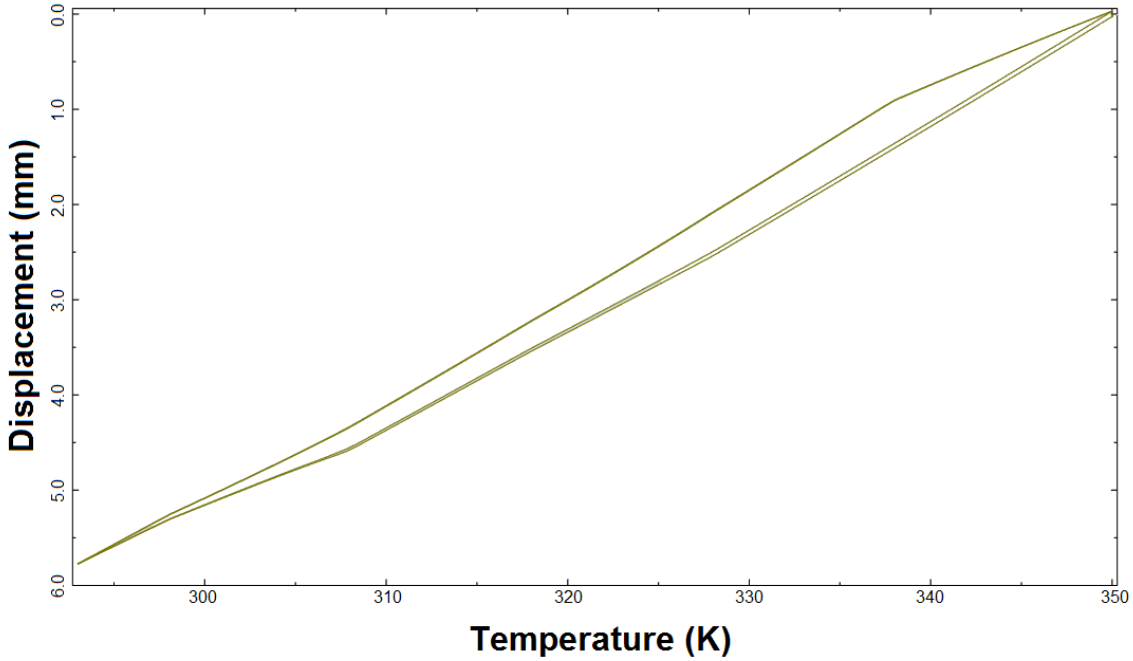

Figure 4-12: Displacement versus temperature graph for spring-SMC actuation

4.3.3 SMC with SMA-SMP bending plates

In order to be able to show that SMC simulations would work for different actuator designs, SMC was created by using the plates of SMP and SMA to work in bending. The NiTi plate has an original curved shape and SMP plate has an original straight shape. The SMP plate was then bended and attached to the SMA plate at a higher temperature than its glass transition temperature. While the load is still applied to the SMP, the temperature decreased. The load was then removed and SMP attached to the SMA plate. By heating them up, the SMP plate generates stress because it wants to bend to its original straight shape and it contracts the SMA plate as well. Figure 4-13 shows the contour plots of bending plates in two positions.

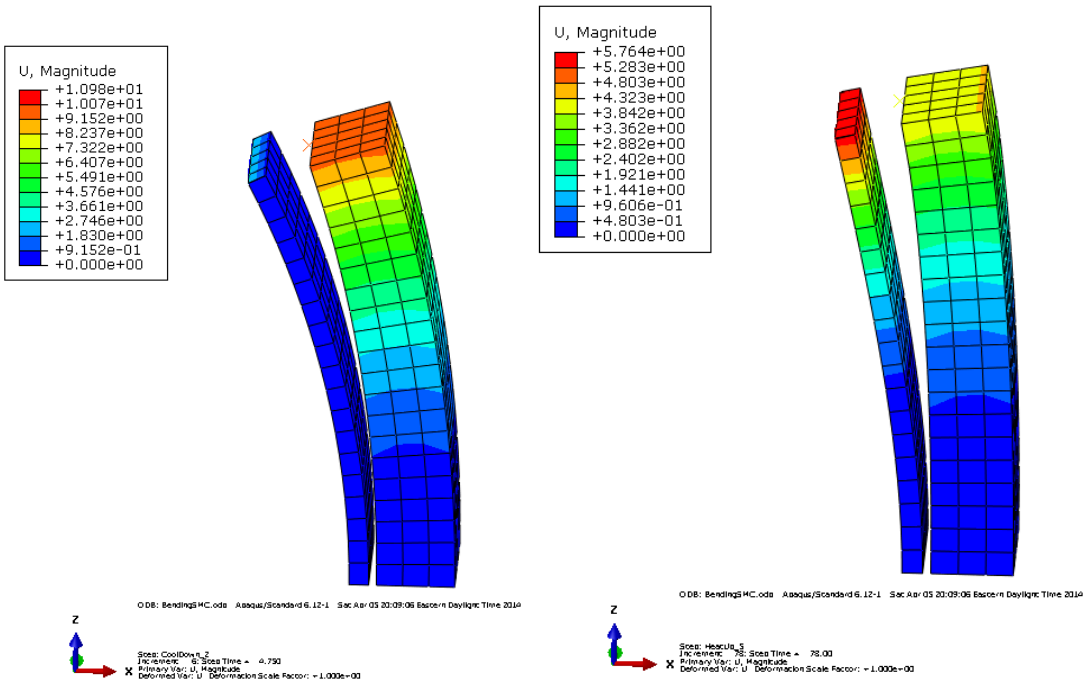

Figure 4-13: Contour plots of SMC bending plates

Figure 4-14 shows the reversible behavior by temperature track but on the rotation angle of the bended plates.

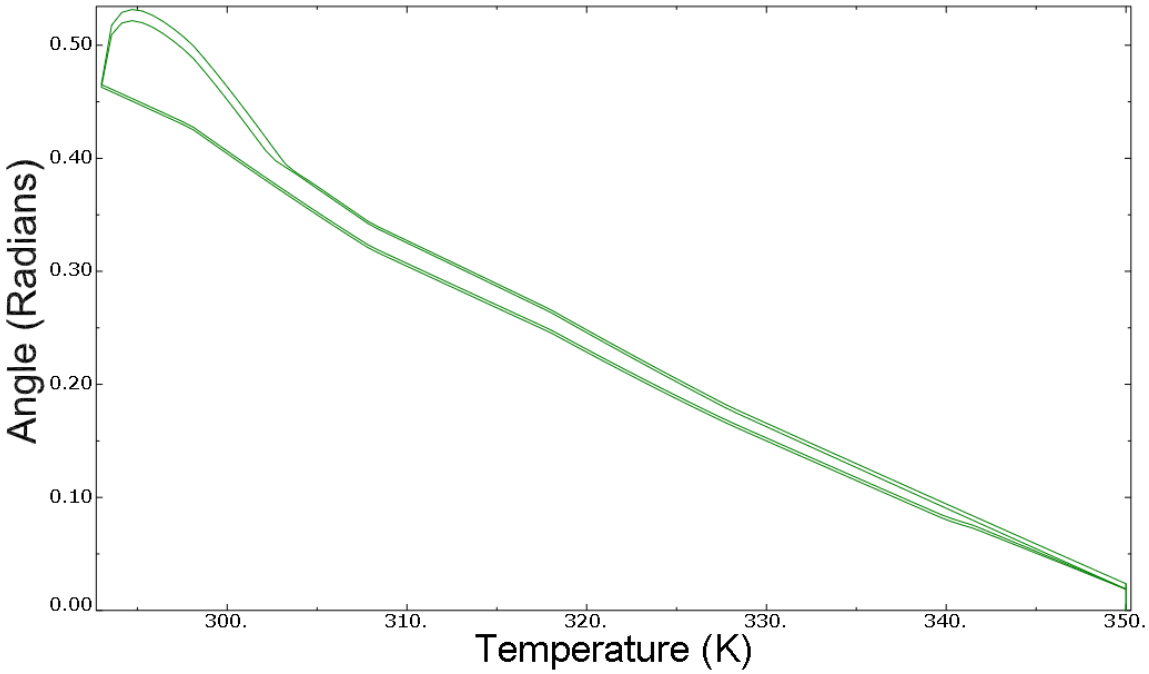

Figure 4-14: Angle versus temperature graph for bending plates SMC

5. CONCLUSIONS

In this work, the thermomechanical properties of epoxy-based SMP were investigated. The glass transition temperature was determined from DSC results and was confirmed by three-point-bending testing at DMA. Failure and compression tests, along with recovery, of the SMP were shown. Two cases for constrained loading of SMP were reviewed. In the constrained load test, two-way shape memory effect under stress was revealed. In the constrained displacement test, 24 MPa stress was generated at glass transition temperature. A simple elastic-plastic model was generated in ABAQUS for SMP that shows shape memory effect; however findings for the cooling section were not consistent with experimental results. Importantly, this simple model of SMP is sufficient for evaluating the kinematic behavior of SMA-SMP shape memory composite.

In Chapter 3, properties of the NiTi wire were discussed. Transformation temperatures were determined by DSC tests. Stress generation and stress-strain tests at room temperature were performed. For modeling of NiTi wire in ABAQUS, a developed subroutine from Lagoudas *et al*. [30] was used. The net cross-sectional area of the total wires in experiments was considered equal to the rod cross sectional area used in the model. The pseudoelasticity graphs in different temperatures were shown for a simple element.

In the last chapter, the SMA-SMP shape memory composite was fabricated and its response with temperature change was revealed. In the experiments, it was confirmed that SMC shows a reversible behavior with temperature cycling. By adjusting the temperature range, the cycle could be more efficient if the plastic deformation of the SMP was not allowed. The model of the SMC in ABAQUS yielded comparable results to those of experiments. Moreover, a spring coil was used instead of wires in the ABAQUS model and another reversible behavior with higher stroke was shown. Since the ABAQUS model indicates a very good estimation of kinematic behavior of the SMA-SMP composite actuator, there is opportunity to simulate the behavior of different SMC designs. Simulation of the actuation behavior of a SMC consists of two bending plates was done in ABAQUS and the results showed a reversible behavior in bending as well

REFERENCES

[1] Liu C, Qin H, Mather P. Journal of Materials Chemistry 2007;17:1543.

[2] Ebine T, Harada H. Jpn. Pat 2002;2002006280.

[3] Terai T. Jpn. Pat 2002;2002086914.

[4] Grablowitz H, Langer RS, Lendlein A, Schmidt A. Biodegradable shape memory polymers. Google Patents, 2000.

[5] Lendlein A, Langer RS. Biodegradable Shape Memory Polymeric Sutures. Google Patents, 2012.

[6] Small W, Metzger MF, Wilson TS, Maitland DJ. Selected Topics in Quantum Electronics, IEEE Journal of 2005;11:892.

[7] Gall K, Yakacki CM, Liu Y, Shandas R, Willett N, Anseth KS. Journal of Biomedical Materials Research Part A 2005;73:339.

[8] Noebe R BT, Padula SA NiTi-Based High-Temperature Shape-Memory Alloys: Properties, Prospects, and Potential Applications. In: Soboyejo WO ST, editor. Advanced Structural Materials: Properties, Design Optimization, and Applications. NW: Taylor & Francis Group, 2007.

[9] LeBlanc L. Part I - 'Smart metals' providing actuation, sealing, and completion functions downhole. Offshore, vol. 61, 2001.

[10] LeBlanc L. Part II - 'Smart metals' providing actuation, sealing, and completion functions downhole. Offshore, vol. 62, 2002.

[11] Murray SJ, Marioni M, Allen SM, O'Handley RC, Lograsso TA. Applied Physics Letters 2000;77:886.

[12] Albertini F, Canepa F, Cirafici S, Franceschi EA, Napoletano M, Paoluzi A, Pareti L, Solzi M. Composition dependence of magnetic and magnetothermal properties of Ni-Mn-Ga shape memory alloys. Elsevier Science Bv, 2004. p.2111.

[13] Mohr R, Kratz K, Weigel T, Lucka-Gabor M, Moneke M, Lendlein A. Proceedings of the National Academy of Sciences of the United States of America 2006;103:3540.

[14] Turner TL. Thermomechanical Response of Shape Memory Alloy Hybrid Composites. Hampton: Langley Research Center, 2001. p.239.

[15] Gall K, Mikulas M, Munshi NA, Beavers F, Tupper M. Journal of Intelligent Material Systems and Structures 2000;11:877.

[16] Ratna D, Karger-Kocsis J. J Mater Sci 2008;43:254.

[17] Hiltz J. Defence RD Canada 2002.

[18] Gall K, Kreiner P, Turner D, Hulse M. Journal of Microelectromechanical Systems 2004;13:472.

[19] Sokolowski WM, Chmielewski AB, Hayashi S, Yamada T. SPIE 1999;3669:179.

[20] Dietsch B, Tong T. Journal of Advanced Materials 2007;39:3.

[21] Tobushi H, Hayashi S, Sugimoto Y, Date K. Materials 2009;2:1180.

[22] Tobushi H, Hayashi S, Pieczyska E, Date K, Nishimura Y. Archives of Mechanics 2011;63:443.

[23] Tobushi H, Pieczyska E, Ejiri Y, Sakuragi T. Mechanics of Advanced Materials and Structures 2009;16:236.

[24] Noeth Z. 2008.

[25] Bollas D, PappaS P, Parthenios J, Gallotis C. Acta Materialia 2007;55:5489.

[26] Pieczyska EA, Nowacki WK, Tobushi H, Hayashi S. Qirt Journal 2009;6:189.

[27] Liu YP, Gall K, Dunn ML, Greenberg AR, Diani J. International Journal of Plasticity 2006;22:279.

[28] Baer GM, Wilson TS, Small W, Hartman J, Benett WJ, Matthews DL, Maitland DJ. Journal of Biomedical Materials Research Part B: Applied Biomaterials 2009;90:421.
[29] Atli B, Gandhi F, Karst G. Journal of Intelligent Material Systems and Structures 2009;20:87.
[30] Lagoudas D, Bo Z, Qidwai M, Entchev P. Texas A&M University, College Station, TX 2003.
[31] Volk BL, Lagoudas DC, Maitland DJ. Smart Materials and Structures 2011;20:094004.
[32] Huang WM, Yang B, Fu YQ. Polyurethane shape memory polymers: CRC Press, 2011.
[33] Tobushi H, Hayashi S, Kojima S. JSME international journal. Ser. 1, Solid mechanics, strength of materials 1992;35:296.
[34] Tobushi H, Hara H, Yamada E, Hayashi S. Smart Materials and Structures 1996;5:483.
[35] Tobushi H, Hashimoto T, Ito N, Hayashi S, Yamada E. Journal of Intelligent Material Systems and Structures 1998;9:127.
[36] Abrahamson ER, Lake MS, Munshi NA, Gall K. Journal of intelligent material systems and structures 2003;14:623.
[37] Liu Y, Gall K, Dunn ML, McCluskey P. Mechanics of Materials 2004;36:929.
[38] Baer G, Wilson T, Matthews D, Maitland D. Journal of applied polymer science 2007;103:3882.
[39] Xie T, Rousseau IA. Polymer 2009;50:1852.
[40] Ded GS. 2010.
[41] Tobushi H, Hara H, Yamada E, Hayashi S. Smart Materials & Structures 1996;5:483.
[42] Tobushi H, Hashimoto T, Hayashi S, Yamada E. Journal of Intelligent Material Systems and Structures 1997;8:711.
[43] Tobushi H, Ito N, Takata K, Hayashi S. Thermomechanical constitutive modeling of polyurethane-series shape memory polymer. In: Saburi T, editor. Shape Memory Materials, vol. 327-3. 2000. p.343.
[44] Bhattacharyya A, Tobushi H. Polymer Engineering and Science 2000;40:2498.
[45] Tobushi H, Okumura K, Hayashi S, Ito N. Mechanics of materials 2001;33:545.
[46] Hong SJ, Yu WR, Youk JH. Thermomechanical deformation analysis of shape memory polymers using viscoelasticity. AIP Conference Proceedings, vol. 907, 2007. p.853.
[47] Srinivasa AR, Gosh P. A simple, Gibbs potential based multinetwork model for shape memory polymers. AIP conference proceedings, vol. 1029, 2008. p.58.
[48] Barot G, Rao I. Zeitschrift für angewandte Mathematik und Physik ZAMP 2006;57:652.
[49] Diani J, Liu YP, Gall K. Polymer Engineering and Science 2006;46:486.
[50] Chen YC, Lagoudas DC. Journal of the Mechanics and Physics of Solids 2008;56:1752.
[51] Chen Y-C, Lagoudas DC. Journal of the Mechanics and Physics of Solids 2008;56:1766.
[52] VOLK BL. Thermomechanical characterization and modeling of shape memory polymers. Texas A&M University, 2009.
[53] Volk BL, Lagoudas DC, Chen Y-C. Smart Materials and Structures 2010;19:075006.
[54] Volk B. Three-Dimensional Modeling of Shape Memory Polymers Considering Finite Deformations and Heat Transfer. 2013.
[55] Khanolkar M, Sodhi J, Rao IJ. Modeling the Behavior of Crystallizable Shape Memory Polymers Subject to Inhomogeneous Deformations. ASME 2010 Conference on Smart Materials, Adaptive Structures and Intelligent Systems: American Society of Mechanical Engineers, 2010. p.105.
[56] Auricchio F, Taylor R. Shape memory alloy superelastic behavior: 3D finite-element simulations. 3rd International Conference on Intelligent Materials: International Society for Optics and Photonics, 1996. p.487.
[57] Tanaka K, Kobayashi S, Sato Y. International Journal of Plasticity 1986;2:59.

[58] Achenbach M. International Journal of Plasticity 1989;5:371.
[59] Seelecke S, Muller I. Applied Mechanics Reviews 2004;57:23.
[60] Liang CR, C.A. Am. Inst. Aeronaut, Astronaut 1989;89-:2011.
[61] Brinson LC. Journal of Intelligent Material Systems and Structures 1993;4:229.
[62] Abeyaratne R, Knowles JK. Journal of the Mechanics and Physics of Solids 1993;41:541.
[63] Govindjee S, Kasper EP. Computer Methods in Applied Mechanics and Engineering 1999;171:309.
[64] Auricchio F, Sacco E. International Journal of Non-Linear Mechanics 1997;32:1101.
[65] Bekker A, Brinson L. Journal of the Mechanics and Physics of Solids 1997;45:949.
[66] Ivshin Y, Pence TJ. Journal of intelligent material systems and structures 1994;5:455.
[67] Paiva A, Savi MA, Braga AMB, Pacheco PMCL. International Journal of Solids and Structures 2005;42:3439.
[68] Rajagopal K, Srinivasa A. Zeitschrift für angewandte Mathematik und Physik ZAMP 1999;50:459.
[69] Patoor E, Eberhardt A, Berveiller M. Acta Metallurgica 1987;35:2779.
[70] Liang C, Rogers C. Journal of Engineering Mathematics 1992;26:429.
[71] Sun QP, Hwang KC. Journal of the Mechanics and Physics of Solids 1993;41:19.
[72] Boyd JG, Lagoudas DC. Journal of Intelligent Material Systems and Structures 1994;5:333.
[73] Auricchio F, Taylor RL, Lubliner J. Computer Methods in Applied Mechanics and Engineering 1997;146:281.
[74] Tobushi H, Yamada S, Hachisuka T, Ikai A, Tanaka K. Smart Materials & Structures 1996;5:788.
[75] Lagoudas DC, Bo Z, Qidwai MA. MECHANICS OF COMPOSITE MATERIALS AND STRUCTURES An INTERNATIONAL JOURNAL 1996;3:153.
[76] Leclercq S, Lexcellent C. Journal of the Mechanics and Physics of Solids 1996;44:953.
[77] Raniecki B, Lexcellent C. European Journal of Mechanics-A/Solids 1998;17:185.
[78] Lagoudas DC, Bo ZH. International Journal of Engineering Science 1999;37:1141.
[79] Qidwai M, Lagoudas D. International Journal for Numerical Methods in Engineering 2000;47:1123.
[80] Govindjee S, Miehe C. Computer Methods in Applied Mechanics and Engineering 2001;191:215.
[81] Brocca M, Brinson L, Bažant Z. Journal of the Mechanics and Physics of Solids 2002;50:1051.
[82] Juhasz L, Schnack E, Hesebeck O, Andrä H. Journal of intelligent material systems and structures 2002;13:825.
[83] Helm D, Haupt P. International Journal of Solids and Structures 2003;40:827.
[84] Anand L, Gurtin ME. Journal of the Mechanics and Physics of Solids 2003;51:1015.
[85] Popov P, Lagoudas DC. International Journal of Plasticity 2007;23:1679.
[86] Reese S, Christ D. International Journal of Plasticity 2008;24:455.
[87] Machado LG, Lagoudas DC. Thermomechanical Constitutive Modeling of SMAs. Shape Memory Alloys, vol. 1. Springer US, 2008. p.121.
[88] Lagoudas DC. Shape Memory Alloys: Modeling and Engineering Applications. New York: Springer, 2008.
[89] Liu Y, Al-Matar B, Newaz G. Metallurgical and Materials Transactions a-Physical Metallurgy and Materials Science 2008;39A:2749.
[90] Furuya Y. Design and material evaluation of shape memory composites. Technomic Publ Co Inc, 1996. p.321.

[91] Hamada K, Lee JH, Mizuuchi K, Taya M, Inoue K. Metallurgical and Materials Transactions a-Physical Metallurgy and Materials Science 1998;29:1127.
[92] Xie CL, Hailat M, Wu X, Newaz G, Taya M, Raju B. Journal of Engineering Materials and Technology-Transactions of the Asme 2007;129:69.
[93] Zhang RX, Ni QQ, Natsuki T, Iwamoto M. Composite Structures 2007;79:90.
[94] Moore CL, Bruck HA. Smart Materials & Structures 2002;11:130.
[95] Davoodi H, Noori, M.N., Hou Z. & Marioni, A. Application of shape memory alloys in vibration control. Proc. 16th Can. Congr. Applied Mechanics, CANCAM. Quebec, 1997.
[96] Zhang RX, Ni QQ, Masuda A, Yamamura T, Iwamoto M. Composite Structures 2006;74:389.
[97] Park JS, Kim JH, Moon SH. Composite Structures 2004;63:179.
[98] Razzaq MY, Frormann L. Polymer Composites 2007;28:287.
[99] Meng QH, Hu JL. Composites Part a-Applied Science and Manufacturing 2008;39:314.
[100] Gunes IS, Cao F, Jana SC. Journal of Polymer Science Part B-Polymer Physics 2008;46:1437.
[101] Cho JW, Kim JW, Jung YC, Goo NS. Macromolecular Rapid Communications 2005;26:412.
[102] Lan X, Liu YJ, Lv HB, Wang XH, Leng JS, Du SY. Smart Materials & Structures 2009;18.
[103] Tobushi H, Hayashi S, Hoshio K, Makino Y, Miwa N. Bending actuation characteristics of shape memory composite with SMA and SMP. Sage Publications Ltd, 2006. p.1075.
[104] Tobushi H, Hoshio K, Hayashi S, Miwa N. Key Engineering Materials 2007;340-341 II:1187.
[105] Jarali CS, Raja S, Upadhya A. Smart Materials and Structures 2010;19:105029.

VITA

Mohammad Souri

http://www.linkedin.com/in/msouri

Education:

Doctorate of Philosophy in Mechanical Engineering, University of Kentucky, Lexington, Kentucky; Anticipated May 2014
GPA: 3.81/4.0
Scope of Dissertation: Design, fabrication, and modeling of shape memory alloy (SMA) – shape memory polymer (SMP) composites.
Honors: Full scholarship from the Materials Center at the University of Kentucky, Fall 2011.
Bachelor of Science in Mechanical Engineering, Sharif University of Technology, Tehran, Iran; August 2007

Publications and Presentations:

- I. Kaya, M. Souri, H. E. Karaca, Y.I. Chumlyakov, "Orientation effects on the shape memory behavior in single crystal $Ni_{51}Ti_{49}$," submission to Acta Materialia is in process (April 2014).
- S. M. Saghaian, H. E. Karaca, M. Souri, H. Tobe, B. Basaran, R. Noebe, Y. I. Chumlyakov**,** "Orientation Dependence of Solutionized and Aged Ni-rich NiTiHf Shape Memory Single Crystal," submission to Acta Materialia is in process (April 2014).
- H.E. Karaca, Y. Chumlyakov, A. Turabi, H. Tobe, M. Souri, Kireeva, B. Basaran, "A Novel Ferrous Shape Memory Alloy with Ultra Large Transformation Strain," submission to Acta Materialia is in process (April 2014).
- M. Souri, Y. C. Lu, A. Erol, S. S. Pulla, H. E. Karaca, "Unconstrained and Constrained Shape Recoveries of an Epoxy-Based Shape Memory Polymer," submitted to the Polymer Testing journal for publication in September of 2013.
- S. S. Pulla, M. Souri, H. E. Karaca, Y. C. Lu, "Characterization of Electrically Conductive Shape Memory Polymer Composites," Proceedings of the American Society of Mechanical Engineers (ASME) ’13 Conference, Salt Lake City, UT, 2013.
- M. Souri, S. S. Pulla, A. Erol, H. E. Karaca, Y. C. Lu, "Thermo-Mechanical Behavior and Constitutive Modeling of Epoxy-Based SMPs and their Hybrid Composites," presented at the Society of Photo-optical Instrumentation Engineers (SPIE) ’13 Conference, San Diego, CA, 2013.
- M. Souri, A. Erol, B. Basaran, H. E. Karaca, "Shape Memory Polymers and Composites and their Properties," presented at the Materials Science & Technology (Ms&T) ’11 Conference, Columbus, OH, 2011.
- M. Souri, A. Erol, B. Basaran, H. E. Karaca, "Thermo-Mechanical Properties of Shape Memory Polymers,” presented at the SPIE ’11 Conference, San Diego, CA, 2011.

- M. Souri, K. Wieman, B. Basaran, H. E. Karaca, "Thermo-Mechanical Properties of Epoxy-Based Shape Memory Polymers and Composites," Proceedings of the Ms&T ’10 Conference, Houston, TX, 2010.
- G. Ded, H. E. Karaca, M. Souri, S. Saghaian, R. Noebe, A. Garg, Y. I. Chumlyakov, "Development of NiTi(Cu,Pd)Hf High Temperature Shape Memory Alloys (HTSMAs) for Aerospace Applications," Proceedings of the Ms&T ’09 Conference, Pittsburg, PA, 2009.
- H. E. Karaca, G. Ded, R. Noebe, A. Hatemi, M. Souri, Y. I. Chumlyakov, "Shape Memory Behaviour of Ni-rich NiTi(Cu,Pd)Hf High Temperature Shape Memory Alloys (HTSMAs)," Proceedings of the European Symposium on Martensitic Transformation (ESOMAT) Conference ’09, Prague, Czech Republic, 2009.